Spatially Resolved Spectroscopy for Detecting Firmness and Internal Disorders of Horticultural Products

A thesis

submitted in fulfilment

of the requirements for the degree

of

Doctor of Philosophy in Electronic Engineering

at

The University of Waikato

by

ZHE (JASON) SUN

THE UNIVERSITY OF
WAIKATO
Te Whare Wānanga o Waikato

2018

Abstract

Nondestructive detection of firmness and internal disorders are critical for New Zealand's horticultural industry. Soft and internally defective products can result both in loss of revenue and the supplier's reputation for quality. This thesis presents evaluation and development of spatially resolved spectroscopy (SRS) techniques aiming to improve the detection performance of these two quality parameters. Original contributions to literature include: (1) an assessment of a SRS reflectance system and a direct comparison of SRS and near-infrared spectroscopy (NIRS) on firmness prediction, (2) quantified understanding of NIRS on detecting internal disorders in terms of light transport and detection limitations, (3) accurate estimations of optical properties of healthy and rotten onion flesh, and (4) development of an SRS transmittance system for detecting onion rot, with the aid of finite element method (FEM) simulations.

By applying SRS measurements on the same 100 'Royal Gala' apples, this work showed that the NIRS interactance system slightly outperformed the SRS-based multispectral imaging (MSI) system when applied to the same samples. The cross validation prediction error was RMSECV = 6.99 N when compared with penetrometer firmness. Before the SRS system can be considered for commercial implementation, SRS firmness system must be further developed to accommodate the conditions and speed (10 samples/second) of a produce grader and demonstrate better performance than the existing online sensors.

Internal disorders that are small and spatially confined inside produce are difficult to detect using NIRS due to its lack of spatial resolution, but improvement might be made with better locations of light illumination and detection on the sample, i.e. optical geometry. Two optical geometries were investigated for detecting small and localised vascular browning (VAB) disorders in 'Braeburn' apples. Monte Carlo (MC) simulations indicated that the 180° transmission geometry allowed the light to travel much further than that of the 90° geometry inside a sample. However, the sensor is still only sensitive to a small portion of the internal volume, which was further validated by the poor results from the actual measurements. The 180° geometry system could detect 80% of defective apples with a misclassification rate of 21% for healthy ones.

An SRS system was then developed for detecting onion neck rots that are often small and localised to the stem end. The FEM software NIRFast was used to simulate light transport with absorption coefficients determined from juice transmittance measurements. The transmittance ratio of 728/805 nm was sensitive to the presence of the rot and was independent of the onion size. This ratio at different source locations formed a spatial profile, which could indicate the size and location of the rots. Finally, the optical system was implemented using a lock-in amplifier for simultaneous measurements of the light of two lasers at 728 nm and 805 nm. A mechanical scanning system was used to investigate multiple source locations. A preliminary test of the system showed a substantial improvement on typical NIRS performance levels. Future work aims to achieve a similar measurement scheme, while the sample is moving at high speed on a grader.

Acknowledgements

First and foremost, I would like to express my gratitude to my two main supervisors: to Rainer Künnemeyer, who encouraged me to take on the challenge of undertaking a PhD, and continued by giving me his moral, academic and financial support; and to Andrew McGlone, who accepted me into the wonderful Applied Sensor team at the New Zealand Institute for Plant and Food Research, and supported my application for a full time job on the team on completion of my PhD. A highlight of my PhD experience was the opportunity to travel with Andrew to China and Europe to attend conferences and to visit fellow researchers. In particular, I would like to acknowledge the patience and willingness of my supervisors in training me to become a competent researcher in various aspects.

Besides my supervisors, I would like to thank Nathan Tomer, whose grasp of mathematical modelling greatly exceeded my own. The research for this PhD would have been limited without the simulation work done by Nathan. I would also like to thank the extended Bioengineering team for all the technical support they gave me throughout my research, with an especial thanks to Keith Sharrock for preparing onion samples, and Paul Martinsen for his assistance in setting up the laser system.

I would also like to thank the New Zealand Institute for Plant and Food Research and the University of Waikato for their financial support by way of scholarships. My time was mainly spent at the Plant and Food Research Ruakura campus, where the people have made it so enjoyable. I want to particularly thank James Pinfold for organising sports activities on the Ruakura campus.

I would like to give special thanks to my parents, Yuzeng and Gaojie, who worked hard to financially support me during my years of undergraduate study. My academic journey would have not started without their overwhelming love and support.

Lastly, I would like to thank my friends in New Zealand, especially Henry and Rachel Fu for their caring, love and spiritual guidance during my PhD studies. They prayed for me and remained positive through all of the ups and downs of my research and life. Also to my long-time friends Lingze Deng, Yong Yu, and Joshua

Sun for all the fun times together. I would like to specifically thank Lucy for coming into my life and for her emotional support during my busiest times.

To all others who have contributed, but whose names I have failed to mention here, thank you.

Abbreviations

AUC	Area under receiver operating characteristics curve
CCD	Charged coupled detector
CMOS	Complementary metal-oxide semiconductor
CW	Continuous wave
DOT	Diffuse optical tomography
FD	Frequency domain
FEM	Finite element method
FPR	False positive rate
HSI	Hyperspectral imaging
IAD	Inverse adding-doubling
MC	Monte Carlo
MLD	Modified Lorentzian distribution
MLR	Multiple linear regression
MSI	Multispectral imaging
NIRS	Near-infrared spectroscopy
PLS	Partial least squares
PLSDA	Partial least squares discriminant analysis
RMSECV	Root mean standard error of cross-validation
RMSEP	Root mean standard error of prediction
ROC	Receiver operating characteristics
SNR	Signal to noise
SRRS	Spatially resolved reflectance spectroscopy
SRS	Spatially resolved spectroscopy
TD	Time domain
TPR	True positive rate
VAB	Vascular browning

Table of Contents

Chapter 1

Introduction

1.1 Background

Near-infrared spectroscopy (NIRS) is a popular optical technique that has been implemented on commercial grader lines for the quality assessment of individual horticultural products. A NIRS system mainly consists of a light source (typically a tungsten halogen lamp) and a spectrometer. The high acquisition speed (a few milliseconds) and a rugged optical structure provided by a photodiode or a charged coupled detector (CCD) array spectrometer facilitated the development of online sensors (that is, sensors built into high-speed graders). Chemometric analysis methods, such as partial least squares (PLS) regression, are often used to build predictive models that interpret the measured absorbance spectra in terms of sample constituents or parameters of interest. NIRS sensors are particularly accurate for measuring concentrations of various constituents, such as dry matter (McGlone et al., 2003; Saranwong et al., 2001) and soluble solids content (McGlone et al., 2002; Nicolaï et al., 2008). There are also applications for firmness (Nicolaï et al., 2008; Sun et al., 2017; Sun et al., 2016) and internal disorders (Clark et al., 2003; Han et al., 2006). There has been ongoing research on optical hardware, spectrometer technologies and mathematical modelling techniques for improving detection performance (Nicolaï et al., 2007). However, firmness prediction and internal defect detection remain difficult for NIRS systems. These two parameters are of great importance for both horticultural producers and retailers since overmature (soft) and/or internally defective products incur consequences for both in loss of revenue and the supplier's reputation for quality. Therefore, any improvements to current NIRS sensors, including the development of new types of sensor for detecting firmness and internal disorders, could provide benefits for the industry.

The detection of relevant signals by the NIRS sensors is based on the change of spectral characteristics through wavelength dependent scattering and absorption processes (Nicolaï et al., 2007). Absorption is primarily due to light-absorbing chemical components in the tissue (for example, sugar, chlorophyll, water, and so on). Scattering depends on microscopic changes in the refractive index caused by extra- and intra-cellular structural components, such as cell walls, by discrete cellular constituents, and by variations in tissue density (McGlone et al., 1997). NIRS cannot distinguish between firmness-related light scattering effects and light absorption effects, the two phenomena interacting to produce the very convoluted absorbance spectra. For internal defects, small and localised ones may not cause

detectable changes in the spectra. There are two main causes of insensitivities: firstly, the transmitted light may simply not travel deeply enough into a sample to interact with the defective tissue, as it is heavily scattered and/or absorbed at shallower depths; and secondly, NIRS is not spatially resolved. Typical light sources broadly illuminate a sample, and any spatial resolution is lost when the resulting diffuse radiation is collected at a distant point (Martinsen and Schaare, 1998). The NIR system typically interrogates an internal region that is much larger than the small internal defect, so the received light is influenced predominantly by the healthy tissue. To detect the small and localised defects in produce, light delivery and collection must be more specifically focussed on different sectional volumes of the produce in order to increase interactions between the defect and the transmitted light.

Spatially resolved spectroscopy (SRS) is a technique that adds spatial information to spectroscopic measurements. SRS is expected to improve the prediction of sample firmness by providing extra spatial information that distinguishes between tissue absorption and scattering properties, so the scattering information can then be used for identifying textural parameters such as firmness. The SRS reflectance technique, often referred to as spatially resolved reflectance spectroscopy (SRRS) or light backscattering imaging, has been extensively studied in recent years (Adebayo et al., 2016; Mollazade et al., 2012), because of its potential for online applications. Among different hardware configurations, laser based systems are particularly suitable since lasers can produce focused high-irradiance illumination spots on the fruit, which allows for deeper light penetration and fast image acquisition (Mollazade et al., 2013; Qing et al., 2008). A multispectral imaging (MSI) system, using lasers at four discrete wavelengths (685, 805, 904, 980 nm), has been previously developed in our research group (Rowe, 2015), and measurements were taken on the flat cut surface of apples. But it is unclear how well this system will perform on intact fruit and, more importantly, how this system will compare with the existing NIRS technique.

Transmittance mode must be used for detecting internal defect since the deeper penetrating light is more likely influenced by the presence of defective tissue. There have been no studies in the literature assessing SRS in transmittance mode for quality evaluation of produce. Diffuse optical tomography (DOT) is a SRS transmittance system used for brain and breast cancer detection (Yamada and

Okawa, 2014). The measurement process of DOT involves spatially localising light delivery and detection at various positions around the sample. This enhances the differentiation of information arising from different discrete internal volumes of the sample. The sensitivity to the small internal defect will increase as the received light will be more affected by the defective tissue. However, the DOT technique is not directly applicable to high-speed graders, high speed and moving samples being the two main obstacles for such systems. Therefore, studies will need to be carried out to investigate the potential of SRS transmittance measurement for internal disorders in produce.

1.2 Research aims

The main aim of this research was to develop SRS-based optical sensors to achieve better detections of firmness and internal defects than those provided by traditional NIRS. We used lasers as the light sources since they provide a powerful light beam with a small illumination area on the object, allowing for fast and spatially-resolved detection. The spatial information was used to extract light scattering properties in order to predict firmness and to improve the sensitivity to small and localised defects by spatially localising source and detection. Specifically, we aimed to 1) compare SRS reflectance system with a NIRS interactance system, for predicting the firmness of 'Royal Gala' apples, and 2) develop a SRS transmittance system for internal disorder detection. An additional aim of the research was to understand or quantify some important technical limitations of NIRS, such as the effects of optical geometry and sample orientation on measurements, through investigative experiments and simulated light transport modelling using Monte Carlo (MC) simulation.

1.3 Thesis outline

This thesis is organised into eight chapters.

Chapter 1

Chapter one gives an introduction to the topic of the thesis.

Chapter 2 (published)

This chapter reviews optical techniques used to measure firmness of fresh produce; in particular, NIRS and spatially resolved reflectance spectroscopy (SRRS) are

discussed, as they have good potential for use on high-speed graders. Fundamental principles for firmness assessment are reviewed as well as reported performance.

Chapter 3

This chapter reviews optical methods that have potential to detect internal disorders, mainly covering NIRS, hyperspectral imaging (HSI) and DOT.

Chapter 4 (published)

SRRS is generally considered to be a better method than NIRS as, in theory, it segregates out the optical scattering properties that are presumed to be affected by sample or tissue firmness. Previous studies have suggested that firmness may also affect the NIRS spectra through absorption changes (Cen et al., 2013; Rowe et al., 2014). Thus, the convoluted NIRS spectra may also contain information that could be used to predict firmness. This paper aims to determine which system might be better. The paper describes the development of a multispectral imaging (MSI) system based on the SRRS technique. The performance was compared with an interactance NIRS system using 100 'Royal Gala' apples. The reference for firmness was measured using a destructive penetrometer. The feasibility of using SRRS for online applications was also discussed.

Chapter 5 (under review)

With more sensitive spectrometers there is a need to assess NIRS specifically on small and localised internal disorders. In an effort to improve the detection of vascular browning (VAB) in 'Braeburn' apples, we investigated two optical geometries and five sample orientations. MC simulations enabled quantified understanding of the light propagation inside the fruit under the influence of different optical geometries.

Chapter 6 (published)

The key inputs to light transport modelling and simulation of measurement experiments are optical properties. The paper presented here concerned research carried out to measure the absorption and scattering coefficients of healthy and rotten onions using a combination of laboratory-based optical measurements on thin tissue slices and extracted juice. The accuracy to the derived tissue data was validated by light transmittance measurements using a NIRS system and a laser-based system.

Chapter 7 (to be submitted)

This chapter describes the development of a DOT-based laser system. The sensor has the potential to be further developed for online applications and it shows good sensitivity to small and localised defects.

Chapter 8

This chapter discusses the work involved in this PhD and presents conclusions. Some possible directions for future work are presented.

1.4 Contributing publications

Throughout this research, the following papers have been published or are ready for publication:

Patent

- Sun, J., Künnemeyer, R., McGlone, A., Tomer, N., 2017. Methods and systems for determining internal quality attribute(s) of articles of agricultural produce, New Zealand Patent Application No. 732719, filed 9 June 2017.

Book chapter

- Sun, J., Künnemeyer, R., McGlone, A., 2017. Optical methods for firmness assessment of fresh produce: a review, Postharvest Handling. InTech.

Journal papers

- Sun, J., Künnemeyer, R., McGlone, A., Rowe, P., 2016. Multispectral scattering imaging and NIR interactance for apple firmness predictions. Postharvest Biology and Technology 119, pp. 58-68.
- Sun, J., Künnemeyer, R., McGlone, A., Tomer, N., 2018a. Investigations of optical geometry and sample positioning in NIRS transmittance for detecting vascular browning in apples. Under review.
- Sun, J., Künnemeyer, R., McGlone, A., Tomer, N., 2018b. Optical properties of healthy and rotten onion flesh from 700 to 1000 nm. Postharvest Biology and Technology 140, pp. 1-10.

- Sun, J., Künnemeyer, R., McGlone, A., Tomer, N., Sharrock, K., 2018. Development of a laser system for detecting internal rot in onions. To be submitted.

Conference papers

- Sun, J., Künnemeyer, R., McGlone, A., Rowe, P., Talele, S., 2015. Development of a multispectral imaging system for apple firmness prediction. 9th International Conference on Sensing Technology IEEE, Auckland, New Zealand, pp. 203-206.

- Sun, J., Künnemeyer, R., McGlone, A., Tomer, N., 2016. Investigation of light transmission in healthy and rotten onions. Electronics New Zealand Conference (pp. 142-145), Victoria University of Wellington.

- Sun, J., Künnemeyer, R., McGlone, A., Tomer, N., 2017. Fruit orientation in NIR transmission for vascular browning in apples. 11th International Conference on Sensing Technology IEEE, Sydney, Australia, pp. 139-142.

Poster

- Sun, J., McGlone, A., Kunnemeyer, R., Tomer, N., Punter, M., 2017. Which optical geometry is best to detect vascular browning in apples? Poster session presented at the meeting of 18th International Conference on Near Infrared Spectroscopy (ICNIRS), University of Copenhagen, Copenhagen, Denmark.

1.5 References

Adebayo, S.E., Hashim, N., Abdan, K., Hanafi, M., 2016. Application and potential of backscattering imaging techniques in agricultural and food processing – A review. Journal of Food Engineering 169, 155-164.

Cen, H., Lu, R., Mendoza, F., Beaudry, R.M., 2013. Relationship of the optical absorption and scattering properties with mechanical and structural properties of apple tissue. Postharvest Biology and Technology 85, 30-38.

Clark, C.J., McGlone, V.a., Jordan, R.B., 2003. Detection of Brownheart in 'Braeburn' apple by transmission NIR spectroscopy. Postharvest Biology and Technology 28, 87-96.

Han, D., Tu, R., Lu, C., Liu, X., Wen, Z., 2006. Nondestructive detection of brown core in the Chinese pear 'Yali' by transmission visible–NIR spectroscopy. Food Control 17, 604-608.

Martinsen, P., Schaare, P., 1998. Measuring soluble solids distribution in kiwifruit using near-infrared imaging spectroscopy. Postharvest Biology and Technology 14, 271-281.

McGlone, V.A., Abe, H., Kawano, S., Kawano, A., 1997. Kiwifruit firmness by near infrared light scattering Journal of Near Infrared Spectroscopy 5, 83-89.

McGlone, V.A., Jordan, R.B., Seelye, R., Clark, C.J., 2003. Dry-matter—a better predictor of the post-storage soluble solids in apples? Postharvest Biology and Technology 28, 431-435.

McGlone, V.A., Jordan, R.B., Seelye, R., Martinsen, P.J., 2002. Comparing density and NIR methods for measurement of Kiwifruit dry matter and soluble solids content. Postharvest Biology and Technology 26, 191-198.

Mollazade, K., Omid, M., Akhlaghian Tab, F., Kalaj, Y.R., Mohtasebi, S.S., Zude, M., 2013. Analysis of texture-based features for predicting mechanical properties of horticultural products by laser light backscattering imaging. Computers and Electronics in Agriculture 98, 34-45.

Mollazade, K., Omid, M., Tab, F.A., Mohtasebi, S.S., 2012. Principles and applications of light backscattering imaging in quality evaluation of agro-food products: a review. Food and Bioprocess Technology 5, 1465-1485.

Nicolaï, B.M., Beullens, K., Bobelyn, E., Peirs, A., Saeys, W., Theron, K.I., Lammertyn, J., 2007. Nondestructive measurement of fruit and vegetable quality by means of NIR spectroscopy: A review. Postharvest Biology and Technology 46, 99-118.

Nicolaï, B.M., Verlinden, B.E., Desmet, M., Saevels, S., Saeys, W., Theron, K., Cubeddu, R., Pifferi, A., Torricelli, A., 2008. Time-resolved and continuous wave NIR reflectance spectroscopy to predict soluble solids content and firmness of pear. Postharvest Biology and Technology 47, 68-74.

Qing, Z., Ji, B., Zude, M., 2008. Non-destructive analyses of apple quality parameters by means of laser-induced light backscattering imaging. Postharvest Biology and Technology 48, 215-222.

Rowe, P., 2015. Optical Techniques for Fruit Firmness Assessment. University of Waikato, Hamilton, New Zealand.

Rowe, P.I., Künnemeyer, R., McGlone, A., Talele, S., Martinsen, P., Seelye, R., 2014. Relationship between tissue firmness and optical properties of ‘Royal Gala’ apples from 400 to 1050nm. Postharvest Biology and Technology 94, 89-96.

Saranwong, S.I., Sornsrivichai, J., Kawano, S., 2001. Improvement of PLS Calibration for Brix Value and Dry Matter of Mango Using Information from MLR Calibration. Journal of Near Infrared Spectroscopy 9, 287-295.

Sun, J., Künnemeyer, R., McGlone, A., 2017. Optical methods for firmness assessment of fresh produce: A review, Postharvest Handling. InTech.

Sun, J., Künnemeyer, R., McGlone, A., Rowe, P., 2016. Multispectral scattering imaging and NIR interactance for apple firmness predictions. Postharvest Biology and Technology 119, 58-68.

Yamada, Y., Okawa, S., 2014. Diffuse optical tomography: present status and its future. Optical Review 21, 185-205.

Chapter 2

Optical Methods for Firmness Assessment of Fresh Produce: A Review

---

An invited book chapter

by

Jason Sun, Rainer Künnemeyer and Andrew McGlone

Published in

Postharvest Handling

As first author, I prepared the initial draft manuscript, which was edited by my supervisors, who have been credited as co-authors. My supervisors provided guidance on the technical part.

Optical Methods for Firmness Assessment of Fresh Produce: A Review

Jason Sun, Rainer Künnemeyer and Andrew McGlone

Additional information is available at the end of the chapter

http://dx.doi.org/10.5772/intechopen.69256

Abstract

This chapter is devoted to a review of optical techniques to measure the firmness of fresh produce. Emphasis is placed on the techniques that have a potential for online high-speed grading. Near-infrared spectroscopy (NIRS) and spatially resolved reflectance spectroscopy (SRRS) are discussed in detail because of their advantages for online applications. For both techniques, this chapter reviews the fundamental principles as well as the measured performances for measuring the firmness of fresh produce, particularly fruit. For both techniques, there have been studies that show correlations with penetrometer firmness as high as $r = 0.8 - 0.9$. However, most studies appear to involve bespoke laboratory instruments measuring single produce types under static conditions. Therefore, accurate performance comparison of the two techniques is very difficult. We suggest more studies are now required on a wider variety of produce and particularly comparative studies between the NIRS and SRRS systems on the same samples. Further instrument developments are also likely to be required for the SRRS systems, especially with an online measurement where fruit speed and orientation are likely to be issues, before the technique can be considered advantageous compared to the commonly used NIRS systems.

Keywords: produce, firmness, spatially resolved reflectance spectroscopy, near-infrared spectroscopy, optical methods

1. Introduction

Firmness is a major quality parameter in grading fresh produce, governed by the mechanical and structural properties of fruit. For producers, it can indicate ripeness and/or storage potential, and for consumers, it directly influences consumer acceptance and satisfaction. The industry standard instrument for firmness assessment is a penetrometer, which drives a metal

plunger into the fruit flesh and records the maximum resistance force. This technique has three main drawbacks [1]: it is destructive, leaving the fruit unsaleable, measurements are highly variable (up to 30%) and it cannot be used in online situations. A fast and nondestructive technique would be desirable for the fresh fruit industry as it offers the benefit of grading and sorting each individual fruit.

Firmness has been a difficult parameter to measure by fruit graders. To date, no commercially successful nondestructive system has been created on a high-speed grader. Most prior research has focused on mechanical methods such as acoustic resonance, impact response, and force-deformation [2–6]. Most of the mechanical methods require contact with the fruit, which limits the grading speed due to the difficulty of achieving reliable physical contact and consistent fruit compliance at high speeds. It also potentially causes physical damage to the fruit. Moreover, mechanical methods are sensitive to each method's specific mechanical property such as deformation force, so they often do not correlate well or consistently with the penetrometer. For this reason, the industry is reluctant to adopt these methods [7]. This has led to more research into the use of optical methods, which have the unique feature of being noncontact. Modern high-speed fruit-grading systems run at speeds in excess of 10 fruit per second and noncontact methods will be advantageous in such circumstances.

This chapter reviews the current optical techniques for firmness measurement. Among these techniques, near-infrared spectroscopy (NIRS) [8–10] and spatially resolved reflectance spectroscopy (SRRS) [11, 12] have been investigated more commonly in recent years, and are more suitable for high-speed operation.

2. Principle of optical methods for measuring firmness

Optical techniques are based on light interactions with fruit tissue. In the visible to near-infrared (Vis/NIR) range of the electromagnetic spectrum, fruit can be considered as semi-transparent or turbid. There are two optical phenomena that describe how light interacts with turbid biological material: absorption and scattering (**Figure 1**). Absorption is primarily due to the chemical composition of the tissue (pigments, chlorophylls, water, etc.). Scattering depends on microscopic changes in refractive index caused by the tissue density, cell composition, and extra- and intra-cellular structure of the fruit, and thus may be useful for assessing textural properties such as firmness. The light transportation in fruit can be characterized by fundamental optical properties of absorption, scattering and refraction, which are defined by the absorption coefficient (μ_a), scattering coefficient (μ_s), refractive index (n), and anisotropy factor (g).

Cen et al. [14] used a hyperspectral backscattering system to measure optical properties of "Golden Delicious" and "Granny Smith" apples over 30 days' storage time. The optical properties from 300 to 1000 nm were compared with acoustic and impact firmness. They found the scattering coefficient generally decreased as the fruit softened ($r > 0.9$ for both mechanical properties). Absorption coefficients also had high correlations with firmness ($r \sim 0.9$ for "Golden Delicious") in the wavelength range that associated with chlorophyll and anthocyanin absorption.

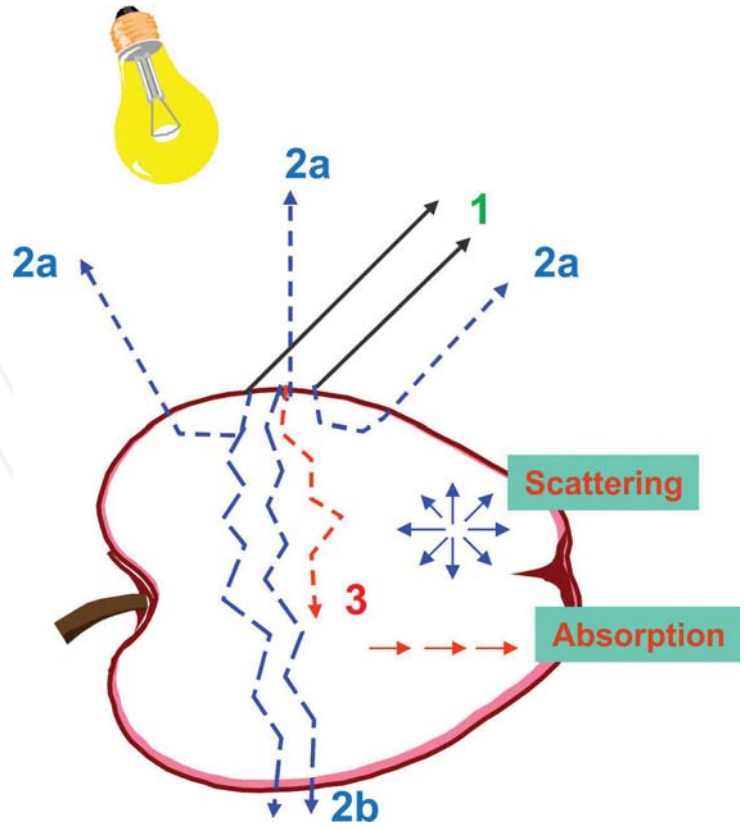

Figure 1. Distribution of incident light in fruits: (1) surface/specular reflectance, (2a) diffuse reflectance, (2b) transmittance, and (3) absorption [13] (Copyright 2016 American Society of Agricultural and Biological Engineers. Used with permission).

The inverse adding-doubling (IAD) technique was used to measure optical properties between 400 and 1050 nm in another study on apples [15]. The reduced scattering coefficient between 550 and 900 nm had an average correlation $r = -0.68$ with penetrometer firmness. Changes in optical properties at carotenoid (400–500 nm) and chlorophyll-a (680 nm) wavelengths correlated with penetrometer firmness with $r = -0.69$ and 0.52, respectively. However, Tomer et al. [16] found that the IAD technique could be quite inaccurate for absorption coefficient measurements on fresh produce at 785 nm, reporting a coefficient for fresh onions that was five times larger than that required for light transport modeling on onions.

There have been some studies based on other optical principles. For example, Costa et al. [17] used a biospeckle laser system to measure the biospeckle images on the *Acrocomia aculeata* fruit pulp. The calculated biological activity (BA) had a negative correlation with penetrometer firmness. The correlation varied depending which tree was evaluated, the highest was $r = -0.903$. Skic et al. [18] used a similar approach for "Ligol" and "Szampion" apples. They achieved a correlation of about $r = -0.5$ for both cultivars. Peña-Gomar et al. [19] used a technique called laser reflectometry near the critical angle (LRCA) to measure the refractive index of mango pulp, which was expected to correlate with acoustic firmness. Their results showed some correlation but the authors did not report the correlation coefficient, and only six fruits were measured.

3. Optical techniques for firmness measurements

Optical methods are noncontact; a feature that distinguishes them from most mechanical methods. In the past two decades, the most common optical sensing method for produce grading is NIRS. Grading lines equipped with NIR sensors are now commercially available from many manufacturers. Firmness is not an attribute commonly assessed using industrial NIR sensors [1], but it has been studied in a number of research applications (**Table 1**).

In theory, the optical scattering properties are more directly related to firmness than absorption properties and have been reported to correlate with firmness, as discussed in Section 2 [14, 15]. Optical techniques that can measure optical properties of biological materials have been studied more recently, aiming to provide a more accurate and robust technique compared to NIRS. These techniques may be divided into three main categories: time resolved, frequency domain, and spatially resolved. Time-resolved and frequency domain techniques have been extensively researched in the biomedical area, but they may not be suitable for applications on a grader line because of expensive instrumentation, slow speed, and the requirement of good contact between the sample and detector [20]. Spatially resolved techniques, and more specifically SRRS, have been researched more commonly for such applications as it can overcome many of those deficiencies.

3.1. Near-infrared spectroscopy

NIRS is widely used to determine fruit quality parameters, particularly compositional parameters such as soluble solids or dry matter content [4, 21]. Standard NIRS measures the spectral pattern of light transmitted through a representative portion of the flesh, and chemometric analysis methods are generally used to interpret the resulting absorbance spectra in terms of the parameters of interest. The disadvantage is that this technique relies on a prior extensive training exercise to develop a predictive model, based on the careful selection and measurement of a representative calibration data set from a suitable population. The model also needs to be checked and updated constantly.

Species	Cultivar	Acquisition mode	Spectral range	Prediction	Reference
Apple	"Royal Gala"	Interactance	500–1100 nm	R = 0.77 RMSEP = 7.5 N	McGlone et al. [25]
Apple	"Gala" "Red Delicious"	Reflectance	400– 1800 nm	R = 0.88	Park et al. [26]
Mandarin	Satsuma	Reflectance	350–2500 nm	R = 0.83	Gómez et al. [10]
Pear	"Conference"	Reflectance	780– 1700 nm	R = 0.59	Nicolaï et al. [9]
Capsicum annuum	Bell pepper	Reflectance	780– 1690 nm	R = 0.6 RMSEP = 7.2 N	Penchaiya et al. [8]
Cherry	"Hedelfinger Sam"	Reflectance	800–1700 nm	R = 0.8 & 0.65 SEP = 0.79 and 0.44 N	Lu [27]

Table 1. Overview of applications of NIR spectroscopy in firmness measurements.

For measuring fruit firmness, the NIRS method is limited in theory because it involves measurement of the apparent light absorbing power of a sample, which does not segregate scattering and absorption properties. However previous studies have suggested firmness may affect the apparent light-absorbing power through chemical changes associated with cell wall degradation, physical changes in intercellular structure and/or indirectly through correlated pigment absorption changes such as a chlorophyll decrease on ripening [14, 15].

3.1.1. Basic concepts

Near-infrared radiation covers the range of the electromagnetic spectrum between 780 and 2500 nm. Often wavelengths below 780 nm are also included in the analysis as these regions contain valuable information on absorbing pigments within the fruit flesh and skin [15]. Therefore, this technique is often referred to as Vis/NIR spectroscopy.

The typical NIRS set-up uses a broadband light source to illuminate the sample and the transmitted or reflected light is measured using a spectrometer. In the design process, it is useful to know that the NIR light intensity decreases exponentially with depth. One study [22] showed that the light intensity dropped to 1% of the initial intensity at a depth of 25 mm inside an apple in the 700–900 nm range. The depth was less than 1 mm in the 1400–1600 nm range. Therefore, the optical arrangement and the effective optical path length for the light are crucial elements to consider in order to collect spectra containing relevant information from the sample. This also explains why NIRS is suited for use with thin-skinned fruit, the thicker skins limiting light penetration [23].

In practice, three measurement set-ups are used (**Figure 2**). In reflection mode, light source and spectrometer are on one side but at a specific angle to avoid specular reflection, while in

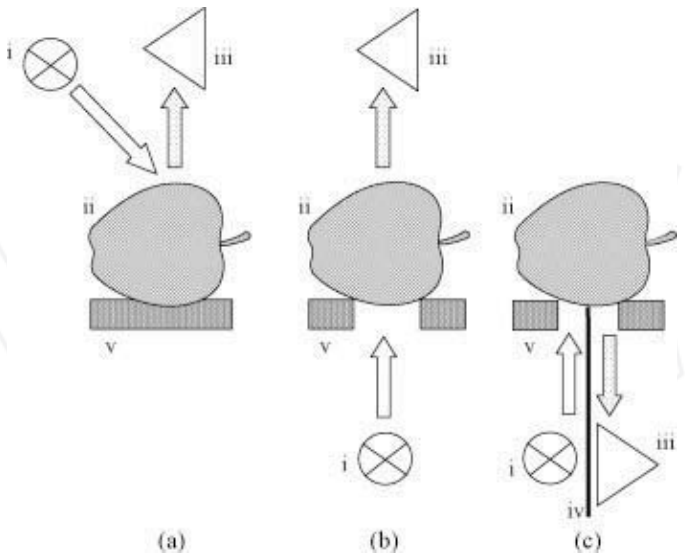

Figure 2. Three different set-ups: (a) reflectance, (b) transmittance, and (c) interactance. (i) Is the light source, (ii) is the sample, (iii) is the detector, (iv) is a light barrier, and (v) is the mechanical support [21] (Used with permission from Elsevier).

transmission mode the light source and detector are on opposite sides. Interactance requires a special optical arrangement so that specular and surface reflection cannot directly enter the detector.

Transmission measurement has the advantages of exploring the largest volume of the internal flesh and all the light measured has interacted with the flesh. Thus it is suitable to find internal defects, but the transmitted light might also contain information of the two layers of skin (front entrance and back exit), and the core of the fruit. For firmness measurement, although light penetration is limited and one skin layer is still present, reflection and interactance set-ups will be more desirable as the light interacts with some portion of flesh without interference from the core. Schaare and Fraser [24] compared reflectance, interactance and transmission measurements for measuring soluble solid content (SSC), density and internal flesh color of kiwifruit and concluded that interactance measurements provided the most accurate results.

3.1.2. Firmness applications

Sensors based on NIRS techniques have been mainly developed for chemical compositions such as SSC, and most of the studies have been carried out under static conditions. The industry is taking the lead in the development of online systems, but there is little scientific evidence of their accuracies [21]. Attempts to use NIRS for fruit firmness prediction have met with varying degrees of success with some studies reporting correlations as high as $R \sim 0.8 - 0.9$. **Table 1** gives an overview of NIRS applications that measure firmness of fruits and vegetables.

Most reported scientific studies consider only a single NIR instrument format for fruit assessment. For example, McGlone et al. [25] used an interactance mode (**Figure 3**). The system contained a broadband light source (50 W quartz halogen, RJL 5012 FL, Radium, Germany) and a nonscanning polychromatic diode array spectrometer (Zeiss MMS1-NIR, Germany). Fruits were placed on a holder with stem-calyx horizontal. Measurements were generally taken on two opposite sides around the circumference, taking care to avoid any obvious surface defects. The absorbance spectrum measured was the average of 5 contiguous acquisitions at 175 ms integration time.

The wavelength range used varies among the reported literature studies (**Table 1**). Walsh [23] suggested that restricted wavelength ranges could improve the robustness of a model and allow for the development of lower cost "multispectral" measurement systems. Prediction performance was generally determined by dividing the fruits randomly into a calibration and a validation set for model development. Walsh [23] also reported that such a model will predict the attribute of interest within the population, but it is likely to fail spectacularly on a new, independent set.

3.2. Spatially resolved reflectance spectroscopy (SRRS)

Figure 1 illustrates two types of light reflectance: surface reflectance and diffuse reflectance. Surface reflectance contains information about the object surface such as color. Only 4–5%

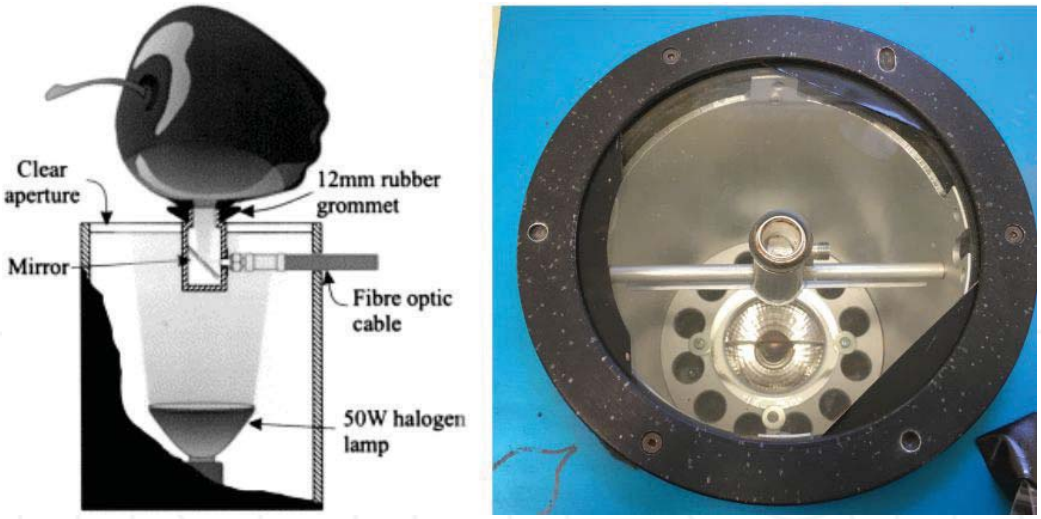

Figure 3. The benchtop NIRS system [25].

of incident light is reflected by surface reflection and external diffuse reflectance, so most reflected light contains the diffuse reflected/backscattered photons that carry information of the internal tissue properties [11].

Figure 4 shows a small continuous-wave light beam perpendicularly illuminates the sample's surface, and the reflected light is measured at different distances from the light source, forming the spatial profile (**Figure 3**). Optical properties/parameters can be obtained by using a phenomenological diffusion model and/or a heuristic modified Lorentzian model from the

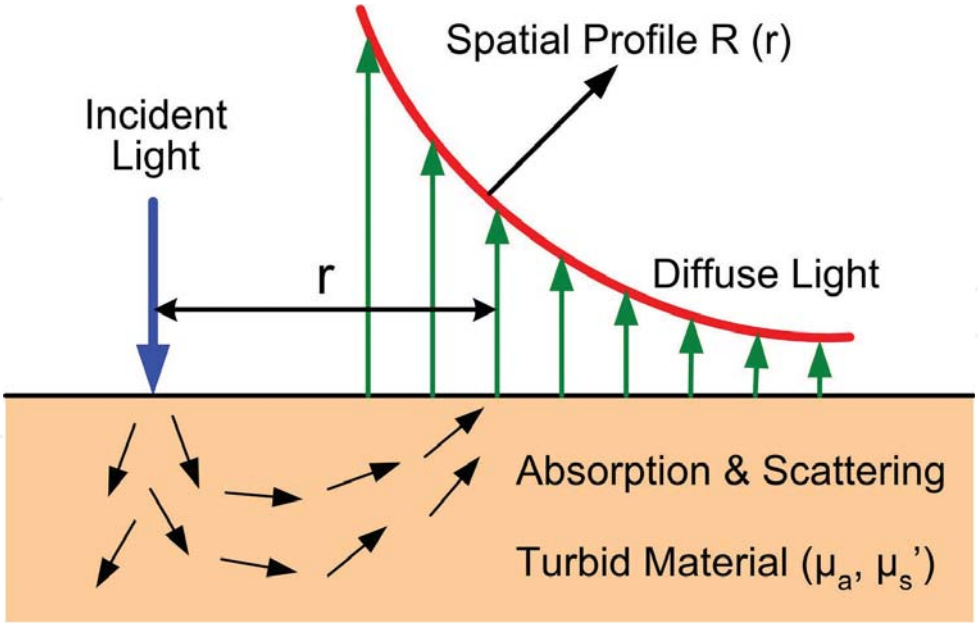

Figure 4. Measuring principle for spatially resolved reflectance spectroscopy (SRRS) [20] (Used with permission from the author).

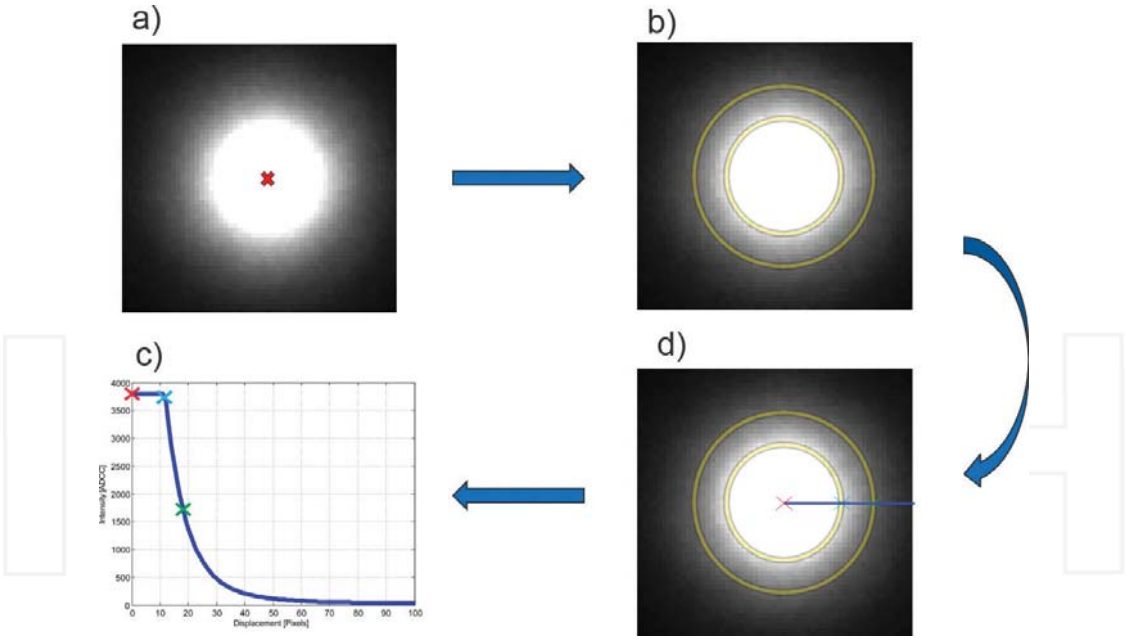

Figure 5. Imaging processing used by Sun et al. [30] for apple firmness measurements: (a) finding center in the raw image, (b) ring average, and (c) & (d) producing the spatial profile.

measured one-dimensional scattering profile. Mollazade et al. [28] used texture-based features methods to build models to predict mechanical properties of various produce. Instead of looking at a single 1D scattering profile, this technique analyzed the entire 2D images, which was expected to improve the correlation to firmness.

The extracted parameters can then be used to predict firmness using statistical models such as multiple linear regression (MLR) and artificial neural network (ANN). Typically, images are first processed to reduce noise and then converted into one-dimensional profile [29]. **Figure 5** illustrates the process used by Sun et al. [30] for measuring apple firmness. The scattering image was first processed to find the center of the illuminated area (**Figure 5(a)**). Then a process called ring/radial averaging was performed. The distance to each pixel was calculated and rounded to the nearest whole number (**Figure 5(b)**). All pixels at each of these integer radii were grouped and averaged providing a vector of intensity values that correspond to single pixel rings expanding out from the center point (**Figure 5(d)**). The intensity profile (**Figure 5(c)**) was finally produced.

3.2.1. Parameters extraction

In turbid material, a diffusion equation is often used as an approximation of the transport of the light. For SRRS under the assumption of inexistence of photon source in the medium, the diffusion equation can be simplified to an equation consisting of three variables: r (source-detector distance), μ_a and $\mu_{s'}$ [11, 31]. Unknown optical properties μ_a and $\mu_{s'}$ can be obtained by applying a curve fitting procedure with respect to r.

Researchers have also used statistical distribution functions to fit scattering profiles as a function of scattering distance. Peng and Lu [32] investigated a number of variations of modified Lorentzian functions aiming to find one suitable for firmness and SSC measurements. They concluded Eq.(1) was the best performing equation, which was also used in other studies for firmness applications [7, 29, 30]:

$$I(x) = a + \frac{b}{1 + \left(\frac{|x|}{c}\right)^d} \tag{1}$$

where I is the intensity along a radial intensity profile, a is the asymptotic value of light intensity when x (distance to center of the light spot) approaches infinity, b is the peak value corresponding to the intensity at the center of the image, c is the full width half maximum (FWHM) of the intensity profile, and d is related to the slope of the profile in the FWHM region.

3.2.2. Hardware

A SRRS system consists of two essential components: light source and imaging system. All the systems can be divided into three types according to the light source and operating wavelength range: laser light backscatter imaging (LLBI), multispectral light backscatter imaging (MLBI), and hyperspectral light backscatter imaging (HLBI).

The LLBI technique requires a small illumination spot on the target fruit, and measurement scattering areas of 25–30 mm diameter have been used for beam diameters of 0.8–1.5 mm by Lu [33] and Peng and Lu [32], respectively. Lasers are particularly suitable for this purpose since lasers can produce focused high-irradiance illumination spots on the fruit, which allows for deeper light penetration and fast image acquisition (shorter integration time). Moreover, LLBI systems are more robust and cost-effective than MLBI and HLBI. Overall, LLBI systems are potentially suitable for online high-speed operations. One of the drawbacks of LLBI systems is the limited operating wavelength. One to four lasers are typically used [28, 30, 34].

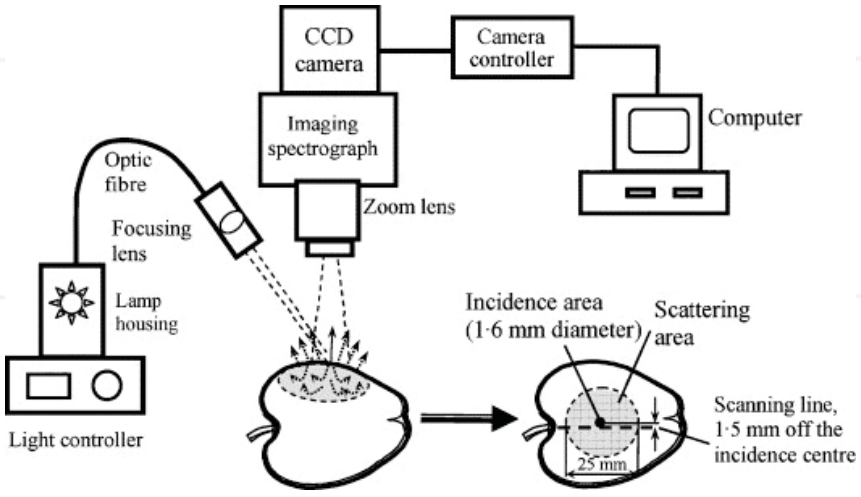

Figure 6. Hyperspectral system (HLBI) for measuring the firmness of peach [36] (Used with permission from Elsevier).

Species	Cultivar	Light source	Detector	Spectral range	Prediction	Reference
Apple	"Golden Delicious" "Jonagold Delicious"	Halogen lamp	CCD camera with spectrograph	500–1000 nm	r = 0.84 − 0.95 SEP = 5.9 − 8.7 N	Mendoza et al. [37]
Apple	"Golden Delicious"	Halogen lamp	CCD camera with spectrograph	450–1000 nm	r = 0.894 SEP = 6.14 N	Peng and Lu [32]
Apple	"Braeburn"	Halogen lamp	CCD camera with spectrograph	500–1000 nm	r = 0.84 RMSEP = 9.68 N	Nguyen Do Trong et al. [38]
Apple	"Braeburn"	Supercontinuum laser with monochromator	CCD camera	550–1000 nm	r = 0.8 RMSEP = 0.75 kg cm^{-2}	Van Beers et al. [35]
Peach	"Red Haven" "Coral Star"	Halogen lamp	CCD camera with spectrograph	500–1000 nm	r = 0.76 − 0.88	Lu and Peng [36]
Apple	"Red Delicious" "Golden Delicious"	Quartz tungsten halogen lamp	NIR enhanced CCD camera with a liquid crystal tunable filter	680, 700, 740, 800, 820, 910, & 990 nm	r = 0.898 SEV = 6.14 − 6.41 N	Peng & Lu [29]
Apple	"Elstar" "Pinova"	Laser diode	CCD camera	680,780,880,940, & 980 nm	r = 0.89 − 0.81 RMSEC V = 4.71 − 5.48 N/cm^2	Qing et al. [34]
Apple	"Royal Gala"	Laser diode	CMOS camera	685,850,904, & 980 nm	r = 0.87 RMSECV = 7.17 N	Sun et al. [30]
Apple Plum Tomato mushroom	"Pinova" & "Elstar" "Jojo" & "Tophit" "Pannovy"	Laser diode	CCD camera	660 nm	r = 0.887 − 0.919	Mollazade et al. [28]
Apple	"Golden Delicious"	Laser diode	CCD camera with spectrograph	408 nm	R = 0.75 SEP = 8.57 N	Noh & Lu [39]

Table 2. Overview of applications of SRRS in firmness measurements.

In the MLBI and HLBI systems, the light source is a tungsten-halogen lamp. The light usually passes through an optical fiber and then focuses on the fruit by a collimating lens, as shown in **Figure 6**. One exception is the system developed by Van Beers et al. [35] where a supercontinuum laser and a monochromator were used for the hyperspectral measurements.

The scattering profiles can be measured using multiple spectrometers at different source-detector distances. The advantage of using a spectrometer is that multiple wavelengths or a specific spectral region can be obtained simultaneously. However, it requires a good contact/focus between the probes and the sample, which will not be suitable for online operations. A CCD camera is more commonly used as it is noncontact, which has been a dominant format in all three types of systems (**Table 2**), except that Sun et al. [30] used a CMOS camera. CCD and CMOS cameras allow only single wavelength operation, but an imaging spectrograph has been used in HLBI systems to provide spectral and spatial information on a single image (**Figure 6**). Filters were also used in MLBI system to enable the image acquisition at specific wavelength [33].

3.2.3. Applications

An overview of SRRS to measure the firmness of fruits and vegetables is given in **Table 2**. The studies show that SRRS achieves similar performance compared with NIRS. The correlations with penetrometer firmness are often in the range of $r = 0.8 - 0.9$. It is not clear which type or instrument format of SRRS is more advantageous. Most studies evaluated the potential of SRRS systems for firmness measurements on static fruit and have not considered the practical challenges of applying SRRS to online situations. Unlike NIRS, there have been no commercially available sensors based on SRRS. All the studies listed in **Table 2** are laboratory systems specifically constructed for measuring stationary fruits. Lu and Peng [7] developed a real-time LLBI system for measuring the firmness of apples on a belt conveyor and achieved a correlation of $r = 0.86$. They claimed that the LLBI system could be integrated into existing grader lines without significant modification. However, their measurements were taken when the conveyor speed was only two fruit per second which is well below the maximum speed of a modern grader. Also, the fruit was manually positioned so that the scattering images could be captured from the equatorial areas of the fruit. The authors suggested the lasers and CCD camera should allow faster acquisition of the scattering images, but the algorithm for processing the images was the bottleneck. Overall, fruit orientation and data processing speed are the main challenges for applying SRRS in online systems.

4. Conclusion

For the main two optical techniques discussed here, NIRS and SRRS, there have been prior studies showing correlations with penetrometer firmness as high as $r = 0.8 - 0.9$. Both techniques can come in many instrument formats, so it is hard to judge from the literature which instrument is more advantageous. A direct comparison of the NIRS and SRRS methods has not been performed on the exact same fruit samples commonly. Sun et al. [30] compared an

interactance mode NIRS system with an LLBI system using "Royal Gala" apples. The two systems had similar correlations with penetrometer firmness of about $r = 0.9$. By contrast, a comparison of a reflectance mode NIRS system and an MLBI system using "Red Delicious" and "Golden Delicious" was conducted by Lu and Peng [40]. Their MLBI system outperformed NIRS system with $r = 0.82$ and 0.81 for two apple cultivars, versus $r = 0.5$ and 0.48 from the NIRS system.

It has been suggested $r = 0.94$ ($r^2 = 0.89$) be considered as a minimum for any useful sorting/grading purposes [41]. Although sometimes very close to that mark, the correlations reported here and in most previous studies are lower. Moreover, NIRS sensors are likely to perform worse across grader lines and seasons because of the low robustness of the calibration models. These may explain why there are no optical sensors for firmness measurements yet commercially available. For SRRS, another concern is the feasibility of online applications; most studies discussed here are bespoke laboratory systems for measuring static fruits. Fruit speed and orientation are normally not a problem for NIRS but might be an issue for the online application of SRRS.

NIRS is a relatively mature technique for quality grading of fruits and vegetables, though not commonly used for firmness. SRRS might well be a better method for firmness, being more robust in practice as it is more directly linked to the optical scattering properties that are presumed to be directly affected by changes in texture properties. However, the SRRS systems will have to be improved and demonstrate better performance than has been achieved to date before they can be considered for commercial implementation. We recommend further research across a wider variety of fruits in the future, and feasibility studies to assess the potential of SRRS for online applications.

Author details

Jason Sun[1,2]*, Rainer Künnemeyer[1,2] and Andrew McGlone[3]

*Address all correspondence to: zhesun89@gmail.com

1 School of Engineering, University of Waikato, Hamilton, New Zealand

2 Dodd Walls Centre for Photonic and Quantum Technologies, New Zealand

3 The New Zealand Institute for Plant & Food Research, Hamilton, New Zealand

References

[1] García-Ramos FJ, Valero C, Homer I, Ortiz-Cañavate J, Ruiz-Altisent M. Non-destructive fruit firmness sensors: A review. Spanish Journal of Agricultural Research. 2005;**3**(1):61-73

[2] Abbott JA. Quality measurement of fruits and vegetables. Postharvest Biology and Technology. 1999;**15**(3):207-225

[3] De Ketelaere B, Howarth MS, Crezee L, Lammertyn J, Viaene K, Bulens I, De Baerdemaeker J. Postharvest firmness changes as measured by acoustic and low-mass impact devices: A comparison of techniques. Postharvest Biology and Technology. 2006;**41**(3):275-284

[4] Ruiz-Altisent M, Ruiz-Garcia L, Moreda GP, Lu R, Hernandez-Sanchez N, Correa EC, Diezma B, Nicolaï B, García-Ramos J. Sensors for product characterization and quality of specialty crops—A review. Computers and Electronics in Agriculture. 2010;**74**(2):176-194

[5] Steinmetz V, Crochon M, Bellon Maurel V, Garcia Fernandez JL, Barreiro Elorza P, Verstreken L. Sensors for fruit firmness assessment: Comparison and fusion. Journal of Agricultural Engineering Research. 1996;**64**(1):15-27

[6] Hitchman S, van Wijk K, Davidson Z. Monitoring attenuation and the elastic properties of an apple with laser ultrasound. Postharvest Biology and Technology. 2016;**121**:71-77

[7] Lu R, Peng Y. Development of a multispectral imaging prototype for real-time detection of apple fruit firmness. Optical Engineering. 2007;**46**(12):123201

[8] Penchaiya P, Bobelyn E, Verlinden BE, Nicolaï BM, Saeys W. Non-destructive measurement of firmness and soluble solids content in bell pepper using NIR spectroscopy. Journal of Food Engineering. 2009;**94**(3-4):267-273

[9] Nicolaï BM, Verlinden BE, Desmet M, Saevels S, Saeys W, Theron K, Cubeddu R, Pifferi A, Torricelli A. Time-resolved and continuous wave NIR reflectance spectroscopy to predict soluble solids content and firmness of pear. Postharvest Biology and Technology. 2008; **47**(1):68-74

[10] Gómez AH, He Y, Pereira AG. Non-destructive measurement of acidity, soluble solids and firmness of satsuma mandarin using Vis/NIR-spectroscopy techniques. Journal of Food Engineering. 2006;**77**(2):313-319

[11] Mollazade K, Omid M, Tab FA, Mohtasebi SS. Principles and applications of light backscattering imaging in quality evaluation of agro-food products: A review. Food and Bioprocess Technology. 2012;**5**(5):1465-1485

[12] Adebayo SE, Hashim N, Abdan K, Hanafi M. Application and potential of backscattering imaging techniques in agricultural and food processing – A review. Journal of Food Engineering. 2016;**169**:155-164

[13] Xie L, Wang A, Xu H, Fu X, Ying Y. Applications of near-infrared systems for quality evaluation of fruits: A review. ASABE. 2016;**59**(2):399-419

[14] Cen H, Lu R, Mendoza F, Beaudry RM. Relationship of the optical absorption and scattering properties with mechanical and structural properties of apple tissue. Postharvest Biology and Technology. 2013;**85**:30-38

[15] Rowe PI, Künnemeyer R, McGlone A, Talele S, Martinsen P, Seelye R. Relationship between tissue firmness and optical properties of Royal Gala apples from 400 to 1050 nm. Postharvest Biology and Technology. 2014;**94**:89-96

[16] Tomer N, McGlone A, Künnemeyer R. Validated simulations of diffuse optical transmission measurements on produce. Computers and Electronics in Agriculture. 2017;**134**:94-101

[17] Costa AG, Pinto FA, Braga RA, Motoike SY, Gracia L. Relationship between biospeckle laser technique and firmness of *Acrocomia aculeata* fruits. Revista Brasileira de Engenharia Agrícola e Ambiental. 2017;**21**(1):68-73

[18] Skic A, Szymańska-Chargot M, Kruk B, Chylińska M, Pieczywek PM, Kurenda A, Zdunek A, Rutkowski KP. Determination of the optimum harvest window for apples using the non-destructive biospeckle method. Sensors. 2016;**16**(5):661

[19] Peña-Gomar M, Arroyo-Correa G, Aranda J, editors. Characterization of Firmness Index for Mango Fruit by Laser Reflectometry around the Critical Angle. XIth International Congress and Exposition; USA: Society for Experimental Mechanics Inc;2008

[20] Cen H. Hyperspectral Imaging-Based Spatially-Resolved Technique for Accurate Measurement of the Optical Properties of Horticultral Products. Michigan, USA: Michigan State University; 2011

[21] Nicolaï BM, Beullens K, Bobelyn E, Peirs A, Saeys W, Theron KI, Lammertyn J. Nondestructive measurement of fruit and vegetable quality by means of NIR spectroscopy: A review. Postharvest Biology and Technology. 2007;**46**(2):99-118

[22] Fraser DG, Künnemeyer R, McGlone VA, Jordan RB. Near infra-red (NIR) light penetration into an apple. Postharvest Biology and Technology. 2001;**22**(3):191-195

[23] Walsh K. Nondestrutive assessment of fruit quality. In: Wills RB, Golding J, editors. Advances in Postharvest Fruit and Vegetable Technology. USA: CRC Press; 2015. pp. 39-64

[24] Schaare PN, Fraser DG. Comparison of reflectance, interactance and transmission modes of visible-near infrared spectroscopy for measuring internal properties of kiwifruit (*Actinidia chinensis*). Postharvest Biology and Technology. 2000;**20**(2):175-184

[25] McGlone VA, Jordan RB, Martinsen PJ. Vis/NIR estimation at harvest of pre- and post-storage quality indices for Royal Gala apple. Postharvest Biology and Technology. 2002;**25**(2):135-144

[26] Park B, Abbott JA, Lee KJ, Choi CH, Choi KH. Near-infrared diffuse reflectance for quantitative and qualitative measurement of soluble solids and firmness of delicious and gala apples. Transactions of the ASAE. 2003;**46**(6):1721-1731

[27] Lu R. Predicting firmness and sugar content of sweet cherries using near-infrared diffuse reflectance spectroscopy. Transactions-American Society of Agricultural Engineers. 2001;**44**(5):1265-1274

[28] Mollazade K, Omid M, Akhlaghian Tab F, Kalaj YR, Mohtasebi SS, Zude M. Analysis of texture-based features for predicting mechanical properties of horticultural products by laser light backscattering imaging. Computers and Electronics in Agriculture. 2013;**98**:34-45

[29] Peng Y, Lu R. Improving apple fruit firmness predictions by effective correction of multispectral scattering images. Postharvest Biology and Technology. 2006;**41**(3):266-274

[30] Sun J, Künnemeyer R, McGlone A, Rowe P. Multispectral scattering imaging and NIR interactance for apple firmness predictions. Postharvest Biology and Technology. 2016; **119**:58-68

[31] Cen H, Lu R, Dolan K. Optimization of inverse algorithm for estimating the optical properties of biological materials using spatially-resolved diffuse reflectance. Inverse Problems in Science and Engineering. 2010;**18**(6):853-872

[32] Peng Y, Lu R. Analysis of spatially resolved hyperspectral scattering images for assessing apple fruit firmness and soluble solids content. Postharvest Biology and Technology. 2008;**48**(1):52-62

[33] Lu R. Multispectral imaging for predicting firmness and soluble solids content of apple fruit. Postharvest Biology and Technology. 2003;**31**(2):147-157

[34] Qing Z, Ji B, Zude M. Non-destructive analyses of apple quality parameters by means of laser-induced light backscattering imaging. Postharvest Biology and Technology. 2008;**48**(2):215-222

[35] Van Beers R, Aernouts B, Gutiérrez LL, Erkinbaev C, Rutten K, Schenk A, Nicolaï B, Saeys W. Optimal illumination-detection distance and detector size for predicting braeburn apple maturity from Vis/NIR laser reflectance measurements. Food and Bioprocess Technology. 2015; **8**(10):2123-2136

[36] Lu R, Peng Y. Hyperspectral scattering for assessing peach fruit firmness. Biosystems Engineering. 2006;**93**(2):161-171

[37] Mendoza F, Lu R, Ariana D, Cen H, Bailey B. Integrated spectral and image analysis of hyperspectral scattering data for prediction of apple fruit firmness and soluble solids content. Postharvest Biology and Technology. 2011;**62**(2):149-160

[38] Nguyen Do Trong N, Erkinbaev C, Tsuta M, De Baerdemaeker J, Nicolaï B, Saeys W. Spatially resolved diffuse reflectance in the visible and near-infrared wavelength range for non-destructive quality assessment of braeburn apples. Postharvest Biology and Technology. 2014;**91**:39-48

[39] Noh HK, Lu R. Hyperspectral laser-induced fluorescence imaging for assessing apple fruit quality. Postharvest Biology and Technology. 2007;**43**(2):193-201

[40] Lu R, Peng Y. Comparison of multispectral scattering and Visible/NIR spectroscopy for predicting apple fruit firmness. Information and Technology for Sustainable Fruit and Vegetable Production, (FRUTIC). 2005;**5**:493-502

[41] McGlone VA, Kawano S. Firmness, dry-matter and soluble-solids assessment of postharvest kiwifruit by NIR spectroscopy. Postharvest Biology and Technology. 1998;**13**(2):131-141

INTECH

Chapter 3

Optical Methods for Detecting Internal Disorders of Fresh Produce: a Review

3.1 Introduction

The internal disorders in fresh produce are very damaging to the reputation of both producers and retailers (Figure 1), and they are difficult to detect by manual inspections as often no symptoms appear externally. Sampling methods that destructively evaluate sample produce by cutting them open are commonly used (Taylor, 2012), but there is a great need to non-destructively examine produce individually, to reject all the defective ones so only defect-free produce is delivered to the consumer.

Using optical techniques to detect small and localised defects of fresh produce is a fairly new approach in horticulture. Near-infrared spectroscopy (NIRS) is routinely used for internal defects if the defect is large and/or generalised in the tissue. However, it becomes less sensitive and more problematic as the defect becomes smaller and particularly if the defect is localised to certain regions. Such is the case for many types of internal rot in produce. With onions, for example, rotten tissue is often localised to the stem end or lies discretely along individual layers. A spatially resolved optical technique, one that can non-invasively examine different sectional volumes of a body, may be the solution. This chapter is devoted to a review of optical spectroscopy and imaging techniques for non-destructively detecting small and localised defect. The emphasis is placed on the imaging techniques particularly diffuse optical tomography (DOT).

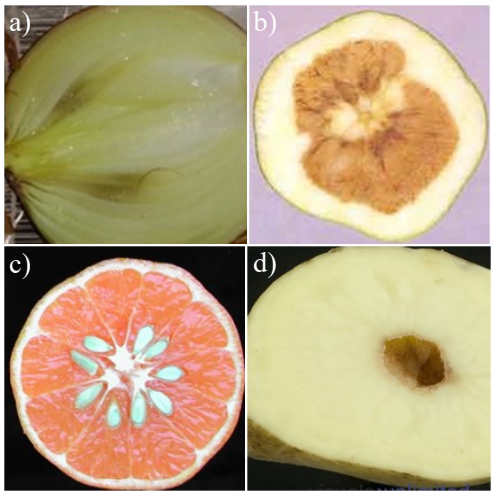

Figure 1. Examples of internal fruit disorders: (a) rots in onion, (b) brown heart of apple, (c) seeds of mandarin orange and (d) hollow heart of potato (Bermejo et al., 2011; Pierson et al., 1971).

3.2 Near-infrared spectroscopy

NIRS is a popular optical technique for quality assessment of fresh produce. The details of the NIRS technique have been summarised in the previous section of the literature review. There are studies on assessing the transmittance mode for different types of disorders in produce (Table 1). The high water content of fresh produce makes it difficult for the light to pass through intact produce in the long wavelength near infrared (LW-NIR) range of 1100 nm to 2500 nm due to the overwhelming presence of strong water absorbance in that range. Hence all the studies summarised in Table 1 used wavelength ranges lower than 1100 nm. There are a number of classification algorithms applied in these studies. Some use discriminate analysis such as Mahalanobis distance (MD) and canonical discriminant analysis (CDA) to segregate the defective produce. Others used regression analysis such as multiple linear regression (MLR) and partial least squares (PLS) to predict the degree or the volume of defectiveness.

NIRS transmission has been implemented on grader line for detecting internal defects. However, NIRS requires frequent model calibrations to maintain good performance (Nicolaï et al., 2007). NIRS systems typically illuminate a large area and detect at only a single spot on the sample, so not providing much spatial information (Ariana and Lu, 2010b; Martinsen and Schaare, 1998) and hence are not sensitive to small and localised defects (Kuroki et al., 2017).

Table 1. Studies using transmittance mode of NIRS for internal disorder detection.

Defect	Species	Spectral range (nm)	Classification algorithm	Reference
brown heart	apple	697-861	MLR and PLS	(Clark et al., 2003)
		650-950	PLS	(McGlone et al., 2005)
	pear	651–1282	MD	(Han et al., 2006)
		400-1028	DA	(Fu et al., 2007)
internal rot	onion	650-950	PLS	(Kuroki et al., 2017)
translucent flesh disorder	mangosteen	640-980	CDA	(Teerachaichayut et al., 2007)
storage disorder	kiwifruit	300 – 1140	CDA	(Clark et al., 2004)

3.3 Hyperspectral imaging

Hyperspectral imaging (HSI) has potential to improve the sensitivity of sensor systems by combining spectroscopy and imaging. The spectral information in spatial details is expected to make the sensor systems more effective for detecting disorders occurring locally in the sample (Pu et al., 2015). Most applications of HSI

use reflectance mode to detect external quality characteristics such as external defects (Wu and Sun, 2013) but this mode is generally not suitable for internal defects (Ariana and Lu, 2010b). In recent years, several studies have been conducted to assess the feasibility of using HSI transmittance mode for internal defect in pickling cucumbers. Ariana and Lu (2010b) developed an online system with the light illumination underneath the conveyor belt with the transmitted light detected by a hyperspectral camera mounted above. They achieved defect classification accuracy of 86%. However, to achieve the operating speed of commercial graders, scanning must be compromised spectrally and/or spatially as acquiring and/or analysing large-scale hyperspectral images is computationally intensive and time consuming. So hyperspectral imaging studies are often carried out as a precursor to the design of a faster multispectral imaging system using 3-4 wavebands for real-time applications (Ariana and Lu, 2010a). Cen et al. (2014) identified a ratio of 887/837 nm could be applied for fast real-time internal defect detection of pickling cucumbers. Overall, with further development, especially the rapid evolution of sensor and computer technologies, HSI in transmittance mode will be a promising technique for detecting internal defect. However, hyperspectral cameras are currently expensive and thus are not suitable for developing a low-cost system, making it less desirable for the industry to adopt the HSI technique. Another concern is that it will probably be difficult for hyperspectral cameras to obtain enough signal in the transmittance mode when applied on larger and/or thick skinned produce than cucumbers, such as apples and onions.

3.4 Diffuse optical tomography

Medical imaging techniques, such as MRI (Clark and Burmeister, 1999; Lammertyn et al., 2003) and X-ray (Lammertyn et al., 2003; van Dael et al., 2016), have been used on produce to detect spatially distributed internal disorders. Table 2 summarises the characteristics of four medical imaging techniques. All these techniques are powerful and have certain advantages, but they suffer from drawbacks which limit their use as continuous, non-contact, non-invasive, portable and low cost quality monitors. With the aim to develop sensors on a high speed grader machine, speed becomes another important factor.

MRI could provide the best imaging quality for the internal evaluation, but MRI is not practical for routine quality testing as this equipment is expensive, slow and difficult to operate (Choi et al., 2006). X-ray can penetrate through most

horticultural products. Studies have shown that it is particular useful for detecting various types of internal defects or foreign objects such as watercore and internal browning in apple (Ruiz-Altisent et al., 2010). However, it uses ionizing radiation and is potentially damaging to the fruit. X-ray systems for sorting potatoes for internal cavities exist but are slow and relatively expensive, and are therefore not regularly used in industry. Ultrasound is entirely safe, but it requires direct contact between the ultrasonic transducers and the biological tissue, and for medical applications its effectiveness depends on the ability of the technician (Yates, 2005).

Table 2. Comparison of various medical imaging modalities (Wang and Wu, 2007).

Characteristics	X-ray Imaging	Ultrasound	MRI	Optical Imaging
Soft-tissue contrast	Poor	Good	Excellent	Excellent
Spatial resolution	Excellent	Good	Good	Mixed[1]
Maximum imaging depth	None	Good	Excellent	Good
Nonionizing radiation	No	Yes	Yes	Yes
Data acquisition	Fast	Fast	Slow	Fast
Cost	Low	Low	High	Low
Non-contact	No	Yes	No	No
[1]High in ballistic imaging and photoacoustic tomography; low in diffuse optical tomography.				

Optical imaging techniques have been mostly developed in the medical field for applications such as disease diagnosis and treatment. They use visible, infrared light to look inside of the body. The advantages to use them in fresh produce assessment are (Wang and Wu, 2007):

- Non-invasive and non-ionizing
- Portable, low equipment cost
- Optical spectroscopy permits simultaneous detection of multiple contrast agents, and different properties of the tissue
- Potential to operate at high speed

Common optical imaging techniques are diffuse optical tomography (DOT), optical coherence tomography (OCT) and photoacoustic tomography (PAT). Diffuse optical tomography (DOT) stands out as a good candidate for detecting spatially distributed internal disorders as it allows light to penetrate deeper into the fruit and can potentially operate at the required speed with fast electronics and image reconstruction algorithm.

Diffuse Optical Tomography (DOT) refers to the optical imaging of biological tissue in the diffusive regime, which is expected to provide physiological information inside thick tissues. It uses NIR light to probe biomedical tissue, which is also referred to as functional near-infrared spectroscopy (fNIR or fNIRS) and near-infrared optical tomography (NIROT); there are also other names too, such as photon migration tomography (PMT), medical optical tomography (MOT), and optical tomography (OT), to name a few. There have been very few studies that have investigated DOT for agricultural use. Kemsley et al. (2008) developed a low-cost mechanical scanning based DOT system for measuring a potato phantom with a black rod as the perturbation (i.e., surrogate internal defect). Their measurements were conducted under highly simplified conditions, and the reconstruction matrix was generated for a single wavelength (689 nm). Nevertheless the results showed DOT has potential for internal defect detection. Numerical models were also used in some studies to simulate and validate the use of DOT for defect detection on potato (Nadhira et al., 2013) and carrot (Nadhira et al., 2015). However, to date there have been no studies assessing DOT on actual agricultural produce. Kemsley et al. (2008) also addressed various problems that will need to be overcome in practical applications on produce: irregular shape and sizes, and their associated 3D effects; skin and dirt on the surface; smaller contrasts between the optical properties of healthy and diseased tissue; variations in detection limits with position from the surface; and constraints on the time available for data acquisition and processing. The following subsections reviews DOT applications, particularly as practiced in the in the medical field.

The whole scheme of DOT can be described generally by two processes (Yamada and Okawa, 2014):

1. Measurement process: transmitted and/or reflected light from the object surface are measured at various positions on the surface. Then the incident position of the source light is scanned over the surface, and the received signal is repeated.
2. Inverse process: a search is made for the spatial distribution of the optical properties inside of medium, to produce agreement between the measured light and the calculated light using the light propagation model.

3.4.1 Measurement type

The three measurement types are illustrated in Figure 2. Each has distinct advantages and disadvantages, and the selection of the appropriate technology largely depends on the specific application. A number of promising hybrid systems have been developed that combine with other imaging modalities such as X-ray mammography, ultrasound, and MRI (Flexman, 2012).

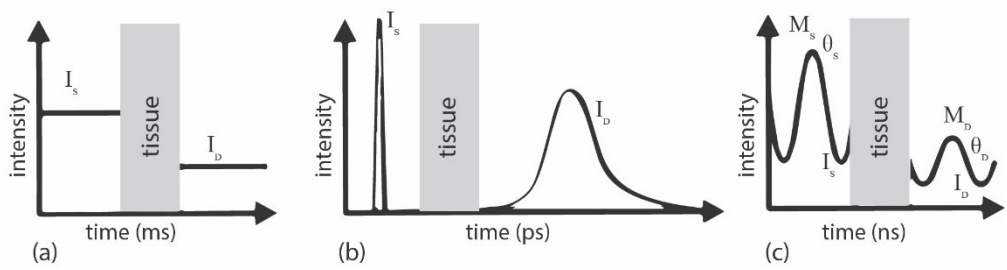

Figure 2. Three measurement types: (a) continuous wave (CW) measurement, (b) time domain (TD), and (c) frequency domain (FD). I_S and I_D are the source and detected light intensities, M_S and M_D are the AC component of the intensity modulated source and detected light respectively. There is also a phase delay between the source and detected light (Michaelsen, 2014; Yamada and Okawa, 2014).

Continuous wave

In some studies, the continuous wave (CW) measurement type is also called Direct Current or Steady State Domain. In CW systems, the light source continuously emits light into the tissue and the transmitted light intensities are measured. The absorption of light is related to the chemical composition, and scattering of light is more related to the physical structure. This approach is the fastest and the least expensive, but has the most limited capability of separating absorption from scattering in a heterogeneous medium. Harrach (2009) demonstrated that it suffices to restrict ourselves to piecewise constant diffusion and piecewise analytic absorption coefficients to obtain unique solution. Under this condition both parameters can simultaneously be determined from complete measurement data on an arbitrarily small part of the boundary. Jiang (2010) stated that in DOT, theoretically infinite absorption and reduced scattering coefficient solutions exist, but practically all solutions that significantly differ from the exact solution can be excluded with a prior knowledge on optical properties of tissue. Several CW systems are in widespread clinical use for brain monitoring. This type of measurement has the lowest image quality, but is potentially fast and cheap. This

method will be useful if the image resolution is high enough for detecting small internal disorders in produce.

Time domain

Among the three measurement types, time domain (TD) can provide highest resolution but is the slowest in data acquisition and the most expensive. Typically a pulsed laser (picoseconds) is used to transmit light signals through the tissue, and the detected pulsed light shows a prolonged temporal profile, due to the optical properties of the tissue. The ultrashort pulsed lasers and the time correlated single photon counting (TCPSC) technique used in the system add to the delay of data acquisition and the complexity of the system.

Frequency domain

Frequency domain (FD) and TD are mathematically related via the Fourier transformation, so that if modulated over a large range of frequencies, the same data in TD systems can be acquired in FD systems. Continuous wave is a zero-frequency special case of FD. FD systems are well suited to acquiring measurements quickly at relatively high detected intensities. However, when imaging across large (> 60 mm) thicknesses the light intensity is very low, possibly only a few photons per second, and sufficient light can only be detected using powerful pulsed laser sources and photon counting techniques such as those used in TD systems.

3.4.2 Optical geometries

All source-detector geometries can be divided into two categories: transmittance and reflectance (interactance is considered as reflectance in this case) (Figure 3). Yamada and Okawa (2014) reported that for small sized biological tissues, transmittance type is possible while reflectance measurement is necessary for objects with a radius larger than about 80 mm. For large objects, information from deeper regions cannot be obtained when the reflectance mode is used, or, if it is possible to get some information at depth, the quality of the reconstructed image becomes low. The maximum depth that can be reconstructed by the reflectance arrangement is thought to be less than 30 mm for the present technology (Yamada and Okawa, 2014).

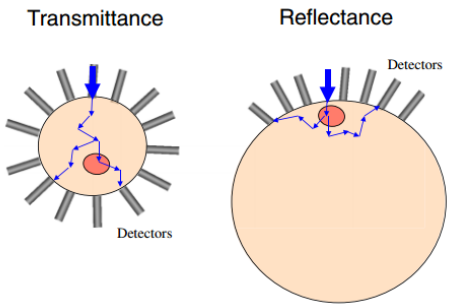

Figure 3. Arrangement of sources and detectors. Reflectance type measurement is necessary for objects with a radius larger than about 80 mm (Yamada and Okawa, 2014).

Pogue et al. (1999) compared six different DOT geometries using a finite element method (FEM) based algorithm, in which there are two possible arrangements for our applications on graders as shown in Figure 4. Transmittance should be possible as most fruits/vegetables are small enough for the received light to reach the detectable level (Nicolaï et al., 2007). Combining the transmittance and reflectance modes as shown in Figure 4b is perhaps a better system, as both the transmitted and reflected light signals are useful for detections. The number of sources and detectors can also be increased to achieve better sensitivity.

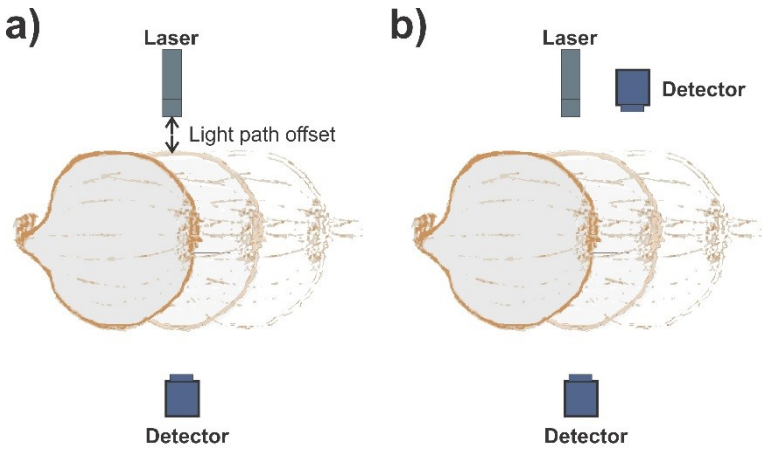

Figure 4. Schematic of two possible source-detector geometries for detecting internal rot in onions on a conveyer belt. The projection shadow geometry (a) is used in several optical mammography scanners, (b) combination of reflectance and transmittance arrangements.

3.4.3 Instruments

Wang (2009) compared the instruments and cost of the CW, FD and TD measurement types in Table 3. Avalanche photodiodes (APDs) are widely used in optical detection due to its high dynamic range. Photomultiplier tubes (PMTs) provide higher sensitivity, although with a limited dynamic range and higher cost. CCD cameras were also used and they have a wide dynamic range. It is not clear

which one is more useful, but maximizing the number of sampling points is clearly a priority for all systems. Using more wavelength is also proven to be useful to estimate the functional properties of breast tissue more effectively (Wang, 2009).

Table 3. Instruments and cost of the three approaches to detect tissue properties.

Systems	Light source	Detection	Parameters estimated	Cost per channel
CW	Lamp or laser Freq<10 MHz	PMTs APDs CCDs	Relative absorption effective attenuation	~$1K laser ~$1K detector
FD	Laser>50 MHz or Modulated lamp output	PMTs APDs	Absolute absorption & scattering coef.	~$1K laser ~$1-10K RF source ~$2K detector
TD	Pulsed laser t<300 ps	SPC-PMTs APDS Streak cameras	Absolute absorption & scattering coef	~$5K laser ~$5K detector

Continuous wave

Yamada and Okawa (2014) reviewed a number of CW systems. An example of such a system is the dynamic near-infrared optical tomography instrument developed at State University of New York (Schmitz et al., 2002). This system can be used to observe the dynamic temporal variations of vascular responses because the system can acquire data and image very quickly at a rate of about 2 Hz with a CCD-based fast detector and a fast image reconstruction algorithm. In this system, two wavelengths are provided by two laser diode. Each detector fibre bundle terminates on a single silicon photodiode.

Frequency-division multiplexing was used in a CW system designed at Massachusetts General Hospital to increase the number of CW measurements (Figure 5). 16 lasers operate at 690 nm, and the same number of lasers operates at 830 nm. The lasers are encoded with 32 frequencies uniformly between 6.4 and 12.6 kHz. The output of each APD is digitized by the ADC, and then the digitally encoded signal is decoded by the computer on the basis of the modulation frequencies to recover the remitted optical signal components originating from each source simultaneously. Since all the sources and detectors function concurrently, the data-acquisition rate is high. The system is well suited to observe rapid physiological phenomena (Wang and Wu, 2007).

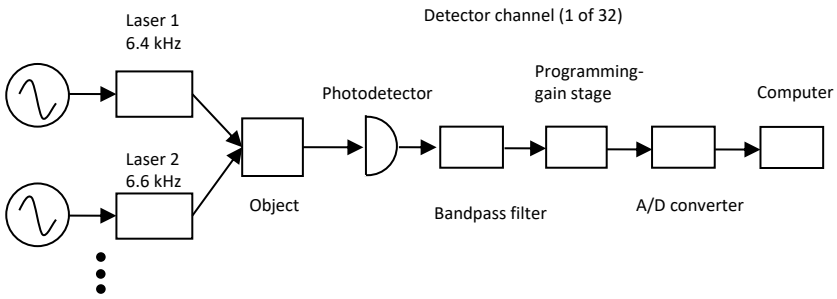

Figure 5. Schematic representation of the CW system at Massachusetts General Hospital (Siegel et al., 1999).

Flexman (2012) has designed a similar dynamic CW system using digital-based detection. The digital system uses multiple digital signal processing (DSP) chips arranged in a master-slave setup to maximize the processing throughout, reduce noise, and provide a system design that can be scaled to accommodate a variable number of detectors and wavelengths.

CW systems could be used for our applications due to its fast data acquisition and image reconstruction rate. Frequency-division would allow simultaneous measurements at multiple wavelengths to improve detection rates as the defective tissue in produce may not have a significant spectral difference at any single wavelength.

Time domain

TD systems developed for breast cancer detection typically take 3-5 minutes for data acquisition (Flexman, 2012). Temporal responses to an ultrashort laser pulse are measured around the scattering object. The responses can be resolved using a streak camera, which records the temporal profile of light intensity with a high time resolution (of about 10 ps), or a time-correlate single-photon counting system. The latter is the most commonly used due to its larger detection area, lower cost, etc. The disadvantage of TD systems is the slow data acquisition, which makes them impractical for high-speed produce grading.

Frequency domain

The FD systems originate from the phase shift method utilized for fluorescence lifetime measurement (Cen, 2011). In some studies, it is called frequency domain photon migration (FDPM) and diffuse photon density wave (DPDW). FD systems use an intensity-modulated (typically in the 100 MHz range) continuous wave light and measure the phase shift and light intensity through a scattering medium. Due

to the compact laser diodes and the well-developed radio frequency (RF) electronics, FD systems are much more robust and cheaper compared with TD systems. The most challenging issue for FD systems is to accurately detect the phase shift and amplitude, and eliminate the effect due to the instrument.

The accuracy of FD system is dependent on the phase measurements. Mei (2014) divided the phase detection schemes into three types: homodyne (Figure 6a), heterodyne (Figure 6b), and single sideband detection (Figure 6c). Both heterodyne and single sideband detection (SSB) down-convert the high frequency signal to low frequency using a frequency mixer, so that the phase difference can be easily detected by detectors such as zero-crossing phase detector, in-phase and quadrature (IQ) demodulator, and lock-in detector. The phase error can be used by employing an IQ demodulator. Some groups used CCD imaging by modulating an image intensifier with a reference signal to produce phase sensitive images (Roblyer et al., 2013).

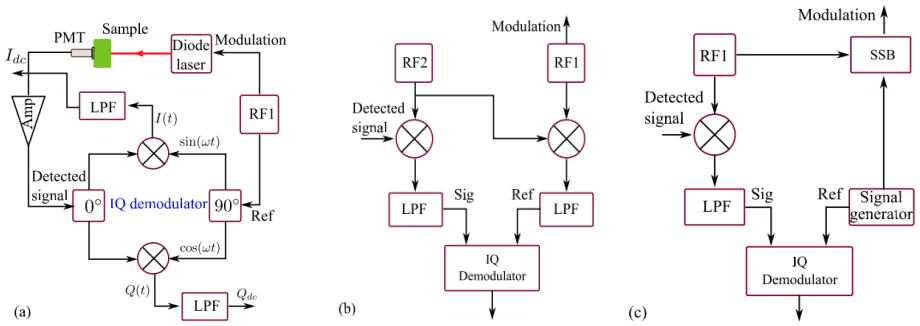

Figure 6. (a) Homodyne, (b) heterodyne, and (c) single sideband (SSB) detection schemes. Amp – amplifier, LPF – low pass filter, IQ – in phase and quadrature (Mei, 2014).

Wang and Wu (2007) presented a single-channel FD sensing system using heterodyne detection (Figure 7). A lock-in detector is used to measure the phase shift between signal and reference signal. Mei et al. (2012) designed a similar system using homodyne detection to detect the optical properties of gas-filled porous media.

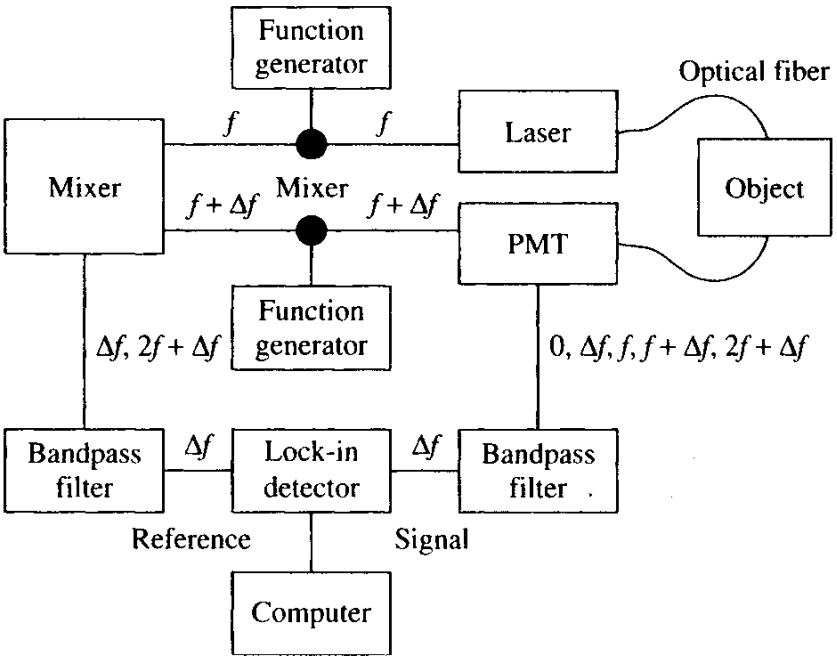

Figure 7. Schematic representation of a single-channel frequency-domain sensing system (Wang and Wu, 2007).

Dartmouth College has been developing FD imaging systems for clinical use. Pogue et al. (1997) have presented a prototype FD system for breast cancer detection. It consists of four parts: light delivery, detection array, fibre optics, control interface and electronics (Figure 8). The NIRFast software package has been developed at Dartmouth to implement the FEM method for the image reconstruction in FD (Dehghani et al., 2008).

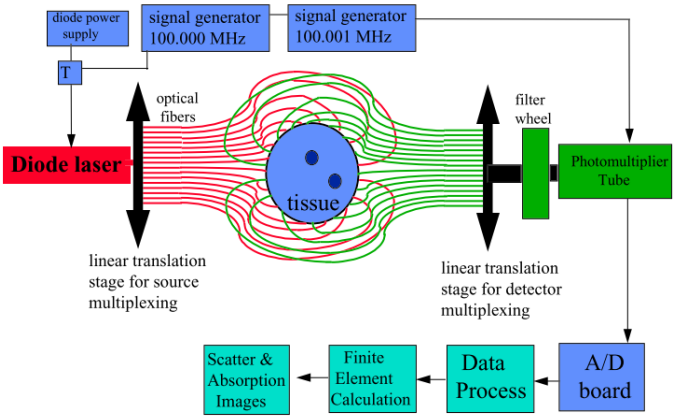

Figure 8. Schematic of the Dartmouth College FD imaging system (Pogue et al., 1997).

A recent study (Roblyer et al., 2013) has proposed a direct digital sampling method in homodyne detection, which reduces the complexity of using analogue electronics. The system includes a 1 gigasample per second (GSPS), 14-bit digital to analogue converter (DAC) to output sinusoidally modulated signals and 3.6 GSPS analogue

to digital converter (ADC) to measure the reference signal and the output of the optical detector. Although it simplifies the design of FD systems, the cost is a concern, requiring a $3000 ADC evaluation board and a $1000 DAC.

The challenge of applying FD technique on produce is the phase measurement. Phase shifts are induced in the electronic equipment, the optical delivery fibres and in the path length offset in air between the sample and the fibres. The resulting total phase shift must be calibrated to retrieve the absolute phase offsets due to the internal light transmission in the sample. This calibration becomes a very challenging issue for on-line grader applications as the measurements are not static, unlike most other FD systems. Every recorded phase shift needs subsequent calibration to take account of the phase offset caused by differences in the path length offset in air, which will be rapidly changing for fast moving samples (10 samples/second). Mei et al. (2014) raised another issue of phase-amplitude crosstalk, i.e., different light intensities inducing different phase shifts

3.4.4 Image reconstruction algorithm

Image reconstruction in DOT is generally categorized as an inverse problem (Figure 9). One of the limitations in DOT development has been that the rapid advances in technological instrumentation have eclipsed the development of accurate image reconstruction algorithms for diffuse tomography (Pogue et al., 1999). Arridge and Schotland (2009) have given a very comprehensive review of mathematical structure and computational approaches to the forward and inverse problems. The inverse process in image reconstruction in DOT is generally classified into two approaches (Dehghani et al., 2009).

1. Linear one-step inversion: This approach provides a means of imaging that is sensitive to changes in optical properties. The advantage is the high computation speed without iteration. This method requires a difference experiment that measures the data as the difference between two states. Care must be taken such that the imaged changes are relatively small, and this method is only suitable for providing qualitative images of measured changes, rather than absolute quantitative changes.
2. Nonlinear iterative inversion: This approach is described by steps as shown in Figure 9. The updating step is the key, and two standard approaches are used: Newton-type and gradient based.

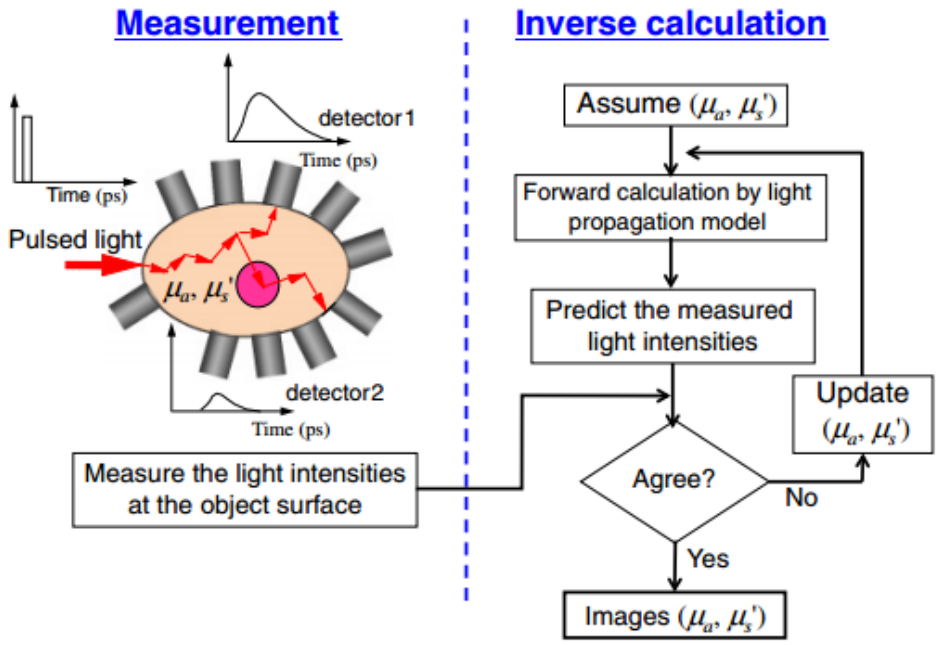

Figure 9. Nonlinear inversion scheme of DOT image reconstruction (Yamada and Okawa, 2014).

3.4.5 Evaluation of different DOT approaches

DOT is a promising technique to detect the internal disorders in clinical area, which is expected to be useful for detecting internal defects of horticultural products. A comparison of the three measurement systems is shown in Table 4. TD systems have complicated instrumentation and slow data acquisition, making it impractical use on the high speed grading machines. CW has the advantage of fast data acquisition and simple setup. However FD is generating more interest as the instrumentation can be largely simplified using digital scheme, and provides better detection capability than CW at a similar speed.

Table 4. Comparison of different measurement types of DOT (Hielscher et al., 2002; Ntziachristos et al., 2005)

Systems	Resolution	Depth	Signal to Noise Ratio	Data Acquisition speed	Separation of absorption and scattering
CW	1 mm	< 50 mm	High	High	No
FD	0.5-1 mm	< 30 mm	Medium	Medium	Yes
TD	0.5–1 mm	< 30 mm	Medium	Low	Yes

Direct and full use of these methods may not be required for two reasons: firstly, the target sensor is aimed at finding the fruit/vegetable with internal defects, but it is not necessarily required to locate the defects, so the system may work without delivering full imaging/tomography capability; secondly, all the DOT systems operate in a static condition, while our design needs to be integrated into the

automated grading machine to detect the fast moving fruit/vegetable, so considerable amount of modifications must be made to the existing DOT systems.

Therefore, our research is to design a spatially resolved spectroscopy technique, so the system can resolve the presence of small and spatially localised defects in fresh produce. The design will still be similar to the existing DOT approaches, but will not require the full and precise reconstruction of the image. A simpler and fast operating system can then be potentially achieved. In the meantime, the potential of generating the image of the inside of fruit/vegetables will still be investigated, but it has to satisfy the speed requirement.

3.5 Discussion and conclusion

NIRS systems are capable of detecting internal defects, but most previous studies have targeted defects that are generalised in the sample tissue and have not specifically focused on defects that are small and spatially distributed. With recent improvements on spectrometry hardware, light sources and chemometric tools, conventional NIRS techniques can be further enhanced but will not provide high spatial resolution. One future work is to improve NIRS, specifically for the detection of small and localised defects, such as small neck rots in onions and vascular browning in apples.

HSI systems integrate spectroscopy and imaging techniques and are thus expected to be more effective for detecting internal defects. Using discrete wavebands could significantly increase the operating speed, but still the current high cost of hyperspectral cameras remains a prohibitive issue for horticultural applications. Moreover, the hyperspectral camera allows the spatial scanning from the detector side only, but the typically large illumination area on the opposite side of a sample probably limits the system to achieve higher spatial resolution due to the highly diffusive nature of light transport in biological tissues.

The DOT technique is not directly applicable to high-speed graders, high speed and moving samples being the two main obstacles for such systems. A simplified version of DOT, with suitable hardware and fast measurement algorithms, may still work. Furthermore, it will probably have a better potential than HSI for being low-cost and more sensitive, because the entire volume of the sample could be examined with inexpensive laser diodes and photodiodes. CW and FD have the potential to operate at the required speed, but phase detection for FD will be very challenging.

FD is generating more interest as the phase information can be used to separate the absorption and scattering properties, which will significantly improve the detection of various parameters of interest. Some studies suggested with some prior information about the typical range of the optical properties (Jiang, 2010), CW system can also simultaneously separate absorption and scattering. Compared to other optical imaging techniques, DOT has a relatively low spatial resolution. The resolution may be further reduced when applied on the commercial graders to accommodate the speed and fast moving samples. Assessment of the limitations of an inexpensive DOT schema in terms of the spatial resolution and measurement speed, should be carried out.

References

Ariana, D.P., Lu, R., 2010a. CHAPTER 14 - Hyperspectral Imaging for Defect Detection of Pickling Cucumbers A2 - Sun, Da-Wen, Hyperspectral Imaging for Food Quality Analysis and Control. Academic Press, San Diego, pp. 431-447.

Ariana, D.P., Lu, R., 2010b. Evaluation of internal defect and surface color of whole pickles using hyperspectral imaging. Journal of Food Engineering 96, 583-590.

Arridge, S., Schotland, J., 2009. Optical tomography: Forward and inverse problems. Inverse Problems 25.

Bermejo, A., Pardo, J., Cano, A., 2011. Influence of gamma irradiation on seedless citrus production: pollen germination and fruit quality. Food and Nutrition Sciences 2, 169-180.

Cen, H., 2011. Hyperspectral imaging-based spatially-resolved technique for accurate measurement of the optical properties of horticultural products, Biosystems Engineering. Michigan State University.

Cen, H., Lu, R., Ariana, D.P., Mendoza, F., 2014. Hyperspectral Imaging-Based Classification and Wavebands Selection for Internal Defect Detection of Pickling Cucumbers. Food and Bioprocess Technology 7, 1689-1700.

Choi, K.-H., Lee, K.-J., Kim, G., 2006. Nondestructive quality evaluation technology for fruits and vegetables using near-infrared spectroscopy, International Seminar on Enhancing Export Competitiveness of Asian Fruits.

Clark, C.J., Burmeister, D.M., 1999. Magnetic Resonance Imaging of Browning Development inBraeburn'Apple during Controlled-atmosphere Storage under High CO2. HortScience 34, 915-919.

Clark, C.J., McGlone, V.A., De Silva, H.N., Manning, M.A., Burdon, J., Mowat, A.D., 2004. Prediction of storage disorders of kiwifruit (Actinidia chinensis) based on visible-NIR spectral characteristics at harvest. Postharvest Biology and Technology 32, 147-158.

Clark, C.J., McGlone, V.a., Jordan, R.B., 2003. Detection of Brownheart in 'Braeburn' apple by transmission NIR spectroscopy. Postharvest Biology and Technology 28, 87-96.

Dehghani, H., Eames, M.E., Yalavarthy, P.K., Davis, S.C., Srinivasan, S., Carpenter, C.M., Pogue, B.W., Paulsen, K.D., 2008. Near infrared optical tomography using NIRFAST: Algorithm for numerical model and image reconstruction. Communications in numerical methods in engineering 25, 711-732.

Dehghani, H., Srinivasan, S., Pogue, B.W., Gibson, A., 2009. Numerical modelling and image reconstruction in diffuse optical tomography. Philosophical Transactions of the Royal Society A: Mathematical, Physical and Engineering Sciences 367, 3073-3093.

Flexman, M., 2012. Dynamic digital optical tomography for cancer imaging and therapy monitoring. Columbia University, Ann Arbor, p. 325.

Fu, X., Ying, Y., Lu, H., Xu, H., 2007. Comparison of diffuse reflectance and transmission mode of visible-near infrared spectroscopy for detecting brown heart of pear. Journal of Food Engineering 83, 317-323.

Han, D., Tu, R., Lu, C., Liu, X., Wen, Z., 2006. Nondestructive detection of brown core in the Chinese pear 'Yali' by transmission visible–NIR spectroscopy. Food Control 17, 604-608.

Harrach, B., 2009. On uniqueness in diffuse optical tomography. Inverse Problems 25, 055010.

Hielscher, A., Bluestone, A., Abdoulaev, G., Klose, A., Lasker, J., Stewart, M., Netz, U., Beuthan, J., 2002. Near-infrared diffuse optical tomography. Disease markers 18, 313-337.

Jiang, H., 2010. Diffuse optical tomography: principles and applications. CRC press.

Kemsley, E.K., Tapp, H.S., Binns, R., Mackin, R.O., Peyton, A.J., 2008. Feasibility study of NIR diffuse optical tomography on agricultural produce. Postharvest biology and technology 48, 223-230.

Kuroki, S., Nishino, M., Nakano, S., Deguchi, Y., Itoh, H., 2017. Positioning in spectral measurement dominates estimation performance of internal rot in onion bulbs. Postharvest Biology and Technology 128, 18-23.

Lammertyn, J., Dresselaers, T., Van Hecke, P., Jancsók, P., Wevers, M., Nicolaï, B.M., 2003. MRI and x-ray CT study of spatial distribution of core breakdown in 'Conference' pears. Magnetic Resonance Imaging 21, 805-815.

Martinsen, P., Schaare, P., 1998. Measuring soluble solids distribution in kiwifruit using near-infrared imaging spectroscopy. Postharvest Biology and Technology 14, 271-281.

McGlone, V.A., Martinsen, P.J., Clark, C.J., Jordan, R.B., 2005. On-line detection of Brownheart in Braeburn apples using near infrared transmission measurements. Postharvest Biology and Technology 37, 142-151.

Mei, L., 2014. Light propagation and gas absorption studies in turbid media using tunable diode laser techniques, Department of Physics Lund Univeristy Sweden

Mei, L., Somesfalean, G., Svanberg, S., 2014. Light propagation in porous ceramics: Porosity and optical property studies using tunable diode laser spectroscopy. Applied Physics A 114, 393-400.

Mei, L., Svanberg, S., Somesfalean, G., 2012. Combined optical porosimetry and gas absorption spectroscopy in gas-filled porous media using diode-laser-based frequency domain photon migration. Optics express 20, 16942-16954.

Michaelsen, K., 2014. Combined digital breast tomosynthesis and near-infrared spectral tomography for breast lesion characterization. Dartmouth College Hanover, New Hampshire.

Nadhira, V., Juliastuti, E., Kurniadi, D., 2015. Image Reconstruction of Continuous Wave Domain Diffuse Optical Tomography for Quality Control on Carrot. International Journal of Tomography & Simulation™ 28, 60-68.

Nadhira, V., Kurniadi, D., Juliastuti, E., 2013. Feasibility study on image reconstruction of continuous wave domain diffuse optical tomography for quality control on seed potatoes, Instrumentation, Communications, Information Technology, and Biomedical Engineering (ICICI-BME), 2013 3rd International Conference on. IEEE, pp. 421-424.

Nicolaï, B.M., Beullens, K., Bobelyn, E., Peirs, A., Saeys, W., Theron, K.I., Lammertyn, J., 2007. Nondestructive measurement of fruit and vegetable quality by means of NIR spectroscopy: A review. Postharvest Biology and Technology 46, 99-118.

Ntziachristos, V., Ripoll, J., Wang, L.V., Weissleder, R., 2005. Looking and listening to light: the evolution of whole-body photonic imaging. Nature biotechnology 23, 313-320.

Pierson, C.F., Ceponis, M.J., McColloch, L.P., 1971. Market diseases of apples, pears, and quinces. U.S. Agricultural Research Service.

Pogue, B., McBride, T., Osterberg, U., Paulsen, K., 1999. Comparison of imaging geometries for diffuse optical tomography of tissue. Optics Express 4, 270-286.

Pogue, B., Testorf, M., McBride, T., Osterberg, U., Paulsen, K., 1997. Instrumentation and design of a frequency-domain diffuse optical tomography imager for breast cancer detection. Optics express 1, 391-403.

Pu, Y.-Y., Feng, Y.-Z., Sun, D.-W., 2015. Recent progress of hyperspectral imaging on quality and safety inspection of fruits and vegetables: A review. Comprehensive Reviews in Food Science and Food Safety 14, 176-188.

Roblyer, D., D O'Sullivan, T., Warren, R.V., Tromberg, B.J., 2013. Feasibility of direct digital sampling for diffuse optical frequency domain spectroscopy in tissue. Measurement Science and Technology 24, 045501.

Ruiz-Altisent, M., Ruiz-Garcia, L., Moreda, G.P., Lu, R., Hernandez-Sanchez, N., Correa, E.C., Diezma, B., Nicolaï, B., García-Ramos, J., 2010. Sensors for product characterization and quality of specialty crops—A review. Computers and Electronics in Agriculture 74, 176-194.

Schmitz, C.H., Löcker, M., Lasker, J.M., Hielscher, A.H., Barbour, R.L., 2002. Instrumentation for fast functional optical tomography. Review of Scientific Instruments 73, 429-439.

Siegel, A.M., Marota, J.J.A., Boas, D.A., 1999. Design and evaluation of a continuous-wave diffuse optical tomography system. Optics Express 4, 287-298.

Taylor, S., 2012. Postharvest handling: a systems approach. Academic Press.

Teerachaichayut, S., Kil, K.Y., Terdwongworakul, A., Thanapase, W., Nakanishi, Y., 2007. Non-destructive prediction of translucent flesh disorder in intact mangosteen by short wavelength near infrared spectroscopy. Postharvest Biology and Technology 43, 202-206.

van Dael, M., Lebotsa, S., Herremans, E., Verboven, P., Sijbers, J., Opara, U.L., Cronje, P.J., Nicolaï, B.M., 2016. A segmentation and classification algorithm for online detection of internal disorders in citrus using X-ray radiographs. Postharvest Biology and Technology 112, 205-214.

Wang, J., 2009. Broadband near-infrared tomography for breast cancer imaging, Physics and Astronomy. Dartmouth College, Hanover, New Hampshire.

Wang, L.V., Wu, H.-I., 2007. Biomedical optics :principles and imaging. Wiley, Hoboken, N.J.

Wu, D., Sun, D.-W., 2013. Advanced applications of hyperspectral imaging technology for food quality and safety analysis and assessment: A review — Part II: Applications. Innovative Food Science & Emerging Technologies 19, 15-28.

Yamada, Y., Okawa, S., 2014. Diffuse optical tomography: present status and its future. Optical Review 21, 185-205.

Yates, T.D., 2005. Time-resolved optical tomography for the detection and specification of breast disease. University of London.

Chapter 4

Multispectral Scattering Imaging and NIR Interactance for Apple Firmness Predictions

---

A journal paper

by

Jason Sun, Rainer Künnemeyer, Andrew McGlone and Philip Rowe

Published in

Postharvest Biology and Technology

I setup the multispectral imaging system with assistance from Philip Rowe, who initially designed the system. I conducted all the experimental work and prepared the initial draft manuscript. My supervisors provided guidance throughout the project and edited the manuscript, Andrew McGlone also carried out the PLS analysis.

Postharvest Biology and Technology 119 (2016) 58–68

Contents lists available at ScienceDirect

Postharvest Biology and Technology

journal homepage: www.elsevier.com/locate/postharvbio

Multispectral scattering imaging and NIR interactance for apple firmness predictions

Jason Sun[a,b,*], Rainer Künnemeyer[a], Andrew McGlone[b], Philip Rowe[c]

[a] School of Engineering, University of Waikato, Hamilton, New Zealand
[b] The New Zealand Institute for Plant and Food Research, Hamilton, New Zealand
[c] Accelerenz Limited, Hamilton, New Zealand

ARTICLE INFO

Article history:
Received 8 January 2016
Received in revised form 12 April 2016
Accepted 26 April 2016
Available online 10 May 2016

Keywords:
Multispectral scattering
Near-infrared spectroscopy
Spatially resolved reflectance spectroscopy
Fruit
Apples
Firmness

ABSTRACT

A multispectral imaging (MSI) system, using four discrete wavelengths (685, 850, 904 and 980 nm), has been developed and validated for making spatially resolved reflectance spectroscopy (SRRS) measurements. The primary aim was to evaluate the potential of MSI for high-speed firmness grading of apples. The MSI system validations were made using Intralipid solutions of known concentration and comparing the results against measurements made using a laboratory based inverse adding-doubling method (IAD). The results compared well for scattering properties with both the MSI and IAD measurements in reasonable agreement with known properties. For the absorption properties only the MSI measurements were close. Performance of the MSI system was then compared with a near-infrared spectroscopy (NIRS) system using 100 'Royal Gala' apples (*Malus domestica* Borkh.). The apples were measured non-destructively by both the MSI and NIRS systems. Cut apple surfaces were also examined by the MSI system and excised slices of apple tissue were measured using the IAD system. Actual apple firmness was measured by destructive penetrometer. The MSI data analysis involved use of both a phenomenological diffusion model and a heuristic modified Lorentzian model for describing the scattering images at each wavelength. The best MSI results of R = 0.87 and RMSECV = 7.17 N were obtained when the Lorentzian model parameters derived at each wavelength were combined using multiple linear regression (MLR). The NIRS system measurements were still a little better, with a best correlation on R = 0.90 and RMSECV = 6.99 N.

1. Introduction

Firmness is a primary concern to the apple industry, as it is a standard quality metric used for regulating fruit consignments in the supply chain. Firmness at harvest can indicate ripeness and/or storage potential, and for consumers it can indicate desirable textural properties such as crispness. The standard measurement technique is destructive, typically carried out using a penetrometer that creates a hole in the fruit and leaves the apple unsaleable. A fast and non-destructive alternative has been desired by industry practitioners for many decades. The main benefit would be the ability to grade and sort every individual fruit in terms of firmness. To date no commercially successful non-destructive system for apple firmness has been created.

Most prior research into non-destructive firmness measurement has focused on mechanical methods such as acoustic resonance, impact response and force-deformation (Abbott, 1999; De Ketelaere et al., 2006; Ruiz-Altisent et al., 2010; Steinmetz et al., 1996). More recently optical methods, particularly using the visible and short-wave near infrared range of wavelengths (400–1100 nm), have been increasingly studied (Nicolaï et al., 2007; Penchaiya et al., 2009; Subedi and Walsh, 2009). Optical methods have the attractive feature of being non-contact, a feature that distinguishes them from the mechanical methods. Modern high speed fruit grading systems run at speeds in excess of 10 fruit per second and non-contact methods will be advantageous in such circumstances.

In recent times two optical techniques have been investigated more commonly for fruit firmness measurement: near infrared spectroscopy (NIRS) and spatially resolved reflectance spectroscopy (SRRS). NIRS is widely used to determine fruit quality parameters, particularly compositional parameters such as soluble solids or dry matter content (Nicolaï et al., 2007; Ruiz-Altisent

* Corresponding author at: The New Zealand Institute for Plant & Food Research limited, Bisley Road, Hamilton 3214, New Zealand.
E-mail address: jason.sun@plantandfood.co.nz (J. Sun).

http://dx.doi.org/10.1016/j.postharvbio.2016.04.019
0925-5214/

et al., 2010). The NIRS method involves measurement of the apparent light absorbing power of a sample by measuring the spectral pattern of light transmitted through a representative portion of the flesh. The literature suggests that firmness may affect the apparent light absorbing power through chemical changes associated with cell wall degradation, physical changes in intercellular structure and/or indirectly through correlated pigment absorption changes such as a chlorophyll decrease on ripening (Rowe et al., 2014). Generally chemometric analysis methods are used to interpret the resulting absorbance spectra in terms of the parameters of interest. Attempts to use NIRS for fruit firmness prediction have met with varying degrees of success but some studies show good correlations as high as $R \sim 0.9$ (Lammertyn et al., 1998; McGlone et al., 2002a; Mendoza et al., 2014; Penchaiya et al., 2009).

In spatially resolved reflectance spectroscopy (SRRS) the spatial distribution of light intensity at the surface of a turbid sample is measured. The addition of spatial information enables light scattering and absorption properties to be segregated. Turbid biological materials, such as apples, scatter light strongly. The amount of scattering is influenced by flesh properties such as tissue density, cell composition, and extra- and intra-cellular structures that affect texture and firmness (Cen et al., 2013). Hence in segregating out the light scatter properties the SRRS method potentially provides a direct link to texture and firmness. SRRS has been studied by others for apple firmness prediction using both hyperspectral (Lu et al., 2009; Peng and Lu, 2008) and single or multispectral (Lu and Peng, 2007; Mollazade et al., 2013; Qing et al., 2008; Van Beers et al., 2015) systems, with the latter being more appropriate for high speed grading operations. Reported correlations of predicted with actual apple firmness have varied but typically are $R < 0.9$.

SRRS is more advantageous in theory, however there are no experimental studies comparing NIRS with SRRS in terms of fruit firmness assessment on the same samples under the same conditions. We present here the results of such a study using both NIRS and SRRS for determination of the firmness of 'Royal Gala' apples. 'Royal Gala' apples are a major apple cultivar exported out of NZ and are known to soften relatively rapidly at times and can be problematic in the supply chain in terms of firmness. Methods of sorting 'Royal Gala' apples for firmness and/or storage potential would be particularly valuable to the industry and success would likely open up opportunities for other cultivars too. The study involved development of a multispectral imaging system (MSI) suitable for SRRS measurement and comparison of results with those obtained using NIRS measurements. Additional measurements of the flesh optical properties were made on excised slices of apple tissue using the popular inverse adding-doubling method (IAD) (Prahl et al., 1993). The primary aim of the work was to validate, or otherwise, the potential of the MSI system for commercial firmness grading of apples.

2. Material and methods

2.1. Apple samples

Approximately 200 'Royal Gala' apples were harvested from an orchard in Havelock North, New Zealand, and then stored in a cool room (0 °C). Half of the apples were moved to a humidified chamber (~85% relative humidity, 20 °C; moisture loss rate of ~0.1% per day) and left to soften for up to 20 days to provide a wide distribution in firmness. Some apples were included directly from the cool room, after warming to 20 °C, to obtain the top range of firmness. A total of 100 apples, all with a diameter between 64.1 and 76.1 mm, was measured over 50 days. The penetrometer firmness of the apples ranged from 38.9 N to 90 N with a mean value of 62.8 N and a standard deviation of 13.9 N.

2.2. Multispectral imaging system

The MSI system (Fig. 1) consists of four lasers operating at different wavelengths which were chosen to provide relevant and

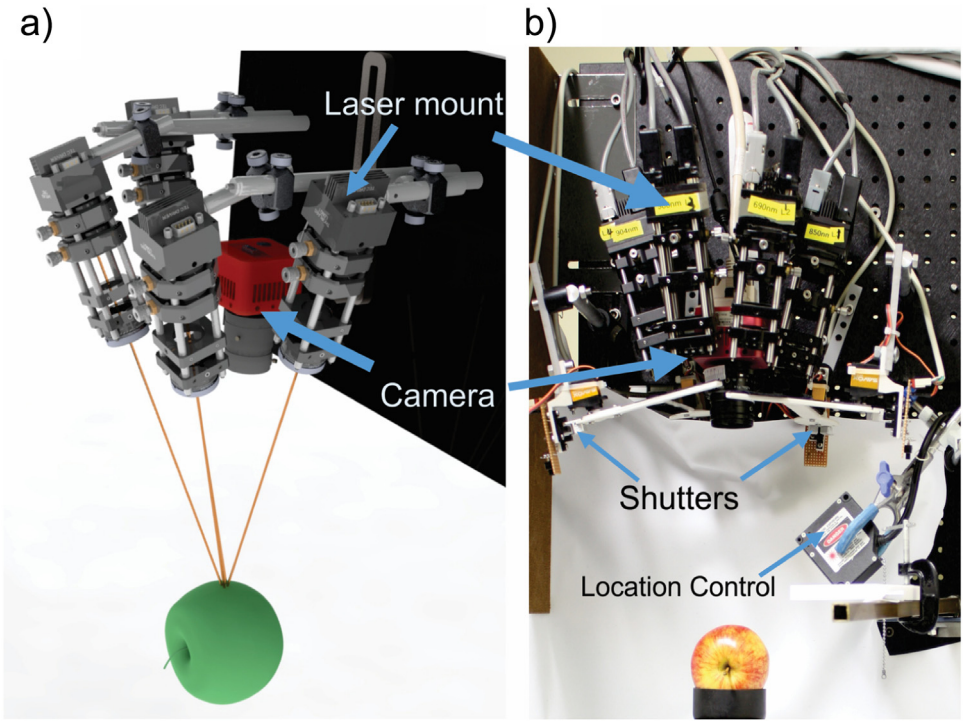

Fig. 1. (a) CAD model of the static MSI system. (b) Actual implementation configured with four lasers, each with electronically controlled shutter.

complementary information and aligned with those selected by others using MSI on apples (Lu, 2004; Noh and Lu, 2007; Peng and Lu, 2008). Two of the lasers, at 685 and 980 nm, are linked to the strong chlorophyll and water absorbance, respectively, that dominate light transport in apples (McGlone et al., 2002a). The 904 nm laser wavelength is linked to soluble solids content (McGlone and Kawano, 1998). At 850 nm apples have relatively low absorbance, suggesting it might best link to optical scattering changes, and the radiation is deeply penetrating (McGlone et al., 1997). Each laser was mounted in a laser diode mount (LDM21, Thorlabs, New Jersey,USA) and driven by a laser diode driver and controller (ITC102, Thorlabs, New Jersey, USA). The laser light intensity was adjusted so the scattering pattern was within the view and sensitivity of the camera.

The scattering images were captured by a high-performance CMOS camera (MV1-D1312I-160-CL, Photonfocus, Switzerland), which was coupled with a Navitar 12.5 mm lens (NMV-25M1, Navitar, Rochester, New York). Exposure time was 10 ms. A fruit location control system that includes a translation stage and a laser displacement sensor was used to ensure the top surface of the fruit was at the same distance to the camera lens for all measurements. Four electronically controlled mechanical shutters enabled single wavelength illumination.

The laser image must be symmetric for the profile extraction in the image processing. Therefore, a 50 μm aperture diameter pinhole (#36-391, Edmund Optics, New Jersey, USA) was used to remove the elliptical shape of the beam and any stray light in the system. A quarter wave-plate was installed to make the laser light circularly polarised, which reduces the scattering asymmetry caused by Mie scattering.

A scattering image was first processed in Matlab (Mathworks, Massachusetts, United States) to find the centre of the illuminated area (red cross in Fig. 2a). The distance to each pixel was then calculated and rounded to the nearest whole number. All pixels at each of these integer radii were grouped and averaged providing a vector of intensity values that correspond to single pixel rings expanding out from the centre point (yellow rings in Fig. 2a). The intensity profile (Fig. 2b) was parameterized using diffusion and modified Lorentzian models. The intensity profile was adjusted to take account of the curved surface (Lu and Peng, 2007). The correction method assumes that the apple has a spherical shape and considers both scattering distance and intensity signal distortion. The Matlab curve fitting toolbox was used to find the best fit to the intensity profiles using the Levenberg-Marquardt non-linear least squares algorithm.

A diffusion model that had previously been successfully used on 'Delicious' and 'Golden Delicious' apples (Cen et al., 2011), their best correlation for firmness prediction was R = 0.892. This model was expected to be suitable for our MSI system. The model is based on the diffusion approximation to the radiation transport equation that attempts to explain light intensity variation with source-sensor distance. The model variant used here is the logarithm transformed diffusion model (Cen et al., 2010) which is essentially the logarithm transformed sum of a set of exponential-type functional forms involving a number of optical coefficients and parameters. Data analysis with the model involves only 4 fitting parameters: the absorption coefficient, the scattering coefficient and two experimental constants that scale the model to match the measured intensity and account for the background light levels respectively.

The modified Lorentzian function (Peng and Lu, 2006) is a heuristic alternative which is expected to handle intensity profiles better. Its model equation is

$$I(x) = a + \frac{b}{1 + \left(\frac{|x|}{c}\right)^d},$$

where I is the intensity along a radial intensity profile, a is the asymptotic value of light intensity when x (distance to center of the light spot) approaches infinity, b is the peak value corresponding to the intensity at the centre of the image, c is the full width half maximum (FWHM) of the intensity profile, and d is related to the slope of the profile in the FWHM region.

Illustration of radially averaging the data to reduce noise. The yellow rings indicate pixels being averaged. Bule and greeen cross

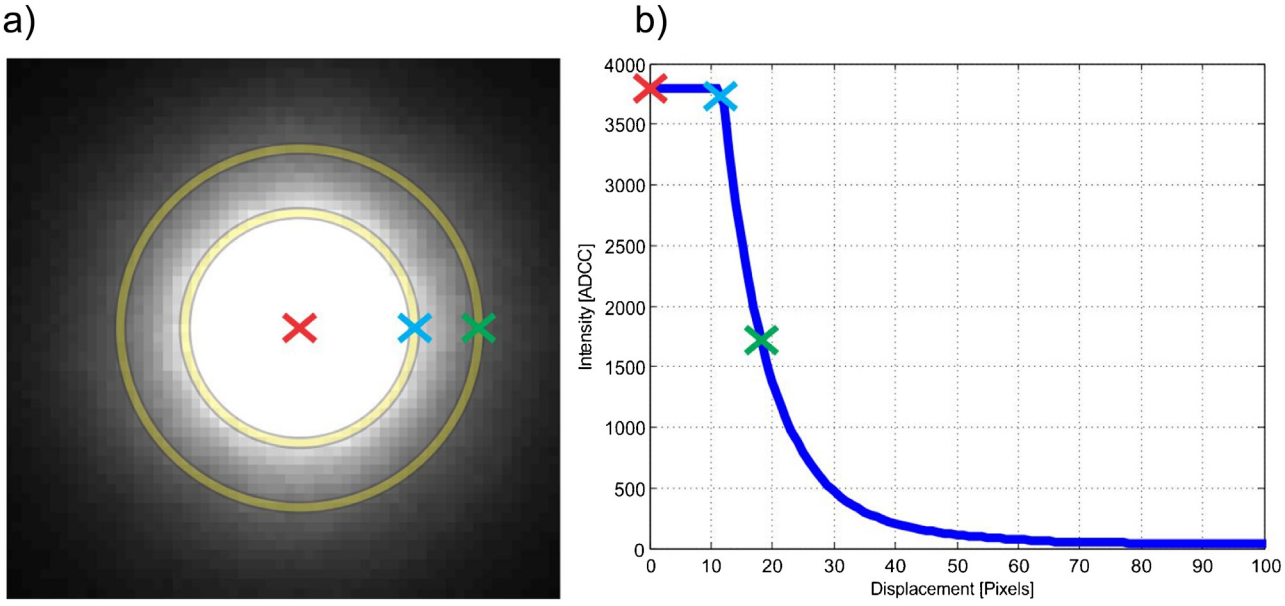

Fig. 2. Illustration of radially averaging the data to reduce noise. The yellow rings indicate pixels being averaged. Bule and greeen cross on the intensity profile (b) correspond to a ring indicated on the image (a).(For interpretation of the references to colour in the text and this figure legend, the reader is referred to the web version of this article.)

on the intensity profile (b) correspond to a ring indicated on the image (a).

2.3. Inverse adding-doubling system

The IAD method consists of a measurement process and computer program for calculating the absorption, scattering, and anisotropy properties of turbid samples (Prahl et al., 1993). Our laboratory system includes an integrating sphere (4P-GPS-033-SL, Labsphere, New Hampshire, USA), a 50 W quartz tungsten halogen lamp (6884, Newport, Irvine, USA), and a Zeiss spectrometer (MMS1, Zeiss, Oberkochen, Germany). The IAD data were processed using version 3.9.10 of the IAD program. Optical properties were calculated assuming an anisotropy of 0 and a refractive index of 1.33.

2.4. NIRS benchtop system

NIRS interactance measurements were taken using a custom built system, which had been previously developed in our group (McGlone et al., 2002b). It contains a broadband light source (50 W quartz halogen, RJL 5012 FL, Radium, Germany) and a non-scanning polychromatic diode array spectrometer (Zeiss MMS1-NIR, Germany). Each spectrum was accumulated over 5 contiguous acquisitions at 175 ms integration time each. Only spectral measurements between 400–1050 nm were used for subsequent data analysis.

2.5. Experimental procedure

Measurements were carried out on both sides of an apple for each measurement cycle (Fig. 3). First the NIRS system was used to record spectra of the fruit on both sides then MSI measurements were taken on the intact surface. Penetrometer firmness was recorded at the two perpendicular sides using a GUSS fruit texture analyzer (Fruit Texture Analyser GS-20, GUSS Manufacturing Limited, South Africa) with an 11 mm diameter probe and forward penetration speed of 30 mm/s. Another set of MSI measurements was taken on the cut surface. The MSI system collected 49 images at each of the four wavelengths for each set of measurement. The 49 images were averaged prior to image processing. Finally, a 5 mm thick slice was obtained by a custom 'guillotine' system and was used for the IAD measurements. Four replicated readings were made with each MSI and IAD measurement, the sample removed and then immediately replaced back for each subsequent replicate reading.

2.6. Data analysis

Most of the data analysis was conducted in Matlab and with the PLS Toolbox (Eigenvector Research, WA). The extracted parameters from curve fitting with the diffusion and modified Lorentzian models were used to build multiple wavelength regression models using multiple linear regression (MLR). There were 8 parameters with the diffusion model (4 wavelengths by 2 optical properties) and 16 parameters with the modified Lorentzian model (4 wavelengths by 4 parameters). The NIRS spectral data had 200 wavelength pixels and was modelled using partial least squares (PLS). In all cases the data were first separated into same calibration (N = 80) and independent validation (N = 20) data sets by rank ordering the apple firmness values and then selecting every 5th sample as a validation sample with the remaining samples left to constitute the calibration samples. The models were then created on the calibration set and a 10-way venetian blind cross-validation procedure was used to provide a root mean square error of cross validation (RMSECV) value that indicates the likely predictive error in using the model on new data. The cross-validation procedure was also used to optimize the latent variable number for the PLS model. The calibrated models were applied to the independent validation data set, and a root mean square error of prediction (RMSEP) value reported, to check the predictive performance on data unseen during the calibration training.

3. Results and discussion

3.1. Validation

An experiment was first carried out to confirm the accuracy of measuring optical properties by both the MSI and IAD system. The liquid optical phantom Intralipid, a fatty emulsion containing mainly lipids and water, was used to simulate light scattering and absorption properties of biological tissues. Measurements were made at four different Intralipid concentrations of 0.5, 1, 1.5 and 2%, covering the range of typical scattering values reported for apples in the literature (Cen et al., 2013; Min et al., 2009; Qin and Lu, 2005). The results are shown in Figs. 4 and 5 where blue and black circles indicate the MSI and IAD measurements, respectively. Each data point is the average of 4 sequential replicate readings taken on the same sample. The resulting coefficients have standard deviations of less than 25 m^{-1} and 1 m^{-1} for scattering and absorption respectively. Corresponding linear regression lines are shown, and a red dotted line illustrates an established empirical model for the optical properties of Intralipid (Van Staveren et al., 1991).

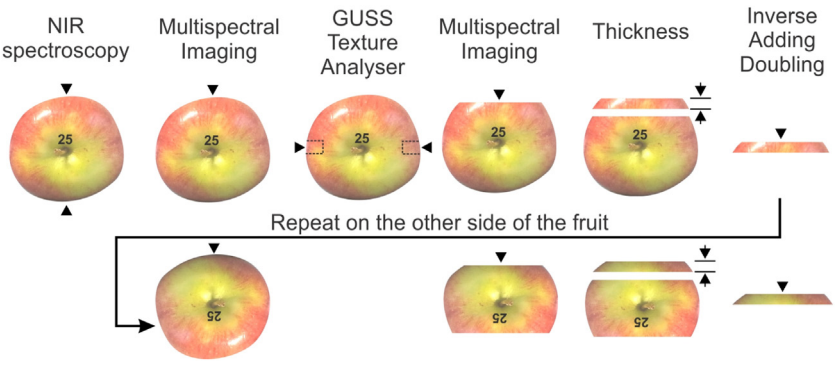

Fig. 3. The sequence and positions of the different measurements. Orientation is indicated by the fruit number.

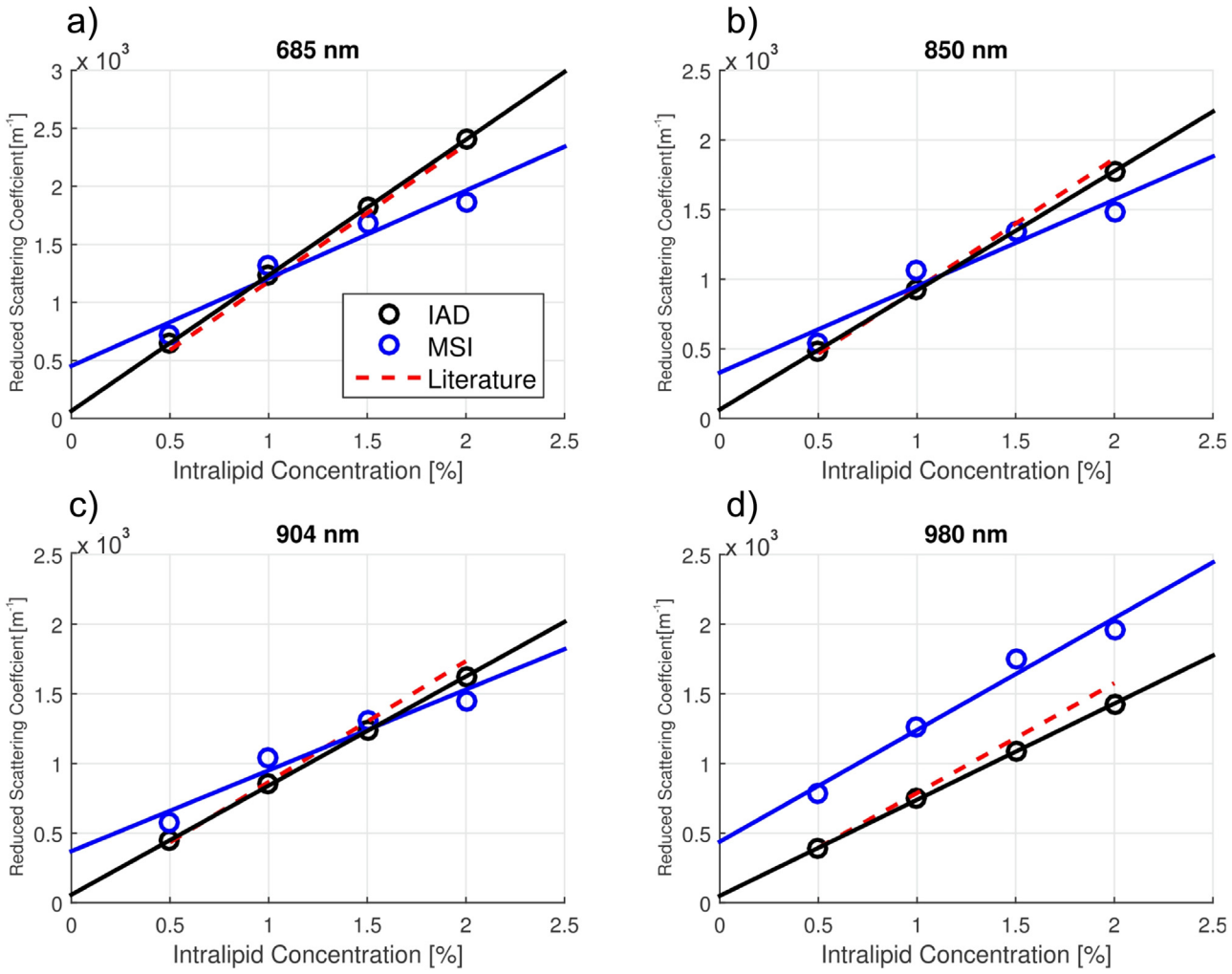

Fig. 4. The reduced scattering coefficient at (a) 685, (b) 850, (c) 904, (d) 980 nm at four concentrations of Intralipid.

At 1.5% Intralipid concentration the MSI reduced scattering coefficient values (Fig. 4) are lower than the empirical model values by 5, 4 and 1% for wavelength 685, 850, and 904 nm respectively. At 2% concentrations, the underestimations increase to 21, 20 and 16%. However at 0.5 and 1% concentrations, the reduced scattering coefficients are overestimated. At 980 nm, the MSI reduced scattering coefficient values are overestimated at all four wavelengths (21, 20, 16 and 24% at 0.5, 1, 1.5, and 2% concentrations respectively). Some studies reported in the literature have shown similar results, with either under or over estimation of the reduced scattering coefficient (Zaccanti et al., 2003; Zhang et al., 2010). The present study shows the relationships are nonetheless highly linear with an average linear correlation coefficient R of about 0.97.

The IAD measurements were closer to the expected empirical model results with differences within 5% for most cases. For 980 nm, the IAD reduced scattering coefficient values are underestimated by 8 and 10% at 1.5 and 2% concentrations respectively, which are the greatest deviations. Both systems provide capabilities to measure the reduced scattering coefficient with good accuracy (within 6% in most cases) and linearity (R is above 0.97), which is expected to provide information regarding fruit firmness.

At the selected laser wavelengths light absorption in Intralipid is almost entirely due to water (Flock et al., 1992; Hale and Querry, 1973; Kou et al., 1993), so the expected empirical values have a slight negative slope with Intralipid concentration (Fig. 5). MSI was best at predicting the absorption coefficient at 850 and 904 nm, with average differences of 5 and 8% respectively. At 685 nm, the expected absorption coefficients are close to zero with an average value of 0.5 m^{-1}. Near the water absorption peak at 980 nm the MSI result is 50–60% lower than the expected empirical model values.

Scattering needs to be significantly higher than absorption if the diffusion model is used to extract optical properties from MSI measurements. A previous study showed that the ratio of reduced scattering and absorption coefficients should be at least 100 to have confidence in the extracted optical properties (Aydin et al., 2004). At 980 nm the ratio is below this, between 25 and 75 depending on the intralipid concentration (Figs. 4 and 5), and may be the cause of the large discrepancy observed. In general, the accuracy of the absorption coefficient measured by the MSI system, and using the diffusion model, is dependent on the extent to which scattering dominates absorption.

At all four wavelengths the IAD method shows grossly inaccurate results for the absorption coefficient (Fig. 5). This is thought to be caused by direct and diffuse light losses not accounted for in the application of the method leading to higher reported absorption values (Cen and Lu, 2010; Rowe et al., 2014; Saeys et al., 2008).

The MSI and IAD systems were also compared using the measurements made on the apple flesh tissues. The reduced scattering coefficients of both systems were moderately correlated at all wavelengths with an average R = 0.6 (Table 1). Some of the

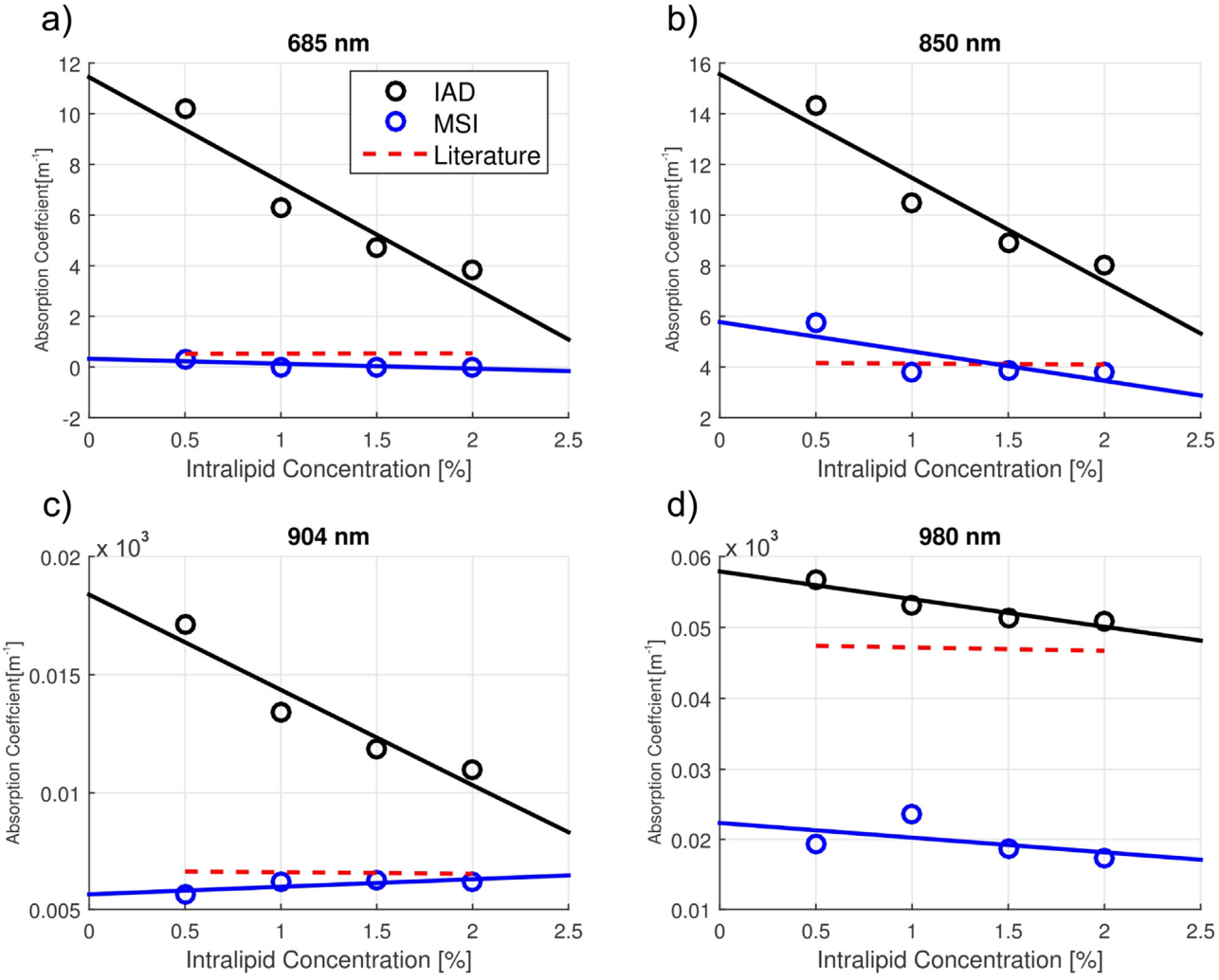

Fig. 5. The absorption coefficient at (a) 685, (b) 850, (c) 904, (d) 980 nm at four concentrations of Intralipid.

variation will be due to the different locations of the respective measurement on the apple flesh. The IAD system measured the 5 mm thick apple slices while the MSI system measured at a small spot (radius r = 10 mm) on the cut surface of a whole apple (Fig. 3). For the absorbance coefficient the correlations between the MSI and IAD measurements were poor (Table 2 and Fig. 6). The absorption coefficient at 685 nm were the most correlated (R = 0.41) but there was a large bias between the two methods (Fig. 6b). The fact that the correlations are significantly higher for the reduced scattering coefficient than for the absorbance coefficient is consistent with the observations made with Intralipid. The highest correlations between both techniques were at 685 nm (Fig. 6). The relative spectral prominence of the chlorophyll absorption might be positively contributing to the slightly better correlation.

Table 1
Correlation coefficient R between MSI and IAD measured reduced scattering and abosorption coefficients at four wavelengths for Apple Flesh Tissues.

	685 nm	850 nm	904 nm	980 nm
Reduced scattering	0.62	0.59	0.59	0.55
Absorption	0.41	0.04	0.01	0.06

3.2. Single wavelength and parameter models

3.2.1. Diffusion model parameters

As the MSI system measures the reduced scattering coefficients reliably we tested the assumption that the reduced scattering coefficient is related to firmness. The correlation between penetrometer firmness and MSI reduced scattering coefficient was investigated. The strongest correlation (R = −0.64) was found at 980 nm measuring the cut surface of an apple (Fig. 7a), but there was a very poor correlation (R = −0.15) for measurements on intact

Table 2
Correlation coefficient R between penetrometer firmness and optical properties at four wavelengths using MSI system and Diffusion Model.

	685 nm		850nm		904nm		980nm	
	Cut surface	Intact apple	Cut surface	Intact apple	Cut surface	Intact apple	Cut surface	Intact apple
Reduced scattering	−0.61	0.5	−0.57	−0.01	−0.64	−0.15	−0.64	−0.15
Absorption	0.53	0.2	0.32	0.04	0.46	0.13	0.59	−0.27

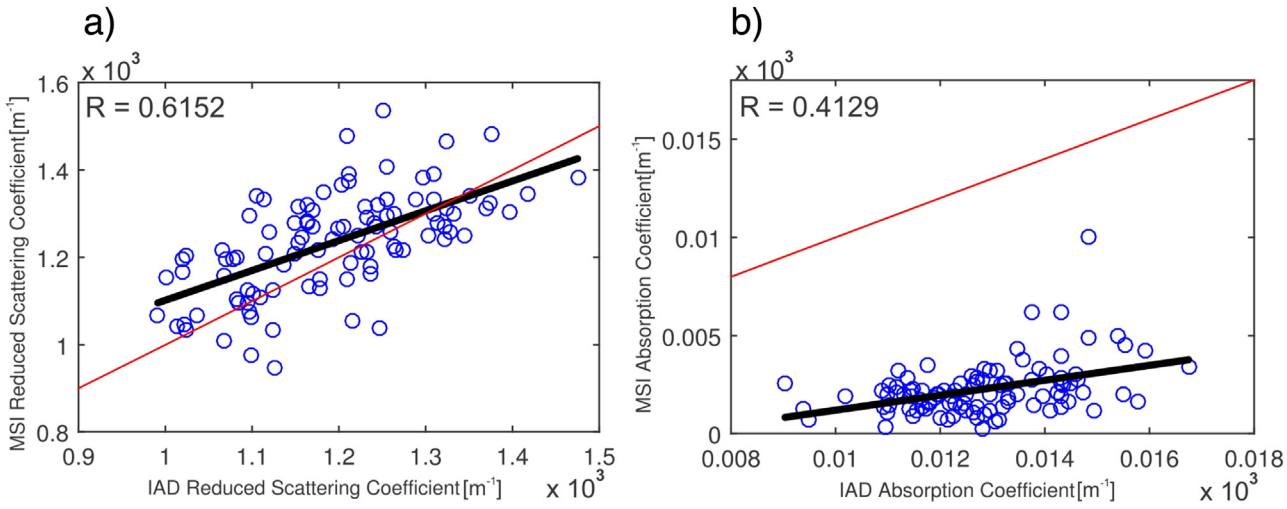

Fig. 6. Comparison between the MSI and IAD system for (a) reduced scattering coeffcient (b) absorption coefficient at 685 nm. Red line indicates the one to one realtioship. (For interpretation of the references to colour in this figure legend, the reader is referred to the web version of this article.)

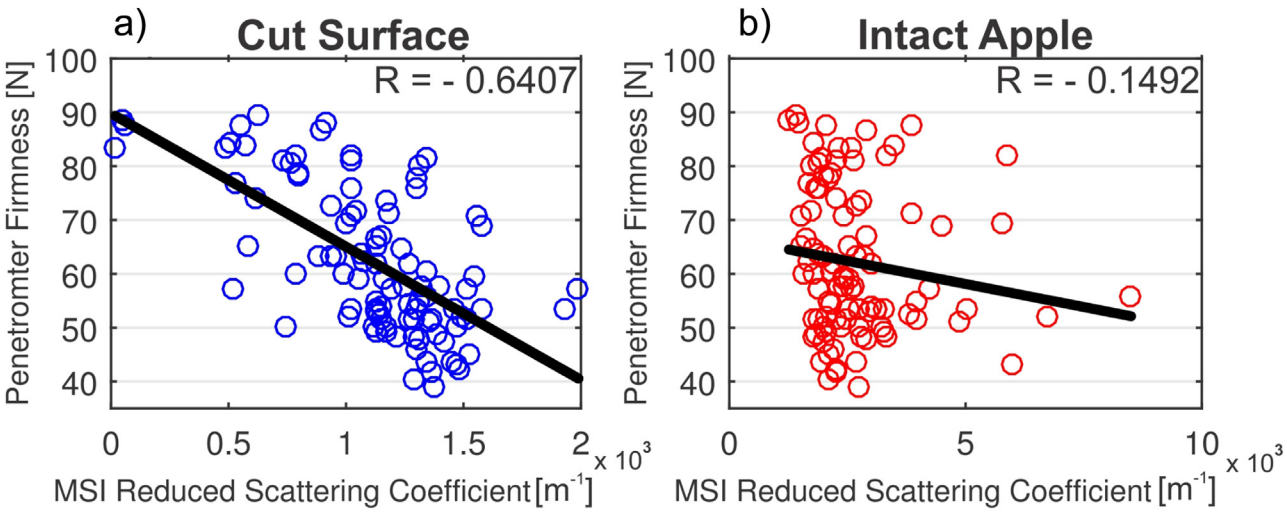

Fig. 7. Relationship between penetrometer firmness and the reduced scattering coefficient for measurements on (a) cut surface and (b) intact apple at 980 nm.

apples (Fig. 7b). For the cut surface measurements, the firmer apples had consistently lower reduced scattering coefficients compared to soft apples across all four laser wavelengths, which corresponds to negative R values (Table 2). These results are similar to previous studies (Cen et al., 2013; Lurie et al., 2011).

Absorption coefficients increased with the firmness for the cut surface measurements and showed a positive correlation which is on average 23% lower than that generated with the reduced scattering coefficient. Both optical properties show poor correlations for the intact apple measurements (Table 2).

3.2.2. Modified Lorentzian model parameters

For the cut surface measurements, the modified Lorentzian parameters *a* and *d* provided the highest overall correlations to the penetrometer firmness (average R = −0.63 and −0.54, respectively). Both parameters have the highest correlation at 980 nm (R = −0.78 and 0.70 respectively), which are stronger than those in a similar previous study (Peng and Lu, 2006) (Fig. 8).

The modified Lorentzian model provides an overall better correlation compared to the diffusion model for the cut surface measurements. The parameters showed poor results for the intact apple measurements in most cases. However, there are some moderate correlations. For instance, parameter *d* has much stronger correlation (R = 0.52) at 685 nm compared to the other wavelengths (Table 3).

Both the diffusion and modified Lorentzian models demonstrate much better performance for cut surface measurements, and the results are comparable to the studies on the other cultivars of apples (Peng and Lu, 2006; Vanoli et al., 2013). Although the effects of instrument response and apple curvature were corrected using a mathematical model with the assumption of a sphere shape, the poor correlation on the intact apple may suggest that this assumption is not valid for the very inconsistently curved surface of 'Royal Gala' apples. The skin itself, and particularly skin pigments, may be another cause of the inferior performance on intact apples. For instance the measurements at 685 nm suggest that the chlorophyll in the skin contributes differently to that in the flesh. This effect caused positive correlations for intact apple measurements and negative correlations for cut surface measurements using reduced scattering coefficient and parameter d of modified Lorenzian model (Tables 2 and 3). The distinctive pigment spots can cause unusually low or high reflectance, so improvement may be achieved by removing those spots in the image processing. The 'virtual peeling' method (Krivoshiev et al.,

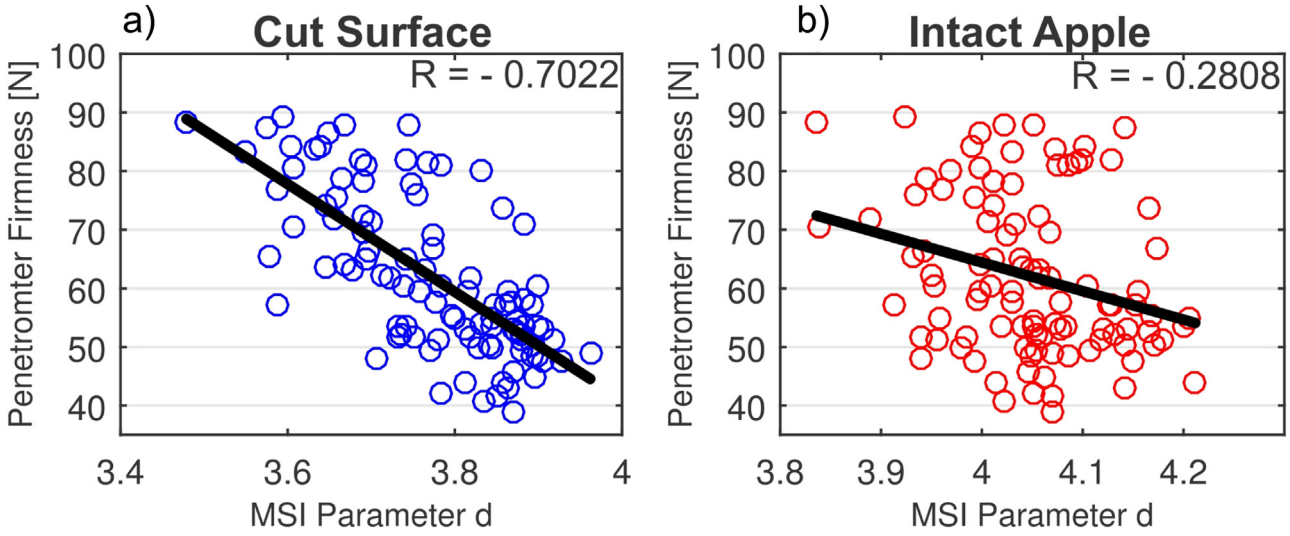

Fig. 8. Relationship between penetrometer firmness and the slope ('d') parameter from the modified Lorentzian model for measurments on (a) cut surface and (b) intact apple at 980 nm.

Table 3
Correlation coefficient R between penetrometer firmness and the modified Lorentzian parameters at four wavelengths using MSI system and modeified Lorenzian model.

	685 nm		850 nm		904 nm		980 nm	
	Cut surface	Intact apple	Cut surface	Intact apple	Cut surface	Intact apple	Cut surface	Intact apple
a	−0.70	−0.02	−0.36	0.14	−0.68	−0.14	−0.78	−0.51
b	0.02	−0.36	0.26	0.05	0.36	0.15	−0.11	0.14
c	−0.20	−0.16	0.48	0.42	−0.06	0.25	−0.07	0.13
d	−0.49	0.52	−0.38	0.12	−0.60	−0.05	−0.70	−0.28

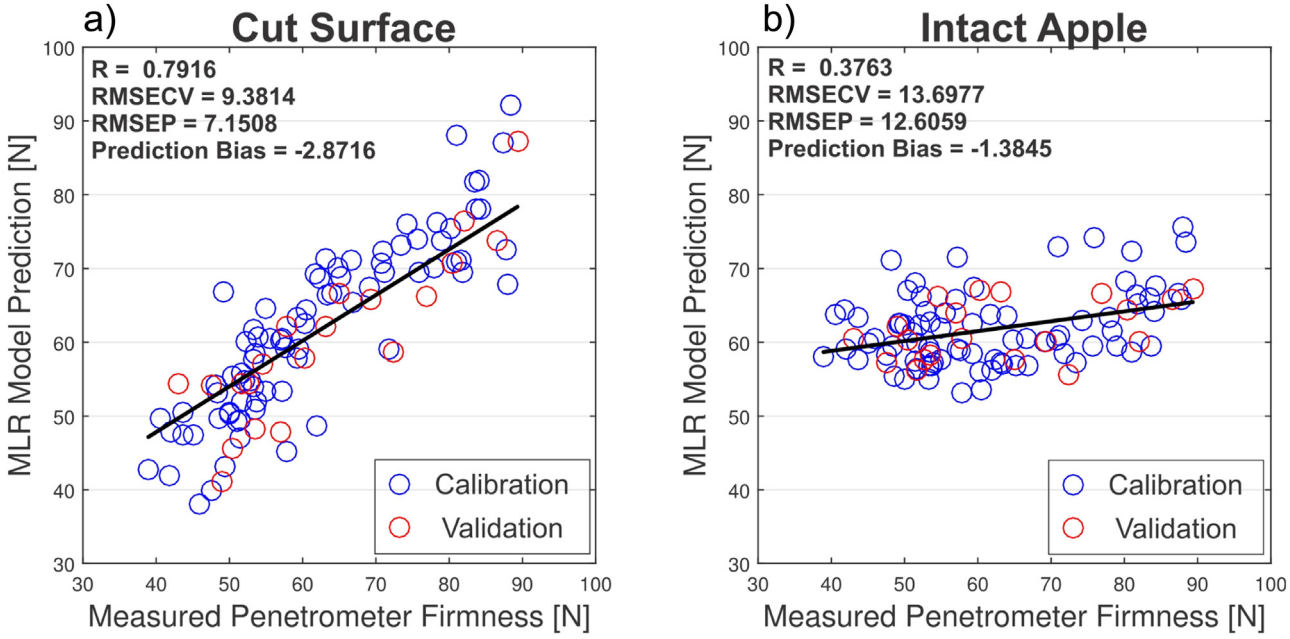

Fig. 9. Predicted vs measured penetrometer firmness. Predictions based on MLR model generated from the optical properties extracted from (a) cut surface and (b) intact measurements using the diffusion model.

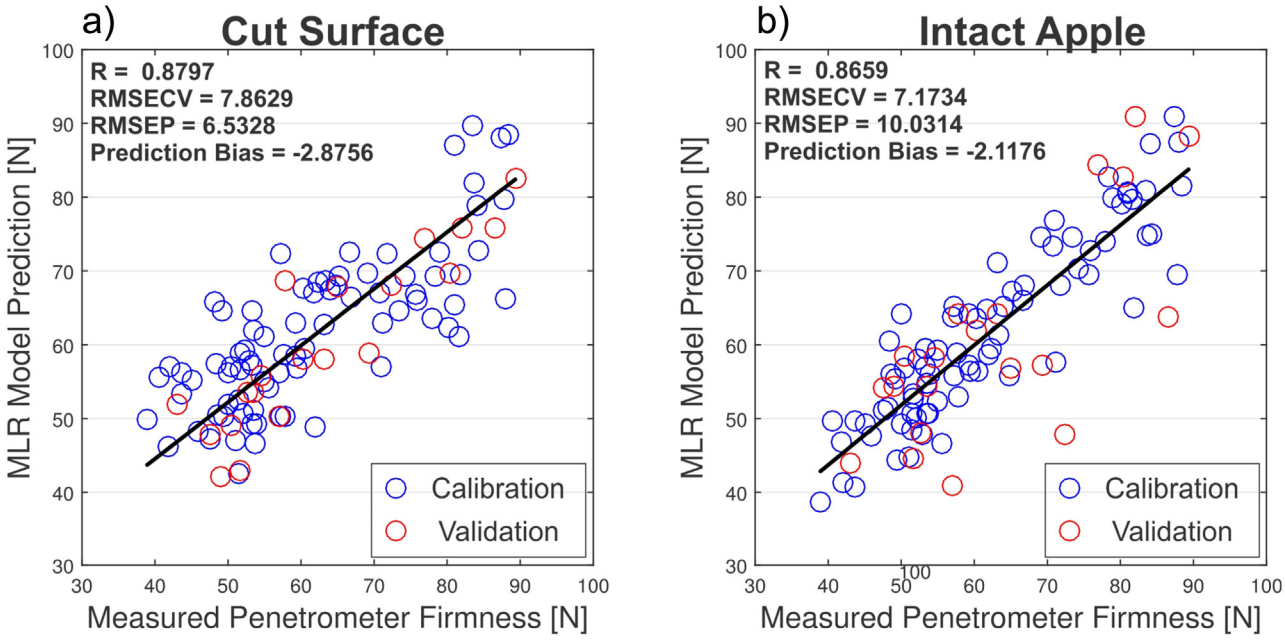

Fig. 10. Predicted vs measured penetrometer firmness. Predictions based on MLR model generated from the modified Lorenzian parameters (a, b, c, d) extraced from (a) cut surface and (b) intact measurements.

2000), which involves additional light reflectance measurements made on the skin, might be useful to minimize such skin affects. However even the best results here, for the cut surfaces, suggest that single wavelength models are not sufficient for accurate prediction of firmness.

3.3. Multiple linear regression

The diffusion model optical properties created an MLR model for firmness with a correlation of R = 0.80 for cut surface measurement, and a poor correlation of R = 0.38 for intact apple measurements (Fig. 9).

With the MLR model using the modified Lorentzian parameters, the correlation for cut surface was improved to R = 0.88 and RMSECV = 7.86 N (Fig. 10a). The correlation for intact apple was similar (R = 0.87) and with a slightly improved RMSECV of 7.17 N (Fig. 10b). This is an outstanding result compared with single wavelength cases and also compared with the diffusion model results. This indicates the MLR model using all 16 modified Lorentzian parameters was able to compensate for the effect of skin interference and non-uniform geometry.

For the strongest performing diffusion model, which was based on cut surface measurements, the largest contributing factor was the reduced scattering coefficient at 904 nm, which was negatively correlated with firmness (Fig. 11a). We have no explanation for that and merely note here that the same wavelength was prominent in the best single wavelength diffusion model (Table 2). The absorption coefficient also had a large contribution at 685 nm. The 685 nm wavelength was dominant in the MLR model using the modified Lorzentian model for the intact apples, being particularly strong for the c and d parameters (Fig. 11b).

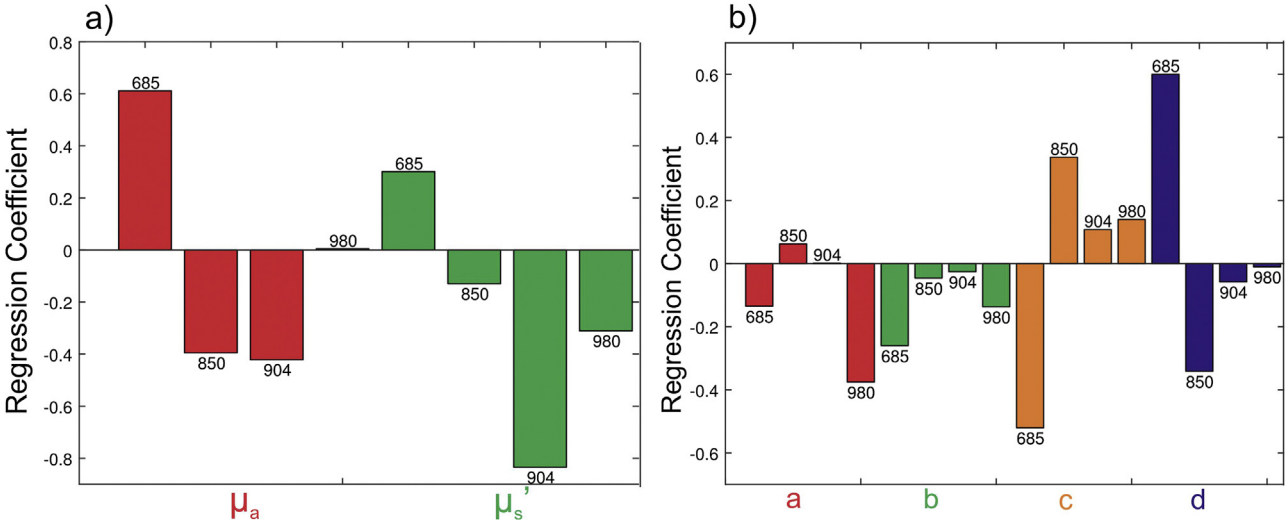

Fig. 11. MLR coefficients for the models built on parameters generated from (a) diffusion model using cut surface measuements and (b) modifed Lorenzian model using intact apple measurements.

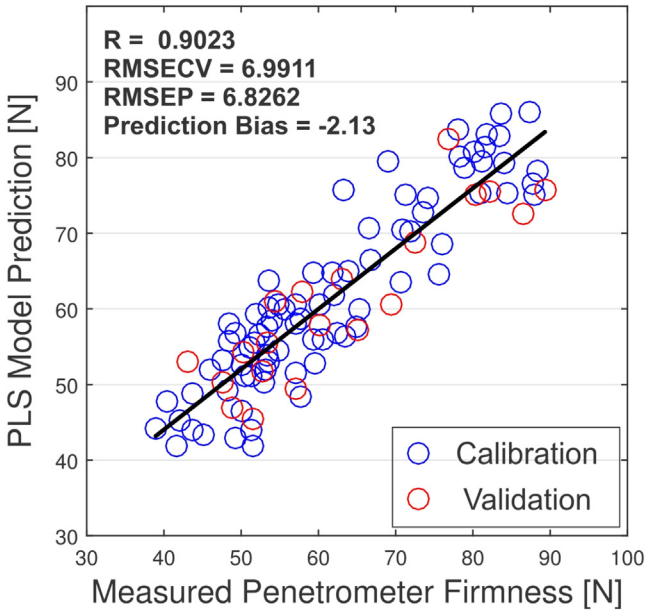

Fig. 12. Predicted vs measured penetrometer firmness. Predictions based on PLS model generated from NIRS spectral data.

3.4. NIR measurements

Partial Least Squares (PLS) was used to build a model with the NIR absorbance measurements on intact apples. The same apples were chosen for the calibration and validation set as before (Fig. 12). The NIR system provided better correlation with R = 0.90 and RMSECV = 6.99 N. The improvement of the correlation coefficient was slight but the scatterplot looks much sharper with decreases in RMSECV and RMSEP. Given that only 6 latent variables were employed, the results shows that the NIR measurement potentially provides better performance for prediction of apple firmness.

4. Discussion and conclusions

An MSI system with four lasers and a CMOS camera has been developed and validated for optical measurements. Reduced scattering coefficient measurements, with Intralipid and excised apple tissue samples, compared well with both the known sample values and/or those derived from separate IAD measurements. Absorption coefficient measurements also compared well with the known values but not with the IAD based measurements which are probably wrong due to unaccounted light loss issues with the IAD method.

For apple firmness prediction the MSI system shows some good potential on intact apples although the results here on 'Royal Gala' apples are inferior to a standard NIRS method. Single wavelength MSI models were poor, correlations with actual apple penetrometer firmness being typically well less than R = 0.7. Multiple wavelength MSI models, combining the model parameters estimated at each wavelength by MLR, significantly improved the correlations to typically R > 0.8. The exception was intact apple measurements using the diffusion model optical properties for which the correlation was very poor at R = 0.38. The modified Lorentzian model parameters outperformed the use of optical properties estimated with the diffusion model and results on cut apple surfaces were typically much better than those on intact apples. Nevertheless the highest correlation with firmness for MSI measurement on intact apples (R = 0.87) was little different to those made on the cut apples surfaces (R = 0.88) when using the modified Lorentzian model parameters. Still the best intact apple measurements were achieved with the NIRS method, the correlation with firmness being R = 0.90 and the prediction error estimated as RMSECV = 6.99 N.

We presented for the first time a comparison of NIRS and MSI systems for measuring firmness on the same samples under the same conditions. Given the small differences here, between NIRS and MSI predictive ability on one set of 100 intact apples, it would be interesting in future work to compare performance across a greater variety of apple sources to observe practically which of the methods might be superior. NIRS systems are commonly in commercial use for fruit grading, although not often for firmness grading, and so an MSI method would need to be demonstrably better performing or have other advantages compared to the NIRS systems to be considered for commercial implementation. For instance, it is possible that the MSI method might be a more robust firmness predictor across apples from a variety of sources and seasons given the method is, at least conceptually, more directly linked to optical scattering properties of the flesh and thus the tissue firmness.

Acknowledgements

The research here was partially funded under MBIE Contract C11X1208. Jason Sun acknowledges the financial support of PhD scholarships from Plant and Food Research and the University of Waikato.

References

Abbott, J.A., 1999. Quality measurement of fruits and vegetables. Postharvest Biol. Technol. 15, 207–225.
Aydin, E.D., de Oliveira, C.R.E., Goddard, A.J.H., 2004. A finite element-spherical harmonics radiation transport model for photon migration in turbid media. J. Quant. Spectrosc. Radiat. Transfer 84, 247–260.
Cen, H., Lu, R., 2010. Optimization of the hyperspectral imaging-based spatially-resolved system for measuring the optical properties of biological materials. Opt. Express 18, 17412–17432.
Cen, H., Lu, R., Dolan, K., 2010. Optimization of inverse algorithm for estimating the optical properties of biological materials using spatially-resolved diffuse reflectance. Inverse Prob. Sci. Eng. 18, 853–872.
Cen, H., Lu, R., Mendoza, F.A., 2011. Analysis of absorption and scattering spectra for assessing the internal quality of apple fruit. 4th International Conference Postharvest Unlimited, Leavenworth, Washington, pp. 181–188.
Cen, H., Lu, R., Mendoza, F., Beaudry, R.M., 2013. Relationship of the optical absorption and scattering properties with mechanical and structural properties of apple tissue. Postharvest Biol. Technol. 85, 30–38.
De Ketelaere, B., Howarth, M.S., Crezee, L., Lammertyn, J., Viaene, K., Bulens, I., De Baerdemaeker, J., 2006. Postharvest firmness changes as measured by acoustic and low-mass impact devices: a comparison of techniques. Postharvest Biol. Technol. 41, 275–284.
Flock, S.T., Jacques, S.L., Wilson, B.C., Star, W.M., van Gemert, M.J., 1992. Optical properties of Intralipid: a phantom medium for light propagation studies. Lasers Surg. Med. 12, 510–519.
Hale, G.M., Querry, M.R., 1973. Optical constants of water in the 200-nm to 200-microm wavelength region. Appl. Opt. 12, 555–563.
Kou, L., Labrie, D., Chylek, P., 1993. Refractive indices of water and ice in the 0 65- to 2.5-μm spectral range. Appl. Opt. 32, 3531–3540.
Krivoshiev, G.P., Chalucova, R.P., Moukarev, M.I., 2000. A possibility for elimination of the interference from the peel in nondestructive determination of the internal quality of fruit and vegetables by vis/nir spectroscopy. LWT—Food Sci. Technol. 33, 344–353.
Lammertyn, J., Nicolaï, B., Ooms, K., Smedt, V.D., Baerdemaeker, J.D., 1998. Non-destructive measurement of acidity, soluble solids, and firmness of Jonagold apples using NIR-spectroscopy. Trans. ASAE 41, 1089–1094.
Lu, R., Peng, Y., 2007. Development of a multispectral imaging prototype for real-time detection of apple fruit firmness. Opt. Eng. 46 123201–123201.
Lu, R., Huang, M., Qin, J., 2009. Analysis of hyperspectral scattering characteristics for predicting apple fruit firmness and soluble solids content. Proc. SPIE 7315, 1–11.
Lu, R., 2004. Near-infrared multispectral scattering for assessing internal quality of apple fruit. Monit. Food Saf. Agric. Plant Health 313–320.
Lurie, S., Vanoli, M., Dagar, A., Weksler, A., Lovati, F., Eccher Zerbini, P., Spinelli, L., Torricelli, A., Feng, J., Rizzolo, A., 2011. Chilling injury in stored nectarines and its detection by time-resolved reflectance spectroscopy. Postharvest Biol. Technol. 59, 211–218.

McGlone, V.A., Kawano, S., 1998. Firmness, dry-matter and soluble-solids assessment of postharvest kiwifruit by NIR spectroscopy. Postharvest Biol. Technol. 13, 131–141.
McGlone, V.A., Abe, H., Kawano, S., Kawano, A., 1997. Kiwifruit firmness by near infrared light scattering. J. Near Infrared Spectrosc. 5, 83–89.
McGlone, V.A., Jordan, R.B., Martinsen, P.J., 2002a. Vis/NIR estimation at harvest of pre- and post-storage quality indices for 'Royal Gala' apple. Postharvest Biol. Technol. 25, 135–144.
McGlone, V.A., Jordan, R.B., Seelye, R., Martinsen, P.J., 2002b. Comparing density and NIR methods for measurement of Kiwifruit dry matter and soluble solids content. Postharvest Biol. Technol. 26, 191–198.
Mendoza, F., Lu, R., Cen, H., 2014. Grading of apples based on firmness and soluble solids content using Vis/SWNIR spectroscopy and spectral scattering techniques. J. Food Eng. 125, 59–68.
Min, H., Jianwei, Q., Renfu, L., 2009. Analysis of hyperspectral scattering characteristics for predicting apple fruit firmness and soluble solids content. Sens. Agric. Food Qual. Saf. SPIE—Int. Soc. Opt. Eng., U.S.A. 731501.
Mollazade, K., Omid, M., Akhlaghian Tab, F., Kalaj, Y.R., Mohtasebi, S.S., Zude, M., 2013. Analysis of texture-based features for predicting mechanical properties of horticultural products by laser light backscattering imaging. Comput. Electron. Agric. 98, 34–45.
Nicolaï, B.M., Beullens, K., Bobelyn, E., Peirs, A., Saeys, W., Theron, K.I., Lammertyn, J., 2007. Nondestructive measurement of fruit and vegetable quality by means of NIR spectroscopy: a review. Postharvest Biol. Technol. 46, 99–118.
Noh, H.K., Lu, R., 2007. Hyperspectral laser-induced fluorescence imaging for assessing apple fruit quality. Postharvest Biol. Technol. 43, 193–201.
Penchaiya, P., Bobelyn, E., Verlinden, B.E., Nicolaï, B.M., Saeys, W., 2009. Non-destructive measurement of firmness and soluble solids content in bell pepper using NIR spectroscopy. J. Food Eng. 94, 267–273.
Peng, Y., Lu, R., 2006. Improving apple fruit firmness predictions by effective correction of multispectral scattering images. Postharvest Biol. Technol. 41, 266–274.
Peng, Y., Lu, R., 2008. Analysis of spatially resolved hyperspectral scattering images for assessing apple fruit firmness and soluble solids content. Postharvest Biol. Technol. 48, 52–62.
Prahl, S.A., Gemert, M.J.C.V., Welch, A.J., Van Gemert, M.J.C., 1993. Determining the optical properties of turbid media using the adding-doubling method. Appl. Opt 32, 559–568.
Qin, J., Lu, R., 2005. Determination of the optical properties of turbid materials by hyperspectral diffuse reflectance. Trans. ASAE: Paper No 053068 1–12.
Qing, Z., Ji, B., Zude, M., 2008. Non-destructive analyses of apple quality parameters by means of laser-induced light backscattering imaging. Postharvest Biol. Technol. 48, 215–222.
Rowe, P.I., Künnemeyer, R., McGlone, A., Talele, S., Martinsen, P., Seelye, R., 2014. Relationship between tissue firmness and optical properties of 'Royal Gala' apples from 400 to 1050 nm. Postharvest Biol. Technol. 94, 89–96.
Ruiz-Altisent, M., Ruiz-Garcia, L., Moreda, G.P., Lu, R., Hernandez-Sanchez, N., Correa, E.C., Diezma, B., Nicolaï, B., García-Ramos, J., 2010. Sensors for product characterization and quality of specialty crops—a review. Comput. Electron. Agric. 74, 176–194.
Saeys, W., Velazco-Roa M. a. Thennadil, S.N., Ramon, H., Nicolaï, B.M., 2008. Optical properties of apple skin and flesh in the wavelength range from 350 to 2200 nm. Appl. Opt. 47, 908–919.
Steinmetz, V., Crochon, M., Bellon Maurel, V., Garcia Fernandez, J.L., Barreiro Elorza, P., Verstreken, L., 1996. Sensors for fruit firmness assessment: comparison and fusion. J. Agric. Eng. Res. 64, 15–27.
Subedi, P.P., Walsh, K.B., 2009. Non-invasive techniques for measurement of fresh fruit firmness. Postharvest Biol. Technol. 51, 297–304.
Van Beers, R., Aernouts, B., Gutiérrez, L.L., Erkinbaev, C., Rutten, K., Schenk, A., Nicolaï, B., Saeys, W., 2015. Optimal illumination-detection distance and detector size for predicting Braeburn apple maturity from Vis/NIR laser reflectance measurements. Food Bioprocess Technol. 1–14.
Van Staveren, H.J., Moes, C.J.M., Van Marie, J., Prahl, S.A., Van Gemert, M.J.C., 1991. Light scattering in Intralipid-10% in the wavelength range of 400–1100 nm. Appl. Opt. 30, 4507–4514.
Vanoli, M., Rizzolo, A., Zanella, A., Grassi, M., Spinelli, L., Cubeddu, R., Torricelli, A., 2013. Apple texture in relation to optical, physical and sensory properties. InsideFood Symposium, Leuven Belgium, pp. 9–12.
Zaccanti, G., Bianco, S.D., Martelli, F., 2003. Measurements of optical properties of high-density media. Appl. Opt. 42, 4023–4030.
Zhang, Y., Wen, X., Xu, Z., Zhu, D., 2010. The accuracy of a commercial spectrophotometer with single integrating sphere for measuring optical properties of turbid sample, optical interactions with tissues and cells XXI. Int. Soc. Opt. Photonics (pp. 756219-756219-756219).

Chapter 5

Optical Geometry and Sample Positioning in NIRS Transmittance for Detecting Vascular Browning in Apples

---

A journal paper

by

Jason Sun, Rainer Künnemeyer, Andrew McGlone, Nathan Tomer

To be submitted

I prepared the initial draft manuscript, which was refined and edited in consultation with co-authors. Nathan and I carried out the experimental work. Nathan Tomer conducted all the simulation work, I processed the data to the form in which it is presented. My supervisors provided guidance throughout this project.

Investigations of optical geometry and sample positioning in NIRS transmittance for detecting vascular browning in apples

Jason Sun[1, 2], Rainer Künnemeyer[1, 2], Andrew McGlone[1], Nathan Tomer[1]

[1]The New Zealand Institute for Plant & Food Research Limited, Hamilton, New Zealand

[2]Dodd Walls Centre for Photonic and Quantum Technologies, Dunedin, New Zealand

Abstract

Two optical geometries and five sample orientations were investigated in an effort to improve the detection of vascular browning (VAB) in 'Braeburn' apples, using near-infrared spectroscopy (NIRS). Classification models were developed by applying partial least squares discriminant analysis on measurements under different conditions. Receiver operating characteristic (ROC) curves were used to measure the discrimination of each case. Monte Carlo (MC) simulations showed the optical geometry was crucial for increasing the light path lengths; longer light path lengths were required to improve the detection of small and spatially distributed defects, such as VAB using a NIRS transmittance system. The five sample orientations studied showed very similar detection rates, although significantly affecting the amount of transmitted light. Overall, it was difficult for NIRS to detect VAB. At the optimal geometry and orientation, 21% of healthy apples were misclassified when the detection threshold was set to detect 80% of defective apples. The simulations indicated that NIRS systems only examined a very limited volume of the sample. New systems, scanning the entire internal volume by spatially examining small discrete volumes, will be required to improve detection efficiencies.

1. Introduction

Near infrared spectroscopy (NIRS) is used for commercial grading of internal quality attributes of fruits and vegetables, such as taste and the presence of rots (Lin and Ying, 2009; McGlone et al., 2002; Nicolaï et al., 2007; Wang et al., 2015). A typical NIRS set-up uses a broadband light source to illuminate the sample, and the transmitted or reflected light is measured using a spectrometer. The spectral data collected are used to make discriminant or quantitative predictions based on the calibration models. For a non-scattering sample, and a constant path length arrangement, the absorbance spectra are linearly proportional to the concentration of the absorbing constituents in accordance with Beer-Lambert's law. However, the absorbance spectra for a turbid or scattering sample do not follow the same law as the light path length for individual photons is variable, the light travelling complicated zig-zag trajectories with a wide distribution of path lengths (Savo et al., 2017). For a typical NIRS measurement system on a scattering sample, the path length distribution of the detected light would change with sample dimension and the locations of light illumination and detection, i.e. optical geometry (Clark et al., 2003). A change in the absorbance spectra caused simply by a different path length distribution can be misinterpreted as due to change in the sample's absorbing constituents (López-Maestresalas et al., 2016). Normalisation methods such as Multiplicative Scatter Correction (MSC) and Standard Normal Variate (SNV) are commonly employed standard methods to assist in minimising the influence of path length variations (Rinnan et al., 2009), typically caused by different sample sizes and sample geometries, and assist in the recovery of absorbance with concentration of absorbing constituents.

NIR light attenuates exponentially with the depth. The penetration depth is often defined as the depth at which the intensity of the radiation decays to 1/e, but this has not been commonly determined for horticultural produce. Fraser et al. (2001) defined the penetration depth as the depth at which the light intensity dropped to 1% of the initial

intensity and measured it in the wavelength range of 500-1690 nm. They reported that the penetration depth in an apple was 35 mm at 716 nm, reducing to less than 1 mm in the 1400-1600 nm range due to strong water absorption. It is well known that, with sufficient integration time, spectrometers can detect light passing through thin-skinned fruit in the 'transmission/biological window' of 700 to 900 nm. In the biomedical field, the two transmission windows at 1000-1350 nm and 1550-1870 nm are also often used (Hemmer et al., 2016), but for produce the radiation in these wavelength ranges is much less penetrating. Water absorption dominates and increases rapidly above 900 nm (Palmer and Williams, 1974; Saeys et al., 2008; Wang et al., 2018). Other than the light penetration, the volume that the detected light interrogates, more specifically the detection sensitivity inside the sample, has not been well studied for horticultural products. However, methods that have been developed for biological tissues (Arridge, 1995; Arridge and Schweiger, 1995; Fukui et al., 2003)can be applied to the similar turbid medium of produce.

Optical geometry in this study is defined by the positions of the source and detector on a sample's surface and can be broadly divided into three sensing modes: reflectance, transmittance and interactance. A transmittance system is probably more appropriate than either a reflectance or an interactance system for internal defect detection since NIR light must pass through the middle of a sample to reach a detector on the opposite side. The deeper penetrating and longer light paths are more likely influenced by the presence of defective tissue (Clark et al., 2003; Kuroki et al., 2017; McGlone et al., 2005; Upchurch et al., 1997). There are different variations of NIRS transmittance set-ups. Clark et al. (2003) measured 'Braeburn' apples with browning defects in four different optical geometries and showed that both, the amount of transmitted light and the detection accuracy, were significantly affected by the optical geometries. Their results also showed that those optical geometries with better signal to noise ratio (SNR), as a consequence of increased transmitted light collection, did not necessarily provide better detection efficiencies.

Moreover, with the development of more sensitive spectrometers (e.g. back-illuminated/back-thinned low noise charge-coupled device (CCD) arrays), sufficient SNR can be achieved even at very low light levels. NIRS is only sensitive to a defect if the detected light is significantly affected by the defect; small and localised defects may not effectively intersect the main transmitted light paths. Improving the sensitivity of transmittance NIRS systems to small and localised defects requires investigations of different optical geometries, particularly the study of light path length and light sensitivity distributions with each geometry. Another factor to be considered is sample positioning. Kuroki et al. (2017) investigated six different sample orientations and discovered that sample orientation had a significant impact on the effectiveness of NIR transmission measurements for detecting internal rot in onions.

Vascular browning (VAB) is a 'Braeburn' Browning Disorder (BBD) (Hatoum et al., 2016), which develops when apples are stored at low temperature under controlled atmosphere conditions. There are many factors contributing to the development of BBD. One strong trigger is high CO_2 concentration (Elgar et al., 1998; Hatoum et al., 2016). VAB is a name used by New Zealand industry as the cavities form around or on the vascular bundles. They are typically small and spatially localised deep inside the apple flesh (Figure 1) and may have a light brown surface. The combination of small size, proximity to the core and the lack of strong absorbance features makes VAB challenging to detect. This study aimed to evaluate the effect of different optical geometries and sample positioning on detecting VAB. Two sub-objectives were formulated.

- To model the light propagation in fruit using Monte Carlo (MC) simulations for quantifying the effectiveness of different optical geometries for defect detection in terms of light path length and sensitivity.

- To build classification models using partial least squares discriminant analysis (PLSDA) and evaluate the detection performances under different geometries and orientations by analysing the receiver operating characteristic (ROC) curves.

2. Methods

2.1. Sample preparation

Approximately 700 ‘Braeburn’ apples were harvested in April 2016 from orchards in Hawke's Bay, New Zealand. Based on sampling results of a set of apples from the same orchards the VAB incidence was estimated to be less than 5% by horticultural specialists. For experimental advantage, the apples were first scanned by a clinical magnetic resonance imaging (MRI) system to find all defective apples and to build a suitably balanced and efficient data set for NIRS analysis. The defect severity was judged on the visual inspection of the MRI and cut surface images. MRI scanning identified 43 apples with clear VAB symptoms, 16 of which were severe (score >1) and 38 symptom-free apples were added to create a sample set of 81 apples (Figure 2). After the NIRS measurements, the apples were cut in half and scored by the defect severity revealed by visual inspection of the cut surface (Figure 1). The scores were further verified by the MRI images which indicated the entire volume of the defect. Heathy apples were given a score of 0 with the severity of the defective apples quantified at three increasing levels labelled 1, 2, and 3.

Figure 1. Cut surface of three ‘Braeburn’ defective apples, which were scored 1, 2, and 3 for vascular browning.

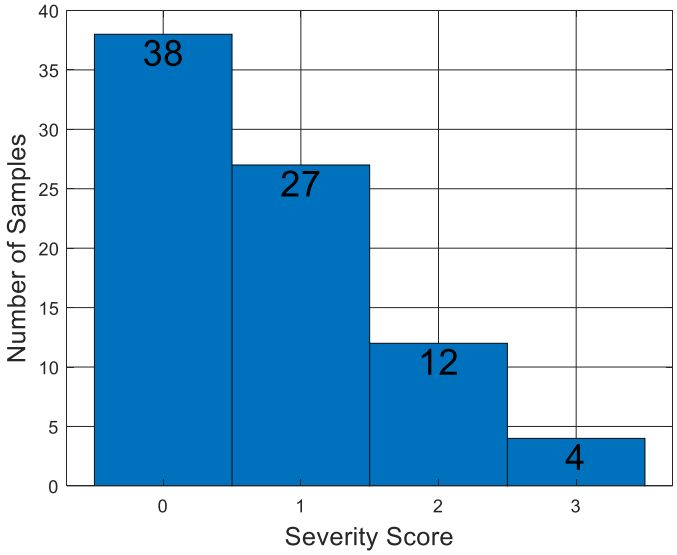

Figure 2. Severity score of the 'Braeburn' apples used in the experiment. Score 0 represents healthy apples with no vascular browning.

2.2. NIRS systems

Two NIRS measurement set-ups of differing optical geometry, termed Systems 1 and 2, were used (Figure 3). System 1 is a popular geometry, first used commercially in Japan in the late 1990s. System 2 is less common in practice, probably due to lower transmitted light levels, but this may change with the recent availability of more sensitive sensors, such as CCD or complementary metal-oxide-semiconductor (CMOS) based spectrometers.

System 1 (Figure 3a) involves three 50 W halogen lamps on each side of the measurement station and a silicon array spectrometer (MMS1-NIR, Zeiss, Germany) on top. The three lamps were aligned horizontally as indicated in the top view. In system 2 (Figure 3b), the light source and detector are at 45° to the fruit, but illuminate it at directly opposing locations. The set-up of System 2 is essentially a 180° transmission arrangement as the light is scattered in a similar manner inside the fruit irrespective of the angle of incidence or collection at the surface. The incident photons lose all knowledge of their original direction after travelling one transport mean free path, which is defined as $\frac{1}{\mu_s'}$ (Martelli et al., 2009). For an apple with μ_s' = 1 mm^{-1}, this distance is 1 mm. The 45° angle geometry

was chosen because, for samples of different spherical sizes, it effectively maintains illumination and light collection at half the height of the sample..

System 2 consists of a single 250 W tungsten halogen lamp (6334NS, Newport, Irvine, CA, USA), powered by a digital radiometric power supply (69931, Newport, Irvine, CA, USA), and an NIR-enhanced, back-illuminated, temperature-stabilised CCD spectrometer (CD024321, Control Development, South Bend, IN, USA) coupled to a 910 µm diameter, NA 0.22, optical fibre (FG910LEC, Thorlabs, Newton, NJ, USA). Both systems use collimating optics to optimise light delivery and collection. System 1 used a faceted reflector to reflect light emitted backwards from the filament and so increasing the light delivery. For system 2, a reflector and collimating lens were used in the lamp housing (66901, Newport, Irvine, CA, USA) to provide collimated light on the sample. Both systems used collimating lenses to gather more light into the collection fibre connected to the spectrometer; System 1 used a 9.24 mm diameter lens with an NIR anti-reflective coating (A397TM-B, Thorlabs, Newton, NJ, USA), while System 2 used a 12.5mm diameter achromatic lens (49-322, Edmund Optics, Singapore).

The light illuminance/irradiance on the fruit for each system is shown in Figure 4. Ray tracing software (Lighttools, Synopsys, CA, USA) was used to simulate the light flux projected onto the plane parallel to the light source. The light flux pattern for System 1 has three high flux regions as a result of illumination from 3 lamps. System 2 was a blurred image of the elongated filament shape, due to the non-faceted back-plane reflector in the lamp housing.

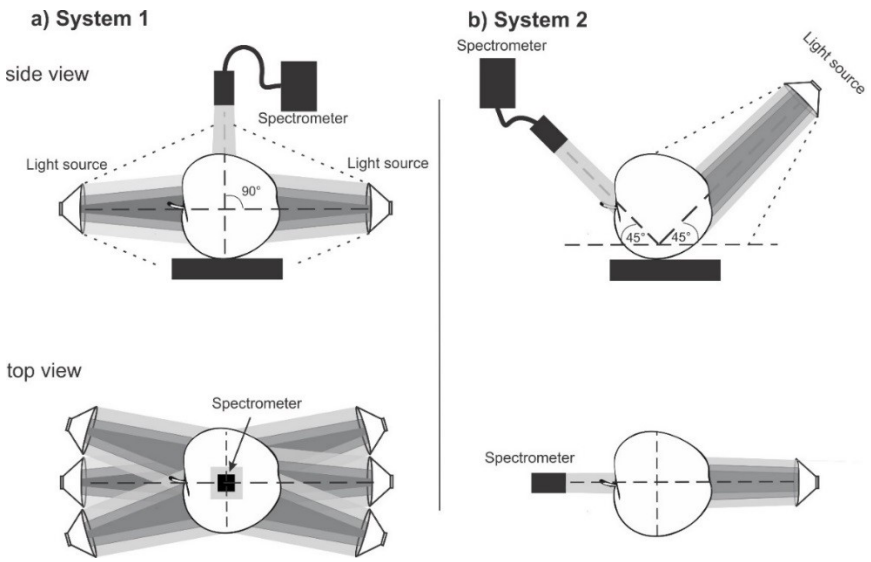

Figure 3. Hardware set-up schematic (side and top view) of a) System 1 and (b) System 2. The dotted line indicates the outer bound of stray light.

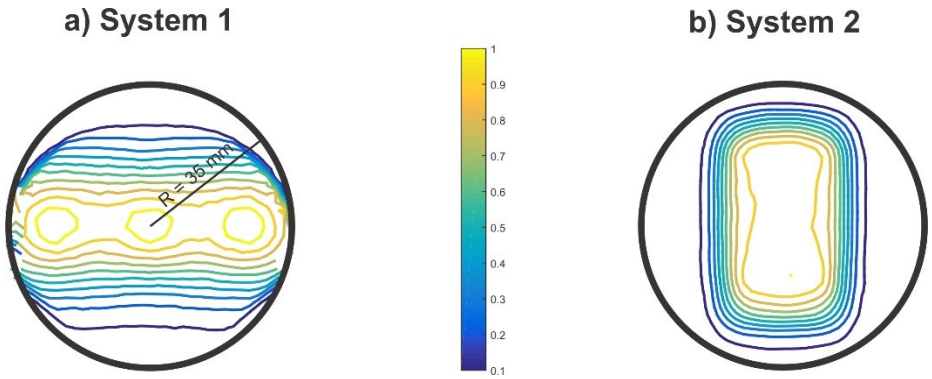

Figure 4. Normalised light flux on the plane parallel to the light source. The black circle represents a cross section of a 70 mm sphere illuminated by the light. The flux values were normalised by the maximum flux value of each system.

2.3. Orientations

The samples were manually positioned on a cup holder for each orientation. All measurements were made relative to the reference position where the stem-calyx axis of the apple was horizontal and aligned as shown in Figure 5. For System 1, the stem and calyx were facing the two light sources. The fruit was then rotated 180° around the stem-calyx axis to provide two orientations. Measurements were taken for the up and down orientation (Figure 5a). For System 2, with the fruit number facing up, the apples were rotated around the vertical axis perpendicular to the detector-source axis. Measurements were taken at five different orientations with the calyx at 0°, 45°, 90°, 135° and 180° relative to the detector-source axis (Figure 5b).

To increase the size of the spectra data set for building more robust classification models when comparing the two optical geometries, a measurement at each orientation was treated as a separate sample with a total of 81 samples for each orientation. Therefore, System 1 and System 2 had data sets of sizes n = 162 and n = 405, respectively. Only System 2 was used for examining the effects of sample orientation.

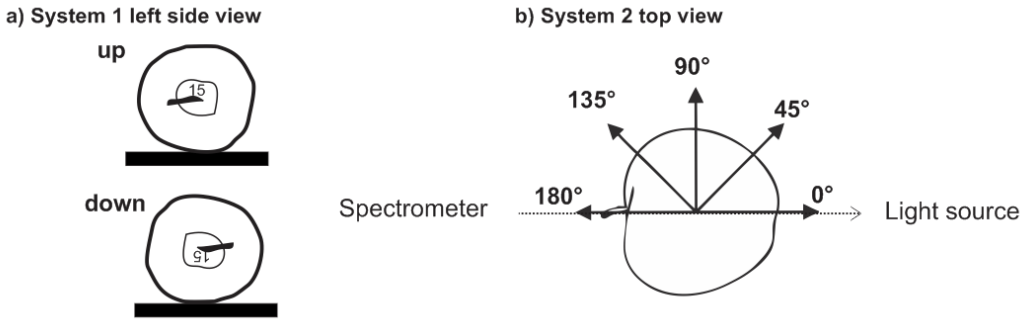

Figure 5. Orientations used in the measurements: (a) up and down orientation indicated by the fruit number on the apple shoulder. (b) Five orientations in System 2, the dotted line indicates the detector-source axis, the arrows indicate the direction of the calyx. The apple in this figure is at 0° orientation.

2.4. Monte Carlo Simulation

Monte Carlo (MC) simulations were carried out using the software package MCX (Fang and Boas, 2009) in Matlab (Mathworks, Massachusetts, United States). The MCX software used 1 mm^3 voxels in its simulations. The fruit sample was modelled with a radius of 35 mm and typical optical properties in the range 700 to 1000 nm (Saeys et al., 2008; Van Beers et al., 2017) for an apple. The refractive index was set to 1.42, the absorption coefficient to μ_a = 0.0035 mm^{-1} and the reduced scattering coefficient to μ_s' = 1 mm^{-1}. The computation time was about 1 hr with 10^9 photons used in the simulation (GeForce GTX780 video card). The path length distribution of each system was the direct output of MCX, and a volume absorption and scattering sensitivity distribution for each system was produced by calculating the photon-measurement density function (PMDF) using the simulation results. The calculation method was described by Arridge (1995). The sensitivity at a location is the gradient of the measured signal with respect to a change in

the optical properties at that location. A location's sensitivity value indicates the portion by which the received signal will be changed if the optical property at that location is changed by a small amount. A higher and positive value means increasing the optical property will increase (decrease for a negative value) the received signal by a higher amount. The absorption sensitivity distribution was then normalised to have a total sensitivity of 1 over the entire volume and quantified in volume terms using a contour plot. The scattering sensitivity distribution was not similarly quantified, as scattering sensitivity is far more localised to the source and detector (Arridge and Schweiger, 1995), and thus shows less interesting features.

2.5. Multivariate analysis

The transmittance spectra were normalised by first dividing them by a reference spectrum taken with nothing between light source and detector at reduced integration time and resulting spectra were further processed using the standard normal variate (SNV) method in an attempt to minimise variations in light path length caused by the varying size and geometry of the fruits. PLSDA was used to build binary classification models using 10-way venetian blind cross-validation (PLS_Toolbox, Eigenvector Research, WA, USA). The optimum number of latent variables (LVs) was selected by choosing the number of LVs after which any additional LV resulted in no meaningful decrease in the average error of cross-validation.

3. Results

3.1. Effect of optical geometry

3.1.1. Spectral Characteristics

The average normalised spectra from each system were quite different irrespective of severity scores (Figure 6). Despite being slightly noisier (less smooth spectra), the transmission spectra of System 2 (Figure 6b) showed two distinctive peaks. The adjacent

troughs were caused by being away from the strong absorption of chlorophyll at 670 nm (Munns et al., 2016) and that of water at 750, 840 and 970 nm (Kou et al., 1993; McGlone and Kawano, 1998). System 1 had similar features, but the relative intensity variations were much smaller (Figure 6a). For example, the dip at about 750 nm was much deeper for spectra from System 2 than System 1, relative to the high peaks at about 710 and 810 nm. Similarly the relative transmittance above about 810 nm was far lower for spectra from System 2 than System 1.

For both systems, the average spectra differed with respect to severity scores, the score 3 spectra being particularly different from the others (Figure 6). VAB-affected apples had lower transmittance in the wavelength range of 680 to 750 nm and higher transmittance above 800 nm. A similar effect was observed for rotten onion (Kuroki et al., 2017; Sun et al., 2016) and brownheart apple (Clark et al., 2003). Clark et al. (2003), in examining brownheart apples, attributed an observed transmittance decrease in the red region (650 to 750 nm) of the spectra to increased absorption by brown-coloured, floury-textured cortical tissue. They also observed increased transmittance above 800 nm and attributed that to decreased water absorption as a consequence of the brown defective tissue being possibly drier. This transmittance decrease on Figure 6 is supposed to be caused by only the change of absorption, if the SNV pre-processing method could fully remove the scattering effects. However, light-scattering properties would likely change too and the combined effect should be considered. Sun et al. (2018) showed that from 800 to 950 nm, rotten onion flesh actually had higher absorption coefficients than for flesh from healthy tissue, but that the scattering coefficients were also lower too. The resulting net effect in that case caused the transmittance to increase from 800 to 950 nm on rotten onions. That explanation may also hold for VAB-affected apples. Nevertheless, the spectral differences indicate that it is quite possible to use NIRS transmittance spectra to build classification models to segregate the VAB-affected apples.

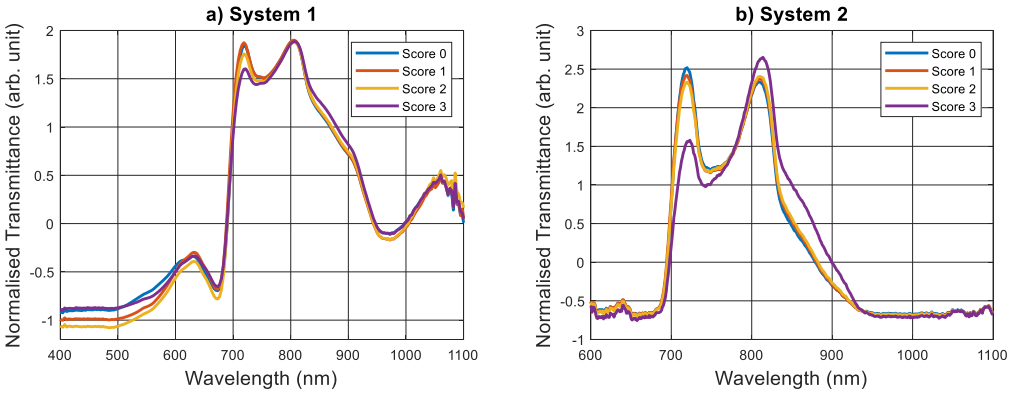

Figure 6. Average spectrum (SNV pre-processed) for each 'Braeburn' apple severity score over all the orientations from (a) System 1 and (b) System 2.

3.1.2. Monte Carlo simulations

The Monte Carlo (MC) simulations revealed quite different light path lengths for the two systems (Figure 7). In System 1, a large portion of the light had path lengths less than 20 mm (Figure 7a), a result of the wide spread of the illumination light. Some of the transmitted light reaches the detection zone on the fruit directly with very little or no interaction with the internal fruit flesh. For System 2 the distribution peaked at 700 mm (Figure 7c), with minimum path lengths at around 250 mm, clearly indicating substantial interaction of the transmitted light with internal fruit flesh. The cumulative photon density plots show the average path lengths (at 0.5 counts/mm) were 259 and 977 mm for System 1 (Figure 7b) and System 2 (Figure 7d), respectively. The longer average path length of System 2 means there is a more light absorption, matching the relative spectral observations previously discussed with respect to the transmittance spectra of Figure 6. System 1 had a much higher photon count density, about 8 times greater when comparing the peak values of both cases. This is consistent with the measured spectra being less noisy (Figure 6a).

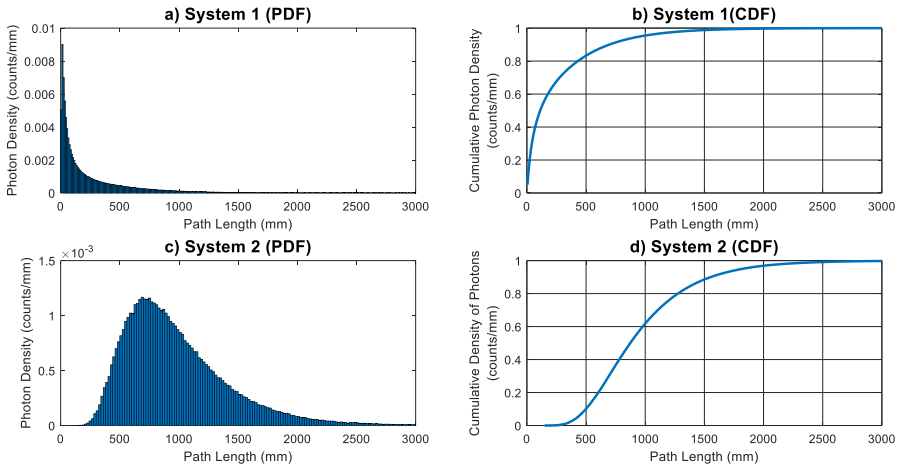

Figure 7. Monte Carlo (MC) simulations of the light path distributions in (a) System 1 and (b) System 2. PDF is probability density function, CDF is cumulative density function.

The longer path length does not necessarily indicate that the light explored a larger volume inside the sample. There is a possibility that the light could simply be scattered more often in the same volume, resulting in longer path lengths but no increased examination of the internal flesh. Figure 8 & 9 are image plots of absorption and scattering sensitivities at each location (represented by a pixel) on the middle slice of a 70 mm diameter sphere.

The absorption sensitivity distribution (Figure 8) shows the sensitive region is localised to the top of the sphere for System 1 next to the detector. In System 2 the sensitive region is substantially increased in size, covering a large part in the middle, but insensitive regions still exist at the top and bottom. The negative values mean increased absorption properties will decrease the received signal. The scattering sensitives (Figure 9) are much more localised to the source and detector positions for both systems, consistent with similar observations made by Arridge and Schweiger (1995) on numerical objects. The scattering values in the regions furthest from the source and detector are positive values, just above zero, indicating increased scattering values in those regions will slightly increase the received signal.

To quantify the absorption sensitivity regions, the volumes that change 20%, 50%, 70%, 99% and 100% of the received signal are shown in a contour plot (Figure 10). Table 1 lists

the percentage of volume in each case. For System 1, some 70% of the received signals were influenced by only 15% of the total volume of the sample. In comparison, 70% of the signal for System 2 is affected by a greater 24% of the sample volume. However, it is clear that both systems are most sensitive to the regions lying directly between source and detector. For example, 50% of the received signal with System 2 was influenced by 14% of the volume lying immediately along the straight line path between source and detector (Figure 10b). For System 1 the equivalent 50% of the signal was affected by a much smaller and shallower 7% of the total volume lying adjacent to the detector. These results indicate that the optical geometry in System 2 is more advantageous, and likely to offer better performances for detecting VAB-affected apples.

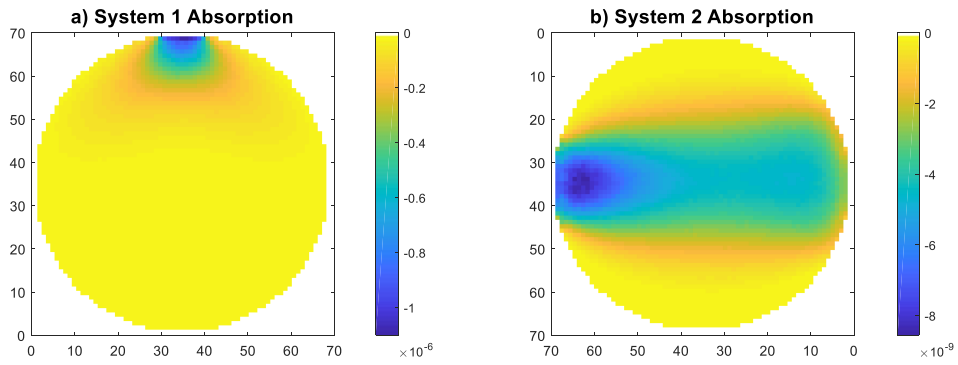

Figure 8: Monte Carlo simulation of the absorption sensitivity distribution in (a) System 1 (detector on top, source to the left and right) and (b) System 2 (source to the right, detector to the left).

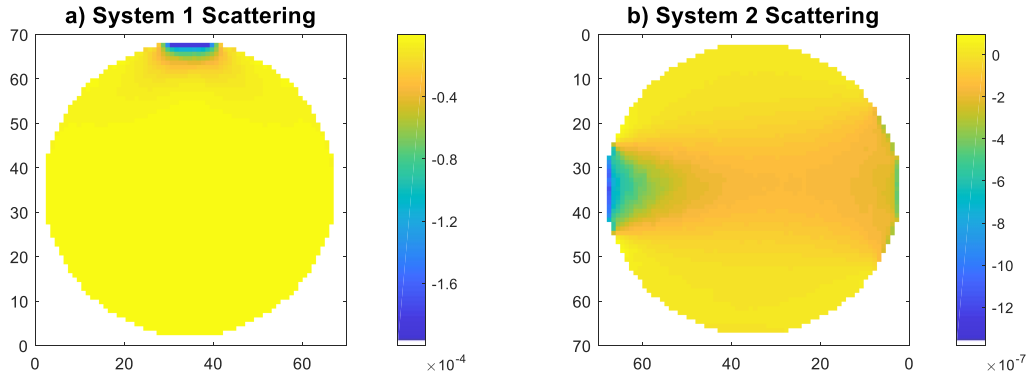

Figure 9. Monte Carlo simulation of the scattering sensitivity distribution in (a) System 1 (detector on top, source to the left and right) and (b) System 2 (source to the right, detector to the left).

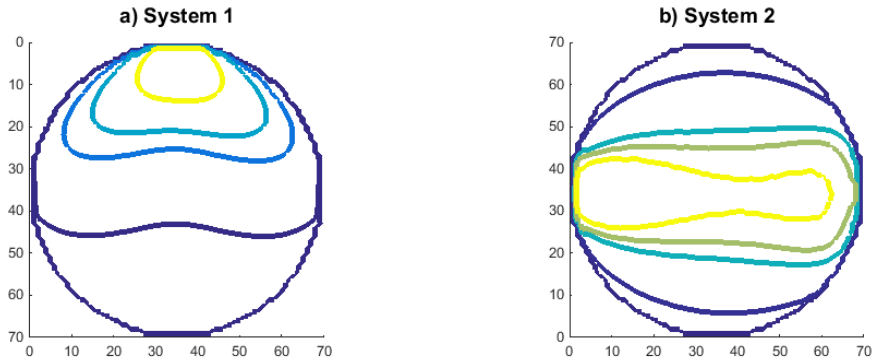

Figure 10. The contour lines indicate the volumes influencing 20%, 50%, 70%, 99% and 100% of the received signal. Table 1 lists corresponding percentage of volume for each case.

Table 1: Coverage of the received photons for the two systems.

Percentage of the received signal that is affected	Percentage of volume affecting the received signal	
	System 1	System 2
100%	100%	100%
99%	61%	73%
70%	15%	24%
50%	7%	14%
20%	1%	4%

3.1.3. Model performance

MC simulations showed that System 2 allows receiving the light that has penetrated deeper into the fruit, so it should be more sensitive in detecting any defects. PLSDA binary classification models were built to distinguish healthy and VAB-affected apples using NIRS transmittance spectra and were evaluated using the cross-validated ROC (Figure 11) curves. The true positive rate (TPR) and false positive rate (FPR) varied depending on the discrimination threshold with a trade-off between them. The area under curve (AUC) is one metric to measure the general capability of a model. System 1 and 2 had an AUC value of 0.81 and 0.86, respectively, indicating that System 2 is potentially a better system.

System 2 was much better when the TPR was higher than about 75%. For example, at 90% TPR System 1 had a FPR of 49%, whereas it was much lower at about 26% for System 2. The smaller FPR means there is a lower chance to misclassify healthy apples, significantly reducing the potential waste of healthy apples while detecting 90% of defective ones.

With TPR< 75%, System 1 showed slightly lower FPR than System 2, indicating System 1 has slightly greater detection ability for some VAB samples. However, direct comparison of results for the two systems here may be unfair, particularly in System 2 which had 2.5 times as many samples due to inclusion of data from all five orientations. As a consequence System 2 may simply be presenting far more reliable and/or robust data, compared to System 1. The down-sampled model using two orientations in System 2 still provided a better performance with higher AUC, particularly so with TPR >75%. In grading practice the model threshold (cut point) would be first set to achieve TPR as high as possible, while maintaining an acceptable false positive rate, since removal of defective fruit is the primary aim, before consideration of the limitations imposed by the cost of the FPR losses of healthy fruit.

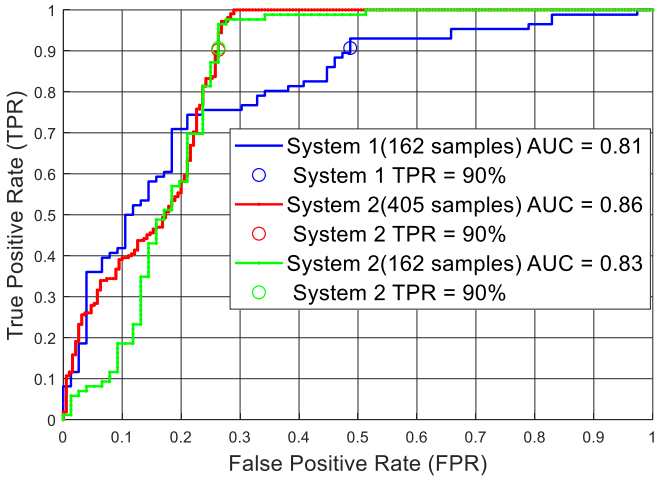

Figure 11. Cross-validated true and false positive rates of detecting 'Braeburn' apples with vascular browning with System 1 and System 2 using all the orientations and using 0° & 180° in System2 The circles indicate TPR = 90% of the two systems.

3.2. Effect of sample orientation in System 2

3.2.1. Spectral characteristics

There was a strong effect due to apple orientation on the amount of transmitted light (Figure 12). The greatest amount of light was transmitted at 0° (calyx end facing the light source). The light level dropped as the calyx end turned away from the light source, although not strictly proportional to increased angle. When placed at 180° and 135° the

healthy apples had the lowest amount of transmitted light, reduced by 42% and 35%, respectively, relative to the 0° orientation (Figure 12a). As expected, the orientation effect was similar for VAB-affected apples (Figure 12b). The highest light level was at 0°, gradually decreasing with the increasing angle. The light level at 45° was 20% and 29% lower than that at 0° for healthy and defective apples, respectively. For the same orientation, the amount of transmitted light also changed relative to the severity scores, but the differences were not consistent. At 0° and 45° the defective apples transmitted 2% and 9% more light, respectively, whereas at 90°, 135° and 180° the defective apples transmitted 17%, 8% and 9% less.

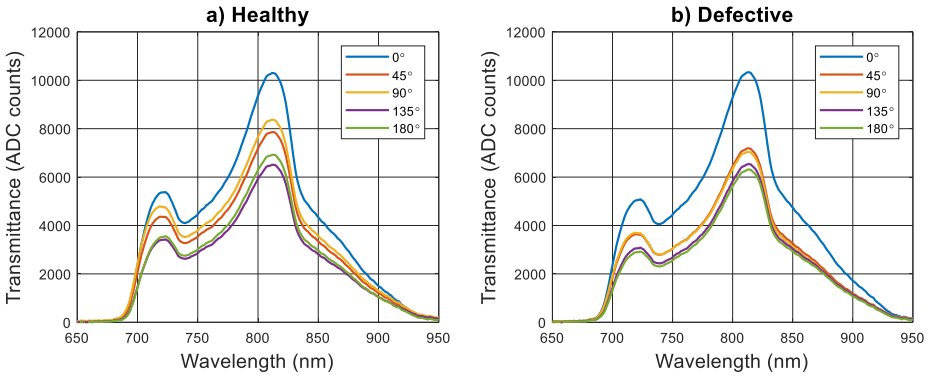

Figure 12. Average raw spectra at five orientations for (a) healthy (b) VAB-affected apples.

Similar to Figure 6b, the normalised spectra were affected by VAB severity (Figure 13). Except at zero degrees, all the orientations showed similar differences for score 0 to 2 (Figure 13b-12e). Based on these spectral observations, illumination at the calyx (0°) would probably provide the worst detection performance.

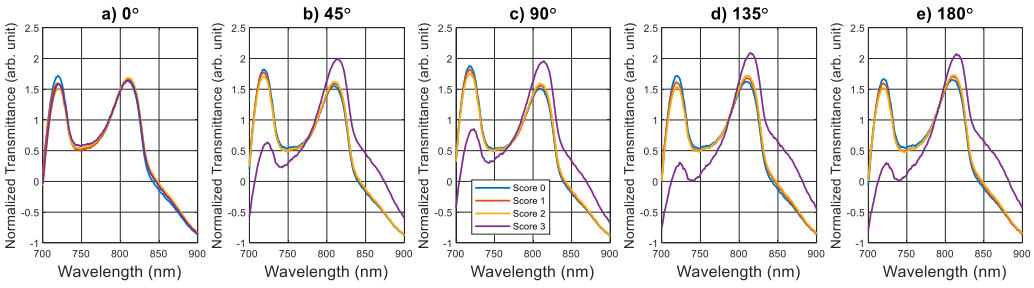

Figure 13. Average spectra at (a) 0° , (b) 45° , (c) 90° , (d) 135° and (e) 180° orientations for System 2.

3.2.2. Model performance

PLSDA models were built using the measurement for each of the orientations. Different orientations performed very similarly, and, there were no major differences in AUC values (Figure 14). The 180° orientation had the lowest AUC value of 0.83, and the 90° orientation had the highest of 0.87. Contradicting the observations in Figure 12, orientation 0° was just as good as the others with AUC = 0.84. This is likely due to the small sample size of score 3.

The threshold can be adjusted to achieve desirable TPR and/or FPR on the ROC curve according to the practical need. The samples used in this study had a VAB incident rate of 5%. The FPR is a concern as high FPR rates result in an intolerable amount of healthy apples being wasted. Table 2 lists the detection rates for each of the severity scores when the TPR rate is set at 80%. The detection rate for the healthy apples (= 1-FPR) will then be a metric to determine the better orientations. The detection rates were generally higher for Score 2 than Score 1, but interestingly for Score 3 the detections were not the highest apart from at 0° and 180°. This was also likely due to the fact that there were only four samples of score 3 severity, probably not large enough to ensure robust detection efficiencies to be determined for Score 3 apples. For the healthy apples, 90° and 135° had the highest rate of 79%, indicating they are potentially the better orientations.

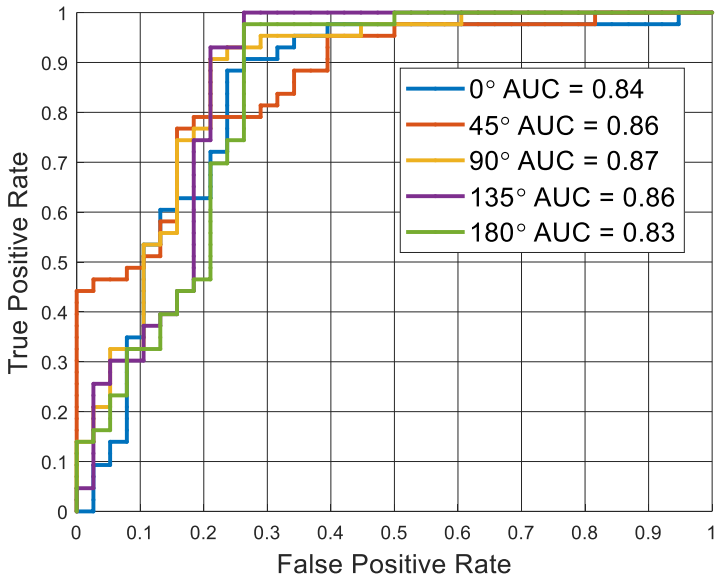

Figure 14. Cross-validated ROC curves for different orientations, area under curve (AUC) values for each orientation is also included.

Table 2. Detection rate for each vascular browning severity score and total defective at 80% TPR (True positive rate).

	Healthy	Score 1	Score 2	Score 3	Total Defective
0°	76%	74%	83%	100%	80%
45°	71%	78%	83%	75%	80%
90°	79%	82%	83%	50%	80%
135°	79%	78%	83%	75%	80%
180°	74%	78%	75%	100%	80%

4. Discussion and conclusion

The optical simulations in this study demonstrated their usefulness for quantified understanding of the effect of optical geometry. The MC simulations (section 3.1.2) revealed that System 2 had much longer light path lengths and explored a larger volume inside the sample. This finding was consistent with the transmission spectra in Figure 6, where the spectra from System 1 were much less affected by the absorbers in the apple. Although System 1 offered superior SNRs to System 2, its optical geometry meant shorter average path lengths, 259 mm vs 977 mm, and its volume sensitivity was lower. System 2 would thus appear to have considerable advantage in terms of internal defect detection. The recent development of more sensitive CCD spectrometers has made System 2

suitable at the same high-speed fruit processing rates required for on-line grader operation.

The classification results presented here, for VAB detection, suggest that System 2 is indeed superior to System 1. The ROC curves for the PLSDA models presented in Figure 11 showed that System 2 had much lower FPR rate for detecting VAB when the TPR was at the higher end above 75%. However, System 1 does not present itself as especially poor either, at least in a relative sense to System 2, with the general performance metric AUC values not being greatly different, at AUC = 0.81 and 0.86 for System 1 and System 2, respectively. System 1 was also slightly better performing for TPR values below 75%, demonstrating slightly lower FPR rates. System 2 provided much longer path lengths, but the volume absorption sensitivity distribution (Figure 8 and Figure 10) indicates it still only explored a small region of the sample, adjacent to the detector, with any relative effectiveness. This may explain why System 2 did not improve the VAB detection significantly. The caution in this analysis is that System 2 classifications involved a 2.5 times larger sample size as a result of inclusion of more and different orientations. In addition, the data sets also had limitations; there were few very severe Score 3 samples for example, and that may have affected the degree to which System 1 and System 2 could be confidently compared. Finally, although System 2 effectively interrogates a larger volume than System 1, the signal from a small VAB defect may still be lost as the received signal is even more dominated by that from healthy tissue. In another words, being sensitive to a larger volume has a negative effect of making the defect less influencing to the received signal.

Orientation of the fruit affected System 2, with the amount of transmitted light reduced as the calyx end rotated further away from the light source (Figure 12). That agrees with the conclusion reached by Upchurch et al. (1997) when examining internal breakdown apples. We speculate that when the light enters the apple from the calyx end, more light directly enters into the core and is thus ‘short-circuited’ to the detector side, resulting in

the light travelling through shorter distances of tissue to the detector. The effective path lengths are then shorter and result in higher transmittance. This speculation cannot explain why stem end illumination permitted the least amount of transmitted light, as some portion of light then should also be 'short-circuited' to the core from the stem end. In future, instead of using a sphere a more realistic model that incorporates the shape of an apple should be used in MC simulations to study these orientation effects. The orientation data of Figure 13 showed that score 3 apples were much less separated from the other apples at 0° orientation, whereas the classification results in Figure 14 and Table 2 showed that detection performances were broadly similar at all orientations. The 90° orientation, where the light enters the fruit through the equator, was perhaps a slightly better orientation overall with a highest AUC value of 0.87. When the PLSDA model for the 90° orientation was set at TPR = 80% then the FPR misclassification rate was the lowest at 21%. However, it is clear from the apple data here that sample orientation with System 2 is not a major issue at all. In future, a larger sample size with more evenly distributed samples over different severities should be used to further validate this finding.

With the better system (System 2) at the best orientation (90°), Table 2 shows that when the TPR was 80%, about 21% of healthy apples would be misclassified. When all the orientations were combined as in Figure 11, the more robust models showed very similar detection rates as in Figure 14. Overall, it was evident that VAB remains a difficult defect to detect using a NIRS transmittance system, high detection rates (TPR values) only come with high losses (PFR values) of healthy apples. Future investigations, to seek improved detection methods, should involve larger sample sizes with more evenly distributed samples over the full range of severity levels.

The simulation results revealed the fundamental limitations of NIRS measurements. Defects such as VAB are localised to a small internal volume, typically deep inside the apples and so outside the very sensitive measurement regions. Rotating the apples and using multiple scans, at different orientations, may be necessary to improve detection

rates. Moreover, investigation of spatially resolved transmission optical systems, such as the methods of hyperspectral imaging (Cen et al., 2014), which combines spectral and spatial scanning, and diffuse optical tomography (Yamada and Okawa, 2014), which can resolve absorption and scattering characteristics to discrete internal volumes, might be necessary to achieve improved detection efficiencies for small and localised defects like VAB in apples.

Acknowledgment

We would like to acknowledge Matt Punter for sourcing the apple samples and Duncan Galbraith for the ray tracing simulations. Jason Sun acknowledges the financial support of PhD scholarships from The New Zealand Institute for Plant & Food Research Limited and the University of Waikato. This research was carried out with funding from the New Zealand Ministry of Business, Innovation and Employment, under programs C11X1601 and C11X1208.

References

Arridge, S.R., 1995. Photon-measurement density functions. Part I: Analytical forms. Applied Optics 34, 7395-7409.

Arridge, S.R., Schweiger, M., 1995. Photon-measurement density functions. Part 2: Finite-element-method calculations. Applied Optics 34, 8026-8037.

Cen, H., Lu, R., Ariana, D.P., Mendoza, F., 2014. Hyperspectral Imaging-Based Classification and Wavebands Selection for Internal Defect Detection of Pickling Cucumbers. Food and Bioprocess Technology 7, 1689-1700.

Clark, C.J., McGlone, V.a., Jordan, R.B., 2003. Detection of Brownheart in 'Braeburn' apple by transmission NIR spectroscopy. Postharvest Biology and Technology 28, 87-96.

Elgar, H.J., Burmeister, D.M., Watkins, C.B., 1998. Storage and handling effects on a CO2-related internal browning disorder of 'Braeburn' apples. Hortscience 33, 719-722.

Fang, Q., Boas, D.A., 2009. Monte Carlo Simulation of Photon Migration in 3D Turbid Media Accelerated by Graphics Processing Units. Optics Express 17, 20178-20190.

Fraser, D.G., Künnemeyer, R., McGlone, V.A., Jordan, R.B., 2001. Letter to the Editor. Postharvest Biology and Technology 22, 191-194.

Fukui, Y., Ajichi, Y., Okada, E., 2003. Monte Carlo prediction of near-infrared light propagation in realistic adult and neonatal head models. Applied Optics 42, 2881-2887.

Hatoum, D., Hertog, M.L.A.T.M., Geeraerd, A.H., Nicolai, B.M., 2016. Effect of browning related pre- and postharvest factors on the 'Braeburn' apple metabolome during CA storage. Postharvest Biology and Technology 111, 106-116.

Hemmer, E., Benayas, A., Légaré, F., Vetrone, F., 2016. Exploiting the biological windows: current perspectives on fluorescent bioprobes emitting above 1000 nm. Nanoscale Horizons 1, 168-184.

Kou, L., Labrie, D., Chylek, P., 1993. Refractive indices of water and ice in the 0.65- to 2.5-µm spectral range. Applied Optics 32, 3531-3540.

Kuroki, S., Nishino, M., Nakano, S., Deguchi, Y., Itoh, H., 2017. Positioning in spectral measurement dominates estimation performance of internal rot in onion bulbs. Postharvest Biology and Technology 128, 18-23.

Lin, H., Ying, Y., 2009. Theory and application of near infrared spectroscopy in assessment of fruit quality: a review. Sensing and Instrumentation for Food Quality and Safety 3, 130-141.

López-Maestresalas, A., Aernouts, B., Van Beers, R., Arazuri, S., Jarén, C., De Baerdemaeker, J., Saeys, W., 2016. Bulk Optical Properties of Potato Flesh in the 500–1900 nm Range. Food and Bioprocess Technology 9, 463-470.

Martelli, F., Bianco, S.D., Ismaelli, A., Zaccanti, G., 2009. Light propagation through biological tissue and other diffusive media: theory, solutions, and software. SPIE Press.

McGlone, V.A., Jordan, R.B., Martinsen, P.J., 2002. Vis/NIR estimation at harvest of pre- and post-storage quality indices for 'Royal Gala' apple. Postharvest Biology and Technology 25, 135-144.

McGlone, V.A., Kawano, S., 1998. Firmness, dry-matter and soluble-solids assessment of postharvest kiwifruit by NIR spectroscopy. Postharvest Biology and Technology 13, 131-141.

McGlone, V.A., Martinsen, P.J., Clark, C.J., Jordan, R.B., 2005. On-line detection of Brownheart in Braeburn apples using near infrared transmission measurements. Postharvest Biology and Technology 37, 142-151.

Munns, R., Schmidt, S., Beveridge, C., 2016. Plants in Action, In: Munns, R., Schmidt, S., Beveridge, C. (Eds.), Plants In Action 2nd Ed, 2 ed. Australian Society of Plant Scientists.

Nicolaï, B.M., Beullens, K., Bobelyn, E., Peirs, A., Saeys, W., Theron, K.I., Lammertyn, J., 2007. Nondestructive measurement of fruit and vegetable quality by means of NIR spectroscopy: A review. Postharvest Biology and Technology 46, 99-118.

Palmer, K.F., Williams, D., 1974. Optical properties of water in the near infrared*. Journal of the Optical Society of America 64, 1107-1110.

Rinnan, Å., Berg, F.v.d., Engelsen, S.B., 2009. Review of the most common pre-processing techniques for near-infrared spectra. TrAC Trends in Analytical Chemistry 28, 1201-1222.

Saeys, W., Velazco-Roa, M.a., Thennadil, S.N., Ramon, H., Nicolaï, B.M., 2008. Optical properties of apple skin and flesh in the wavelength range from 350 to 2200 nm. Applied Optics 47, 908-919.

Savo, R., Pierrat, R., Najar, U., Carminati, R., Rotter, S., Gigan, S., 2017. Observation of mean path length invariance in light-scattering media. Science 358, 765-768.

Sun, J., Künnemeyer, R., McGlone, A., Tomer, N., 2016. Investigation of light transmission in healthy and rotten onions, Electronics New Zealand Conference, Victoria University of Wellington, pp. 142-145.

Sun, J., Künnemeyer, R., McGlone, A., Tomer, N., 2018. Optical properties of healthy and rotten onion flesh from 700 to 1000 nm. Postharvest Biology and Technology 140, 1-10.

Upchurch, B.L., Throop, J.A., Aneshansley, D.J., 1997. Detecting internal breakdown in apples using interactance measurements. Postharvest Biology and Technology 10, 15-19.

Van Beers, R., Aernouts, B., Watté, R., Schenk, A., Nicolaï, B., Saeys, W., 2017. Effect of maturation on the bulk optical properties of apple skin and cortex in the 500–1850 nm wavelength range. Journal of Food Engineering 214, 79-89.

Wang, H., Peng, J., Xie, C., Bao, Y., He, Y., 2015. Fruit Quality Evaluation Using Spectroscopy Technology: A Review. Sensors 15, 11889.

Wang, M., Wu, C., Sinefeld, D., Li, B., Xia, F., Xu, C., 2018. Comparing the effective attenuation lengths for long wavelength in vivo imaging of the mouse brain. Biomedical Optics Express 9, 3534-3543.

Yamada, Y., Okawa, S., 2014. Diffuse optical tomography: present status and its future. Optical Review 21, 185-205.

Chapter 6

Optical Properties of Healthy and Rotten Onion Flesh from 700 to 1000 nm

---

A journal paper

by

Jason Sun, Rainer Künnemeyer, Andrew McGlone, Nathan Tomer

Published in

Postharvest Biology and Technology

I prepared the initial draft manuscript, which was refined and edited in consultation with co-authors. Nathan designed and carried out the juice transmittance measurement. Andrew McGlone collected the IAD data. I conducted the NIRS and laser transmittance measurements, and processed the data to the form in which it is presented. My supervisors provided guidance throughout this project.

Postharvest Biology and Technology 140 (2018) 1–10

Contents lists available at ScienceDirect

Postharvest Biology and Technology

journal homepage: www.elsevier.com/locate/postharvbio

Optical properties of healthy and rotten onion flesh from 700 to 1000 nm

Jason Sun[a,b,*], Rainer Künnemeyer[a], Andrew McGlone[b], Nathan Tomer[b]

[a] Dodd Walls Centre for Photonic and Quantum Technologies, School of Engineering, University of Waikato, Hamilton, New Zealand
[b] The New Zealand Institute for Plant and Food Research, Hamilton, New Zealand

ARTICLE INFO

Keywords:
Onion
Optical property
Juice
Sensor
Laser
NIRS

ABSTRACT

To facilitate the design of an optical system for detecting internal rot in onions, the light propagation properties in healthy and rotten onions were studied in the 700 to 1000 nm range. The absorption and reduced scattering coefficients of internal onion tissues were measured using a combination of measurements on excised onion slices, using the Inverse-Adding Doubling method (IAD), and light transmittance measurements on extracted onion juice. Standard NIRS transmittance measurements were made on intact onions, revealing a transmission window in the range of 670 to 950 nm. From 700 to 750 nm, more severely rotten onions had lower transmittance, whereas from 850 to 900 nm onions with larger rotten tissue had higher transmittance. A multi-laser light transmittance system was implemented to make accurate measurements for different source-detector positions around intact onions, enabling calculations of attenuation coefficients at 636, 700, 728 and 804 nm. The results showed the onion juice measurements yielded much more accurate absorption coefficients than the IAD method on the onion slices. The attenuation coefficients calculated using accurate optical properties were generally matched with the light transmission characteristics, and were in good agreement (6% on average) with the measured attenuation coefficients for both healthy and rotten onions at 700, 728 and 804 nm.

1. Introduction

Onion is an important vegetable with a production of approximately 93 million tons in 2016 (FAOSTAT, 2016). Consumers have increasingly high expectations of quality in terms of nutritional value, appearance, flavour, and absence of defects (Griffiths et al., 2002). To meet the quality demand from consumers, particularly with regard to individual onion quality, non-destructive methods for quality assessments must be developed. Optical methods have the inherent advantage of being typically non-destructive, fast and low-cost. NIR spectroscopy (NIRS) is one optical technique routinely used for detecting internal defects in horticultural produce. It is particularly effective if the defect is large and/or of a generalised nature in the tissue (Khatiwada et al., 2016; McGlone et al., 2005; Nicolaï et al., 2007). The typical NIRS set-up uses a broadband light source to illuminate the sample, and the transmitted or reflected light is measured using a spectrometer. The spectral data collected by the spectrometer is used to create predictive models. The set-up can be in transmittance mode (light source and sensors positions on opposite sides of the produce), reflectance mode (source and sensor on the same side) or some in-between interactance mode (source and sensor separated by a light barrier to avoid specular reflection) (Schaare and Fraser, 2000; Sun et al., 2017). The choice of mode is a design consideration relying on NIRS knowledge and the practicalities of measurement.

Onion defect detection by NIRS has been examined previously by other researchers. Ito and Hattori (2012) and Ito and Morimoto (2014) used a portable interactance mode NIRS system (K-BA100R) to measure the stem end (shoulder part) of the onion. They used the spectra in the Herschel region of the NIR (750–1100 nm) to build multivariate models to predict the rottenness of the onion, and their models could detect 83.2% and 91.4% of the rotten onions, respectively. However, the measurements were manually targeted on the stem end where the symptoms occurred, and the degree of rot in the samples was not clearly stated. Among the three modes, a transmittance system is probably most appropriate for internal rot detection as the longer and deeper penetrating light paths mean that the light will likely be more affected by the rotten tissues. Kuroki et al. (2017) investigated NIRS transmittance system at six bulb positions. The onions were divided into 6 levels from 0 to 6 according to the degree of rot. At the optimal bulb position, the authors achieved a high accuracy (98.4%) for onions above level 1, but the accuracy was significantly lower for level 1 (slightly rotten) onions (56.3%), and the detection rate for healthy onion was only 81.8%. An NIRS system is only sensitive to a defect if the detected light is affected by the defect to a detectable level; some of the transmitted light paths must intersect with the defect. This may not be the case for small internal rots in onion as the rotten tissue, for instance, may be

* Corresponding author at: Dodd Walls Centre for Photonic and Quantum Technologies, School of Engineering, University of Waikato, Hamilton, New Zealand.
E-mail address: jason.sun@plantandfood.co.nz (J. Sun).

https://doi.org/10.1016/j.postharvbio.2018.02.006
Received 25 October 2017; Received in revised form 9 February 2018; Accepted 13 February 2018

strongly localised to the stem end and so effectively not intersecting with the typical transmitted light paths for NIRS. Quantified understanding of light propagation is then required to effectively and efficiently design improved NIRS systems, so the small and localised defect can be detected. Reliable knowledge about the optical properties in healthy and rotten onions becomes important then as key inputs for the necessary light transport modelling.

Light propagation in biological materials can be characterised by the fundamental/bulk optical properties of tissue, namely the bulk absorption coefficient (μ_a), bulk scattering coefficient (μ_s), refractive index (n), and anisotropy factor (g). Typically the scattering and anisotropy factors are further combined to yield a reduced scattering coefficient (μ_s'), a coefficient more useful for describing the very diffuse nature of light transport in strongly scattering biological materials such as fruit and vegetables (Rowe et al., 2014; Wang et al., 2014). A primary method for measuring optical properties of biological tissue is the Inverse Adding Doubling (IAD) method that involves a combination of transmittance and reflectance measurements on thin slices of tissue followed by iterative data processing to calculate the optical properties (Prahl, 2011; Prahl et al., 1993). The method has been used extensively on biomedical materials (Kim and Wilson, 2011) but also more recently on horticultural products such as apple (Rowe et al., 2014; Van Beers et al., 2017), potato (López-Maestresalas et al., 2016) and onions (Wang et al., 2012; Wang et al., 2014). The IAD method is considered the 'gold standard' method for optical properties if a thin homogenous slab or slice is available (Van Beers et al., 2017). Wang et al. (2014) used the IAD method to measure optical properties of dry skin and the flesh of healthy and botrytis infected onion, reporting typical values of μ_a = 0.02 and 0.1–0.3 mm^{-1} and μ_s' = 1 and 0.8 mm^{-1} for the flesh of healthy and rotten onions respectively, in the wavelength range of 450–850 nm.

However, Zhu et al. (2007) suggested the IAD method will work best on samples with relatively high absorption ($> 0.02\ mm^{-1}$) or scattering ($> 16\ mm^{-1}$), which is generally not the case for fresh produce in the Herschel region of the NIR. Moreover, Prahl (2011) stated in the IAD manual that the light loss, where light escapes outside edges of the sample, leads to erroneously high absorption coefficients because all lost light is attributed to absorption by the sample. Zhu et al. (2007) investigated this effect by comparing IAD measurements with Monte Carlo (MC) simulations. They concluded that the light loss greatly increases the estimated error of the absorption coefficient and only slightly affects the scattering coefficient. They also found that increasing the sample port size, or decreasing the thickness of the sample, can reduce the light loss effectively. However with biological specimens, like onion tissue, it can be very difficult to prepare uniformly thin slabs of enough area to cover the sample port in a typical IAD system setup, particularly so with rotten onion tissue.

A newer version of IAD (since 3.6.0 - c. 2011) has incorporated MC code to account for the light loss from the edge of the sample (Prahl, 2017). Rowe et al. (2014) measured the optical properties of four concentrations of Intralipid® solutions, which had the typical optical properties of fresh produce, and discovered that with the newer version of the IAD program, the scattering was accurately determined, but there was still a considerable baseline offset for the absorption values due to the light loss effect. Saeys et al. (2008) arrived at the same conclusion, they found the reduced scattering coefficient for apple flesh was reliably determined by the IAD method but not necessarily the absorption coefficient. Tomer et al. (2017) similarly concluded that while the reduced scattering coefficient at 785 nm for healthy onion flesh was correct, the absorption coefficient was probably being overestimated by a factor of 5. Other than inaccurate absorption values, Rowe et al. (2014) reported a small amount of crosstalk in the reduced scattering coefficients, in the wavelength range from 400 to 1050 nm for apple flesh.

This study was aimed at providing accurate light propagation properties for healthy and rotten onions, particularly focused on the wavelength range from 700 to 1000 nm. Optical properties of excised onion tissue, both healthy and rotten, were then estimated using a new method, which is a combination of both the IAD method on this tissue slices, for the reduced scattering coefficients, and a transmission method on extracted juice for the absorption coefficients. To validate the accuracy, NIRS transmittance measurements were made on whole onions to establish the key spectra characteristics distinguishing different degrees or levels of rots. A multi-laser system was then used to study the light transport in whole onions, generating intensity as function of source-detector distance data for measuring the light attenuation coefficient at different key wavelengths. The accuracy of the optical properties was then judged by comparing attenuation coefficients calculated indirectly from the optical properties with those measured directly by the multi-laser system on the whole onions.

2. Optical property estimation

2.1. Methodology

2.1.1. Sample preparation

In order to provide rotten onions for the measurements two types of inoculum were used. Botrytis fungus, which causes neck rot, and pseudomonas bacteria, which causes slippery skin rot (Harrison et al., 2008). Each onion was trimmed at the stem end to reveal a small amount of healthy white tissue. A fresh puncture wound in the centre of the leaf stalk scar was created with a hot (200 °C) 1 mm diameter copper wire attached to a soldering iron gun. The hot wire was briefly pushed about 10 mm into the crown of the onion. Once the wound had cooled, a 50 µL aliquot of inoculum was applied to the surface of the stalk scar, centred on the visible hole just created by the hot wire. After allowing a few minutes for the inoculum to soak into the stalk scar, the onions were placed inside a cardboard box, covered with high density polyethylene box liner film, to loosely seal them and incubated at 22 °C in saturated humidity. After two weeks the temperature of the incubator was reduced to 2° in order to slow down rot growth. All the measurements began after the onions were kept at room temperature for five hours. Three types of onions were prepared: healthy control, botrytis infected and pseudomonas infected.

2.1.2. IAD on onion slices

Our IAD measurement method was as described in detail by Rowe et al. (2014), involving a 83.8 mm diameter integrating sphere (4P-GPS-033-SL, Labsphere, New Hampshire, USA) with a 38.1 diameter sample port, a 50W quartz tungsten halogen lamp (6884, Newport, Irvine, USA), and a spectrometer (MMS1, Zeiss, Oberkochen, Germany). The system measured the reflectance and transmittance of an onion slice held between two panes of glass of thickness 1.12 mm. The onion slice samples were about 2–3 mm thin longitudinal onion slices taken parallel to the stem-root axis and from a zone about 10 mm in towards the central core from the surface. Taking slices of healthy tissue was easy if the samples were not too thin, but excising rotten tissue slices was a difficult and delicate manual exercise as rotten tissues do not have the mechanical integrity of healthy tissue. There were many failed attempts before getting intact samples of sufficient size to cover the sample port of the integrating sphere, eventually two healthy and two rotten slices were measured. The reflectance and transmittance spectra were processed to provide absorption and reduced scattering coefficients using version 3.9.10 of the IAD program, with assumed a refractive index of 1.33 and 1.52 for the onion tissue and the glass panes respectively.

The scattering anisotropy factor, g, was set at g = 0.5 and 0.7 for healthy and rotten onions in the IAD calculations. The factor is a measure of the average degree of forward scattering occurring during a single scattering event, with g = 0 being isotropic scattering and g = 1 being full forward scattering. It has been established that the value of g is largely irrelevant, and difficult to accurately measure, when using the IAD method on thick sample slabs of highly scattering materials

(Aernouts et al., 2013; Saeys et al., 2008). Measurement variation of up to ± 50% has been reported for g measurements on onions, with average g around 0.5 and 0.7 for the healthy and rotten onion flesh in the 700–1000 nm range (Wang et al., 2012). Our calculations of absorption and scattering coefficients varied very little, less than 5%, when varying g between 0 and 0.8. Essentially, for our types of samples, it is an arbitrary constant that we are free to choose. Typically biological materials have a g-value of about 0.8 (Jacques, 2013).

A Mie scattering model (Dehghani et al., 2008) was used to estimate reduced scattering coefficients that are close to the actual ones without crosstalk (solid line in Fig. 2b):

$$\mu_s'(\lambda) = a\lambda^{-b} \quad (1)$$

where a is the scattering amplitude, b is the scattering power, λ is the wavelength of light in μm. Suitable values of a and b were found manually by fitting the equation to the experimental scattering results. We set a to be 1.28 and 0.57, b to be 0.22 and 0.67 for healthy and rotten tissues.

2.1.3. Direct transmittance on onion juice

One healthy, one pseudomonas and one botrytis onions were selected for this experiment. The healthy and rotten onion tissue were each blended (Model 900, Nutribullet LLC, Pacoima, CA, USA) and then centrifuged at 10,000 rpm to provide a lightly coloured clear juice as a supernatant (light yellow for healthy tissue and light brown for rotten tissue). The juice was carefully removed and its absorption coefficient was measured by direct light transmittance through a 40 mm fused silica cuvette of side width 1 mm. Preparation by centrifuging removed most of the particulate matter and minimised light loss caused by scattering. The transmission cell set-up used a 400 μm (P400-1-VIS-NIR, Ocean Optics, FL, USA) and a 50 μm (P50-1-VIS-NIR, Ocean Optics, FL, USA) optical fibres with collimators (F260SMA-B, Thorlabs, Newton, NJ, USA) for light delivery and collection (Fig. 1). The spectrometer and light source as mentioned in Section 2.1.2 were used. Multiple reflection events occurred when the light went through the interfaces between air and cuvette, and between cuvette and liquid. The associated light loss was accounted for through Markov chain processing (Hébert et al., 2007). Laboratory tap water was also measured separately, and then compared with water reference data (Kou et al., 1993) to evaluate the accuracy of the measurement system.

2.1.4. Attenuation coefficient

The attenuation coefficient, also sometimes called the effective attenuation coefficient or extinction coefficient, indicates how much light is attenuated per mm across a path in a medium due to the combination of absorption and scattering losses. It is calculated as:

$$\mu_{eff} = \sqrt{3\mu_a\mu_s'} \quad (2)$$

where μ_a is the absorption coefficient and μ_s' is the reduced scattering coefficient, with the formula being derived from the diffusion approximation to the fundamental light transport equations (Martelli et al., 2010).

2.2. Results

2.2.1. IAD on onion slices

The absorption coefficient spectra measured on healthy and rotten onion tissue showed the expected strong water absorption peak at about 980 nm (Fig. 2a). For healthy tissue only, there was also a small peak at around 680 nm that is presumably due to chlorophyll-a (Munns et al., 2016). That the peak was missing for the rotten tissue absorption spectra indicates either a lack of chlorophyll-a content or the overwhelming dominance of other absorption in that wavelength range for the rotten tissue. The baseline of the rotten tissue absorption coefficient spectra was 2 to 3 times higher than that for the healthy tissue, and it rose more steeply for lower wavelengths in the visible range down to 500 nm. As discussed in the introduction, both from our laboratory (Tomer et al., 2017) and others (Saeys et al., 2008; Zhu et al., 2007), the absorption coefficient values calculated through the IAD method, as employed here, are likely incorrect in absolute magnitude although spectrally correct in a relative sense across the wavelength range. This inaccuracy in magnitude lead to the development of the new method described in this paper of estimating the absorption coefficient from transmittance measurements on extracted onion juice.

The reduced scattering coefficient spectra calculated from measurement on the onion slices is believed to be quite reliable (Saeys et al., 2008; Tomer et al., 2017). There were large differences between healthy and rotten onion tissue (Fig. 2b). The rotten tissue spectra were about 1.5 to 2 times lower and dropped more steeply with increasing wavelength. There are crosstalk features at 670 and 980 nm for healthy onion tissues, which correspond to peaks in the absorption coefficient spectra.

2.2.2. Light transmittance on onion juice

Light transmittance measurements of the absorption coefficients of the laboratory tap water were in good agreement (mean absolute difference of 7.35% from 700 to 950 nm) with the literature values (Kou et al., 1993) for water in the NIR range, verifying the accuracy of the method (Fig. 3a). For all the onion juices, there was a significant departure from water absorption below 900 nm (Fig. 3b). The absorption coefficient was fairly flat at 600–700 nm for juice from healthy onions. Juice from rotten onions had much higher absorption coefficients than that of healthy onions, the difference generally increasing with the decreasing wavelength. It is noted that rotten onion juice had slightly higher absorption coefficients at 700 nm than that of 800nm, which is the opposite case for healthy onions.

3. Light transmittance measurement

3.1. Methodology

3.1.1. NIRS transmittance

As the rots in the onions were localised towards the stem end, the light source and detector were arranged in a 'V' shape (Fig. 4) in which more light would go through the rotten tissues. It was expected that the

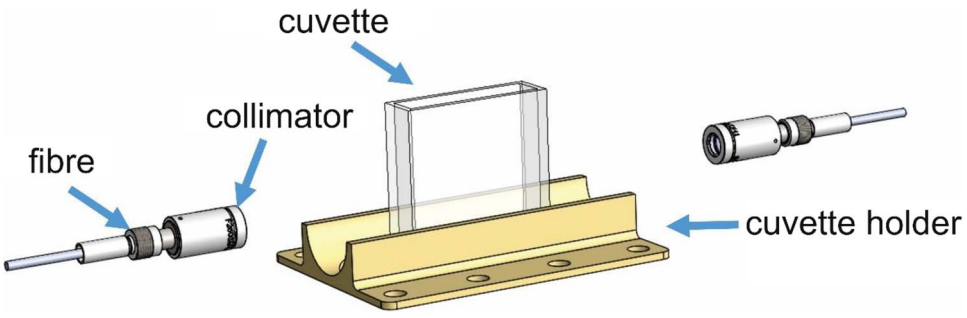

Fig. 1. Schematic of the experimental setup for the juice transmittance measurement.

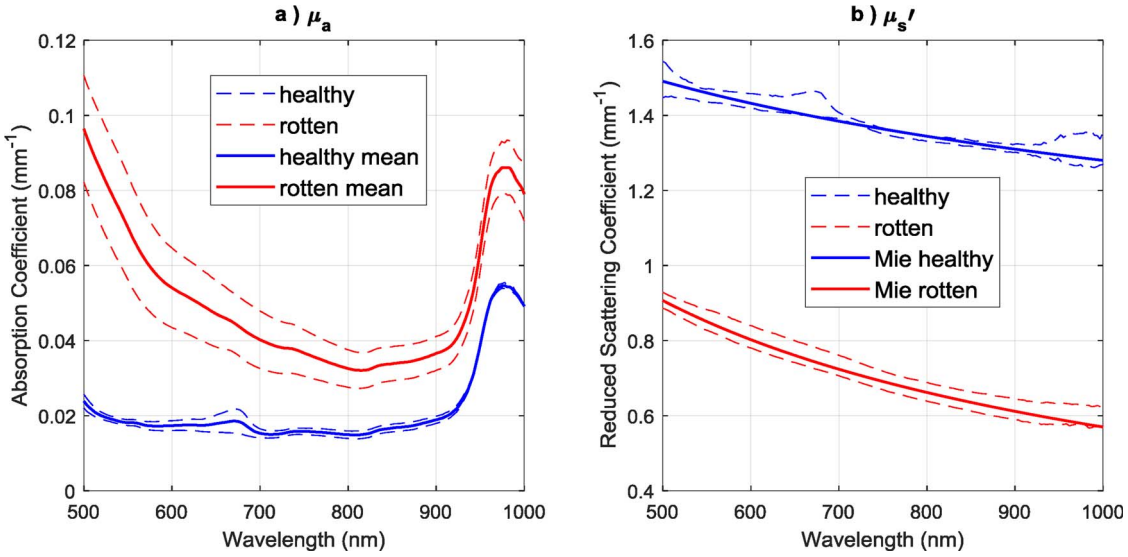

Fig. 2. Optical properties of healthy and rotten onion tissue slice: (a) the absorption coefficient and (b) the reduced scattering coefficient.

spectra collected by the spectrometer would then be more affected by the rot. The light source was a 250 W tungsten halogen lamp (6334NS, Newport, Irvine, CA, USA) driven by a digital radiometric power supply (69931, Newport, Irvine, CA, USA). The source light was coupled to the onion using a 14 mm diameter light pipe. The transmitted light was detected by a CCD spectrometer (CD024321, Control Development, South Bend, IN, USA) through a 1000 µm core diameter multimode fibre (M35L01, Thorlabs, Newton, NJ, USA). The integration time was 0.1 s. Both light pipe and fibre had an in-house designed adaptor for attachment to the onion, which had rubber seals to prevent unwanted stray light.

The measured raw spectra were processed to minimise effects due to variation in the light source output, the detector sensitivity, and variation in light paths due to differences such as onion size and shape. Normalised transmittance spectra were first obtained from the raw spectra by subtracting the dark current spectra and dividing by a reference spectra of the light source. The reference spectra were recorded by removing the onion from the light path and using a reduced integration time. To minimise variation due to intensity changes, such as those arising from differences in onion size and shape, the spectra were further normalised to have the same unit area of 1.

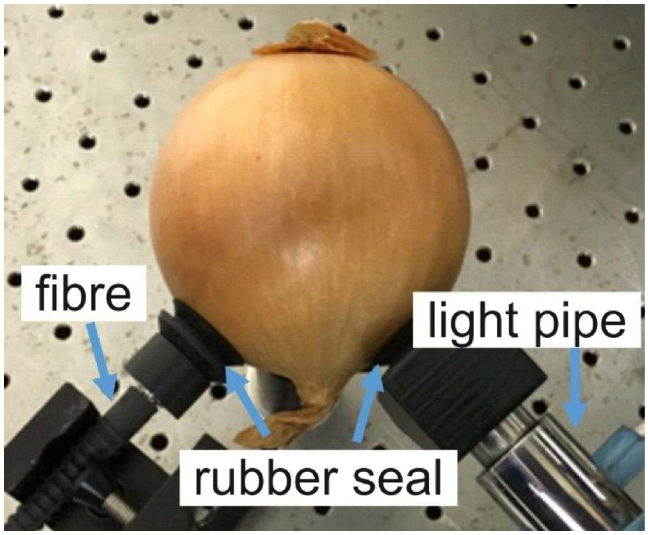

Fig. 4. Hardware setup of NIRS transmittance measurements. The light entered from the light pipe, and is collected by the fibre.

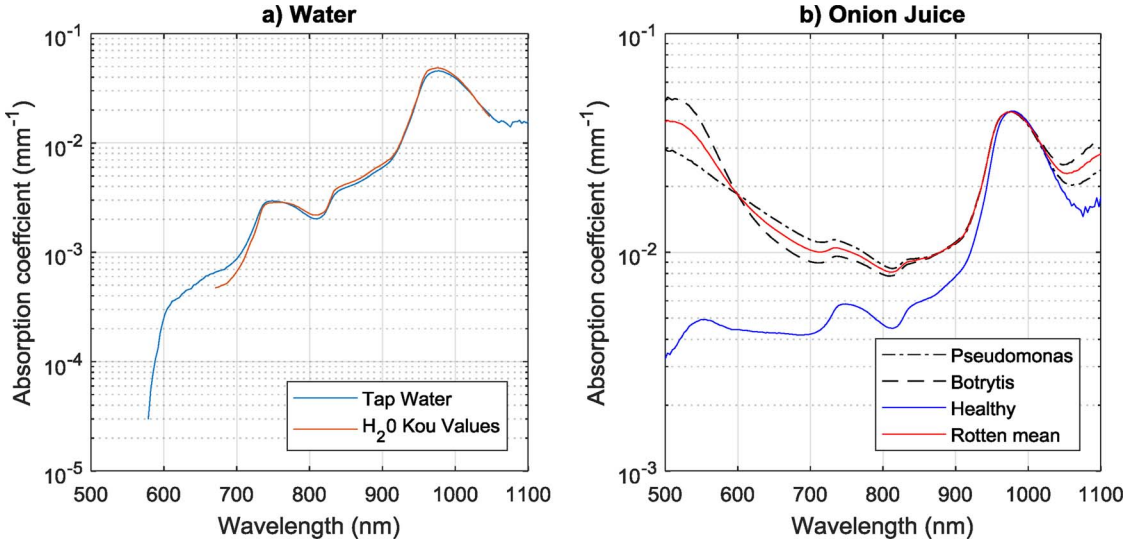

Fig. 3. (a) Comparing water measurement to literature values to validate the system. (b) The absorption coefficient for onion juices.

Fig. 5. Severity score according to the degree of rot from the cut surface. For these examples, Score 1 and 4 were caused by botrytis, score 2, 3 and 5 were caused by pseudomonas.

Onions were cut vertically (from the neck to the basal plate) after the measurements and were scored visually according to the degree of rot on the cross section (Fig. 5). It can be seen that pseudomonas caused rotten tissues on certain layers (Score 2, 3 and 5 in Fig. 5), while botrytis infected more layers and occupies a whole area (score 1 and 4 in Fig. 5). Both types of rots are more localised to the stem end where the inoculation took place, which is also the case for naturally occurring rots in onions. For quantification of degree of rot, Kuroki et al. (2017) used a scalpel to section the rotten tissue, the degree of rot was the weight of rotten tissue divided by the whole onion. They later found the visual scoring method was almost equivalent to the weighing method with r = 0.9868.

The onion were also scored based on the size of sprouting on the cross section image using a similar assessment method. Onions with significant internal sprouting growth were removed from the analysis to avoid any interference and/or confusion due to the sprouting. In total, 41 healthy and 92 rotten onions were measured by the NIRS transmittance system (Fig. 6). Most onions were not severely rotten; of the rotten ones 68 were below severity score 4.

3.1.2. Multi-laser transmittance

The laser system consists of four lasers operating at different wavelengths: 636, 700, 728 and 804 nm. The laser wavelengths were chosen on the basis of previously measured NIRS transmittance spectra, selecting wavelengths near the two main peaks (see Fig. 9), although the convenient (commercial) availability of some lasers was an important factor too. The 700 and 728 nm lasers were chosen as they were in the close vicinity of the first major transmittance peak (~710 nm), that changes significantly with the degree of rot. The 804 nm laser was selected as it was close to the second major peak, at c. 810 nm, and also light is most penetrating at around this wavelength. The small difference between healthy and rotten onions at this wavelength makes it a useful reference point to account for onion geometry and any drifts in the system, such as light source variations. The lower wavelength laser, at 636 nm, was selected as it was possibly interesting in terms of chlorophyll absorption, which typically peaks at c. 670 nm but can be quite broad with a measurable presence down at 636 nm. However the visible region below 700 nm is of very high light absorption for onions and so the usefulness of a laser in that region may be less than at the other higher laser wavelengths. Each laser diode was mounted in a laser diode mount (LDM21, Thorlabs, Newton, NJ, USA) driven by a laser diode driver and controller (ITC102, Thorlabs, Newton, NJ, USA). Two lenses were used to focus the light to a 5 mm radius spot. An adjustable pinhole was used to remove the elliptical shape of the beam and any stray light.

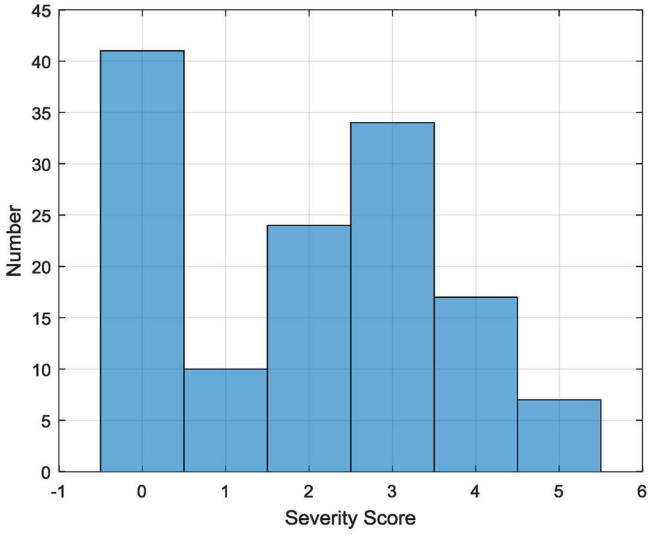

Fig. 6. Rot severity scores of onions used in the NIRS transmittance measurements.

The detector consisted of a silicon photodiode (FDS100, Thorlabs, Newton, NJ, USA) and a trans-impedance amplifier (DLPCA-200, Femto, Berlin, Germany) which was mounted on the turn table (Fig. 7a). The connection was made as short as possible to reduce noise. The stepper motor was used to rotate the turn table, which was driven by an Arduino based controller with a micro-step driver (JK1545, Jingkong Motor & Electric Appliance, Changzhou, China). A Matlab GUI was written to control the turn table and record the subsequent data.

The onion was put on a cup so that it would stay stationary while the table was rotating. As the detector was mounted on the rotating table, it is stationary in the reference frame of the onion. In each scan, the detector position was fixed, and the source (laser beam) location was rotated around the onion as illustrated in Fig. 7. The table rotated 11.25° each time, which formed 21 source locations from 67.5° to 292.5°. For examining the whole onion, measurements were carried out on three latitudes: top, middle and bottom (Fig. 7b). In total, each onion was measured with 63 source and 3 detector positions. Three replicate measurements were carried out on each onion.

Three intact onions were selected as their skin had relatively uniform colour and thickness by visual inspection, their cut surface shown in Fig. 8. The uniform skin allowed us to calculate the attenuation coefficient without the skin interference. The botrytis and pseudomonas infected onions had at least 50% (Score 5) infected tissue (Fig. 8) so that we could investigate the light transmission which was strongly affected by rotten tissue. The diameter of each latitude was measured for the source-detector distance calculations.

The laser system allowed us to calculate the actual light transmittance through onion using Eq. (3):

$$Transmittance = \frac{V}{RG\,P_{in}} \quad (3)$$

where V is trans-impedance amplifier, P_{in} is the input laser power (W) measured by a light power meter (Nova, Ophir Optronics, Jerusalem, Israel), R is the responsivity of the photodiode (A/W), and G is the transimpedance gain of the amplifier (V/A).

3.2. Results

3.2.1. Light transmittance

There is high transmittance in all onions between 670–950 nm, yielding low noise spectra in that range (Fig. 9). The displayed spectra

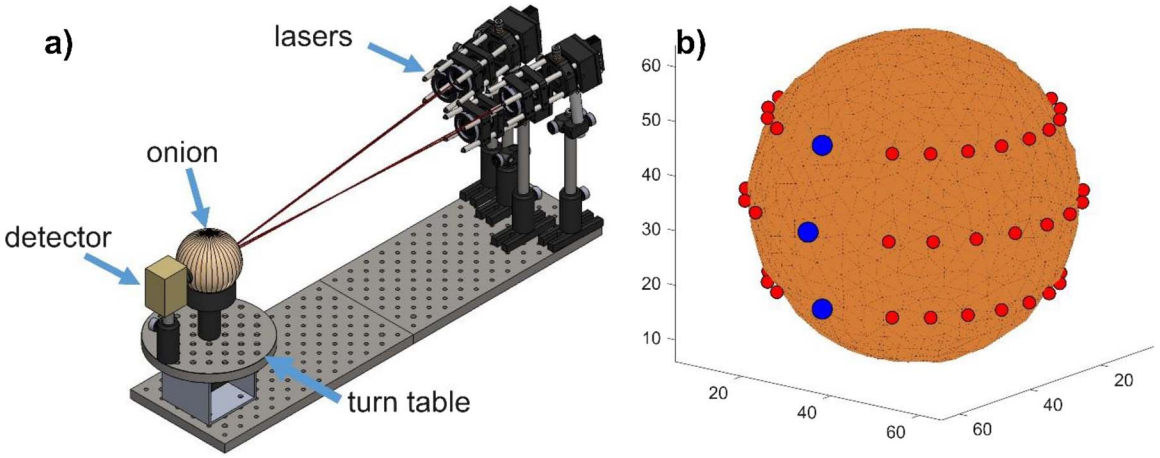

Fig. 7. (a) Experimental setup of the multi-laser system. (b) Source and detector locations; blue and red dots are the detectors and sources respectively. Mesh sphere represents an onion.

are area normalised to minimise intensity differences due to sample geometry, such as size and shape features of the onions that affect the average light transmission path-length and thus the measured light intensity. Area normalisation cannot fully eliminate path-length variations, but relative spectral features, such as peaks and dips, should largely be preserved. Useful inferences about the fundamental optical properties involved should be possible.

The normalised signal is rapidly attenuated below 700 nm, presumably the light strongly absorbed by high levels of chlorophyll (broad peak absorbance c. 670 nm); the normalised signal is also rapidly attenuated above 900 nm, due to the strong water absorbance peak at c. 960 nm (Clark et al., 2003; Kuroki et al., 2017; Rowe et al., 2014; Saeys et al., 2008; Van Beers et al., 2017). The healthy (score 0) and rotten (score > 0) spectra both had two transmittance peaks at about 710 and 810 nm. The error bar in Fig. 9 represents one standard deviation at the double peaks and 875 nm, the standard deviation at each wavelength point of all the spectra in Fig. 9 is less than 0.013 units and the average is less than 10% of the peak at 800 nm.

The amount of internal rotten tissue affected the normalised light transmission, especially in the range of 700–750 nm and 850–900 nm. From 700 to 750 nm, the more rotten the onions were, the lower the transmission and presumably due to the increased absorbance of the brown rotten tissue in that range. That trend was reversed in the range 850–900 nm, with the more rotten onions having higher transmission and is attributed to the net effect of a higher absorption coefficient for rotten tissue being countered by a simultaneous lowering of the scattering coefficient, as indicated in Figs. 3b and Figure 2a. From about 780–810 nm, all spectra were very close and/or overlapping, suggesting a less rot sensitive region although the area normalisation process may be minimising the observation of sensitivity in that region. The results

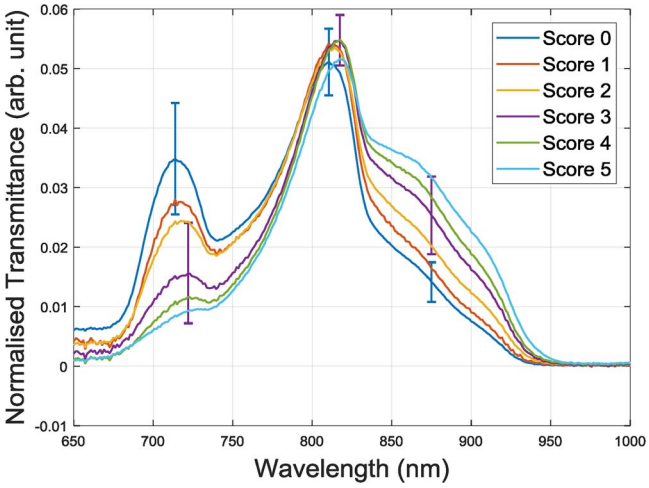

Fig. 9. Effect of the internal rot, each trace is the mean transmission of onions with severity scores from 0 to 5. The error bars were at the two peaks and 875 nm for score 0 and 3 spectra.

were matched to the normalised absorbance spectra reported by Kuroki et al. (2017), who used a similar measurement setup, and are also consistent with those made on apples afflicted with brownheart (Clark et al., 2003).

The average laser light transmittance, as a function of laser incident angle, demonstrated a broad 'U" shaped pattern with a minimum transmittance at about 180° (Fig. 10). The basic pattern was consistent for each laser wavelength and for each onion type, the Control

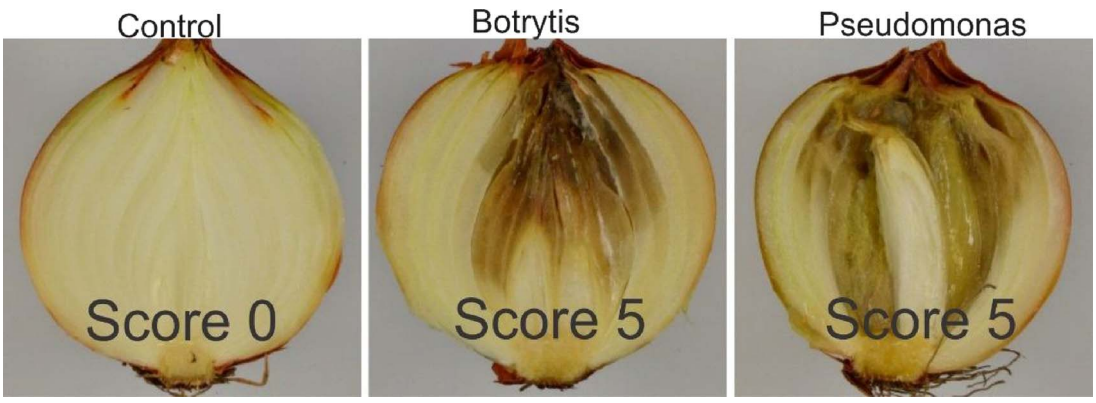

Fig. 8. Cross sections of the three onions measured: control, botrytis and pseudomonas.

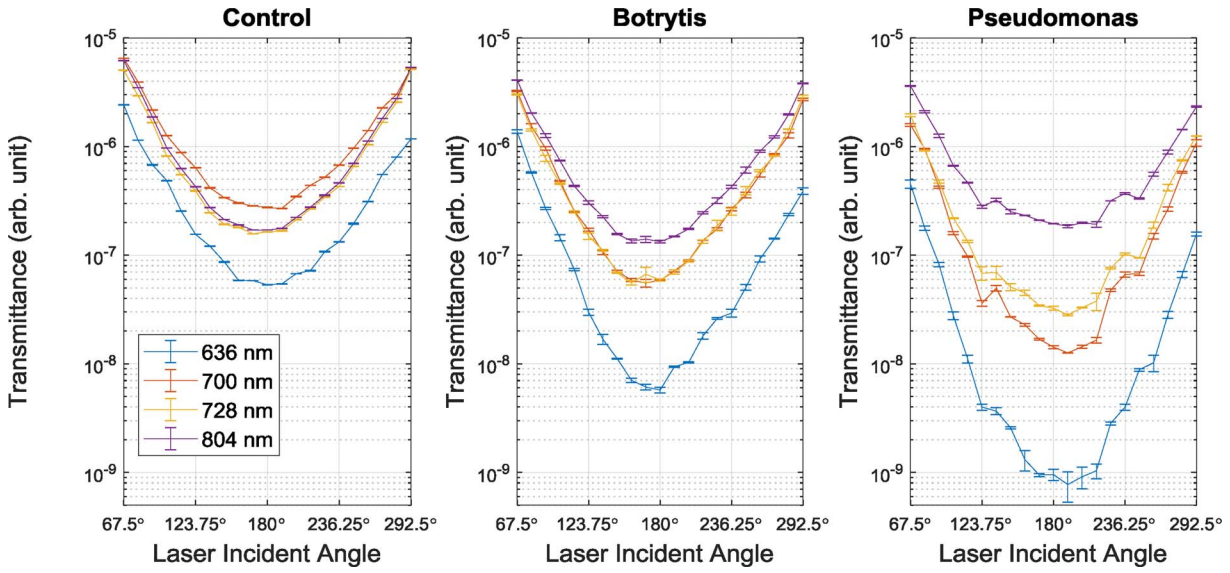

Fig. 10. Average laser light transmittance as a function of the laser incident angle at the top latitude on each of three onions. Error bars are 5 times standard deviations calculated from 3 replicate readings on the same onion.

(Healthy), Botrytis or Pseudomonas infected onions. The patterns were not perfectly symmetric, around 180°, probably due to slightly skewed features in the shape and/or internal structure of the onions. The measurements were very stable. The error bars in Fig. 10 were set to five times the standard deviation of the three replicates to make the error bars visible. The 804 nm laser light had the highest transmittance and did not vary greatly in average magnitude between the Control and the two infected onions, which is also the case in Fig. 9 for the normalised spectra. The 636 nm laser light transmittance was at least an order of magnitude lower than that at the other laser wavelengths, and much lower again for the infected onions compared to the Control - this was not observable in Fig. 9 as the signal there was too low. The 700 and 728 nm laser light transmittances were in between the values of the other two lasers, and much closer to the 804 nm transmittance. The light transmittance at 636, 700 and 728 nm was closer to 804 nm transmittance for the Control, the difference increased for the rotten onions. The same general trends were observed at each of the three measurement latitudes, and were consistent with spectral characteristics shown in Fig. 9 for the area normalised transmission spectra.

Fig. 11 shows laser light transmittance as a function of wavelength for the 180° laser incident angle. In most cases the top latitude measurements were the lowest; the middle and bottom were similar for Healthy and Botrytis. The Pseudomonas had similar measurements for all three latitudes, its rotten tissue was more spread in the Pseudomonas onion (Fig. 8), so the attenuations were similar across the three latitudes. The upper limit of chlorophyll absorption is about 710 nm (Munns et al., 2016). The Control onion had similar trends for middle and bottom latitude, where the transmittance at 700 nm was about 2.5 times higher than that of 728 nm. For the top latitude, the Healthy onion had similar transmittance at 700 and 728 nm. This indicates there were more green tissue on the top than the bottom for the Healthy, which is indicated in Fig. 8.

3.2.2. *Attenuation coefficients*

The laser light transmittances were turned into attenuation coefficients by first converting the laser light incident angles into the equivalent of source-detector distances, assuming the onions had constant diameter on each measurement latitude. For example, for the control onion at 728 nm, the transmittance changed linearly with source-detector distance on a log scale (Fig. 12). The pattern was similar for different onions and wavelengths. Using a linear regression on each set of measurements attenuation coefficients could be calculated for each onion and wavelength.

For all three onions at all four wavelengths, the middle position had the lowest attenuation coefficients, while the bottom position (stem-basal plate axis) had the highest (Fig. 13). The higher attenuation from the top and bottom of the onion agreed with results from Kuroki et al. (2017). Using the control onion as a reference, the attenuation was directly linked to the degree of rot in onions. Pseudomonas had a larger area of rotten tissue across the three latitudes (Fig. 8), so its attenuation

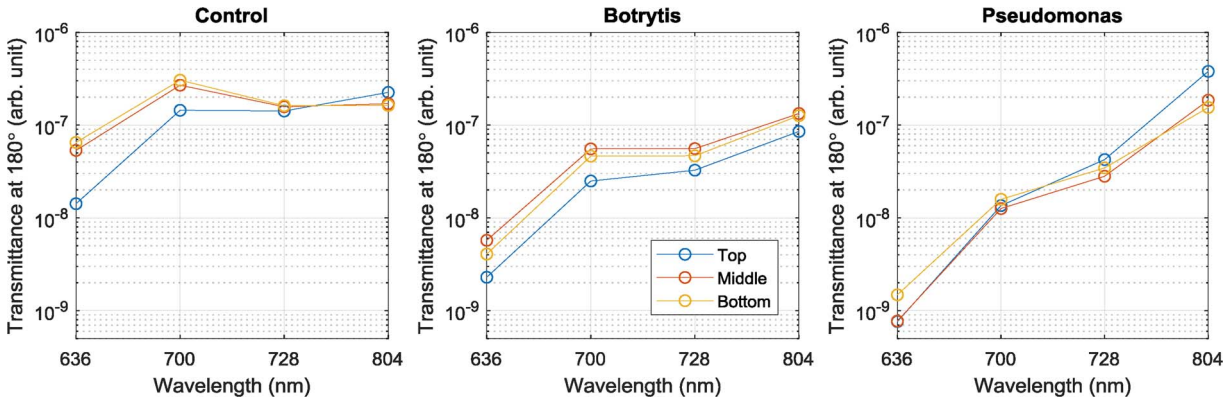

Fig. 11. Light transmission at laser incident angle 180° on three different latitudes for the three onions. Each data point is the mean of the three scans.

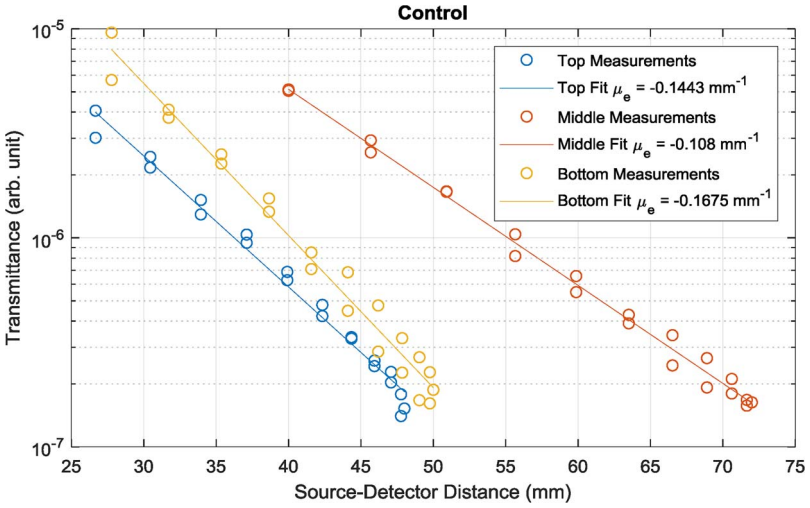

Fig. 12. Light transmission versus source-detector distance for the control onion at 728 nm. The slope of the fit line is μ_e, which is the effective attenuation coefficient.

coefficients were the highest for 636, 700 and 728 nm. Fig. 9 shows that 804 nm was not sensitive to the rotten tissue, Pseudomonas in this case had the lowest attenuation coefficients.

The effective attenuation coefficients of onion tissue can be calculated using equation 2. This allows comparison of attenuation through idealized onion tissue with optical properties measured in two different ways, shown in Fig. 14. The Juice & Slice method used average μ_a from the juice transmittance measurements and average μ_s' from the IAD slice measurements (Fig. 14a). Average values for rotten juice were calculated by averaging the μ_a values from the botrytis and pseudomonas measurements. The Full Slice method used both average μ_a and μ_s' from the IAD slice measurements (Fig. 14b).

It is clear that the absolute attenuation coefficients derived using the Juice & Slice method are in good agreement with those measured directly from the laser light transmittance measurements (Fig. 14 and 15). The average discrepancy for Juice & Slice and Full Slice method were 6.0% and 90% respectively. The large discrepancy for the Full Slice method was mainly caused by the elevated absorption coefficient values as its spectral shapes were similar to those of Juice & Slice method.

For both methods, the healthy onion had higher attenuations around 850 to 1000 nm, which was consistent with the observations made on the NIRS transmittance spectra (Fig. 9). Above 730 to 810 nm, the Juice & Slice method showed that the healthy onion had slightly larger attenuations than the rotten onions, while in the Full Slice method the healthy onions had slightly lower attenuation coefficients over the range 700 to 840 nm. It appears that the attenuation coefficient from the Full Slice method over the lower range from 700 to 840 nm is relatively more consistent with the observations in Fig. 9. Rotten tissue should have relatively higher attenuation coefficients than healthy tissue, even though the absolute magnitudes are wrong. So while the Juice & Slice method appears more accurate in average level it may not be very precise at the detailed level in comparing healthy and rotten tissue types, which is likely caused by not using the same onions for the juice transmittance and IAD measurements. Understanding that failure at that lower detailed level requires further experimental investigation, perhaps involving accurate measurement of the anisotropy g value and using a larger number of samples (Fig. 15).

4. Discussion

The IAD absorption values had similar spectral shape to that from the juice transmittance measurements, but the absolute values were

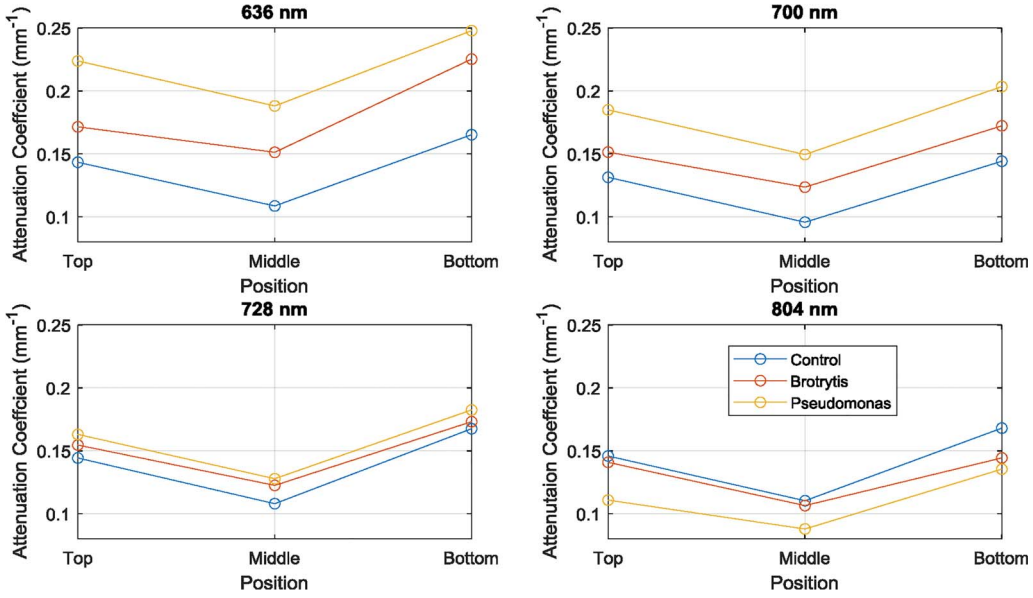

Fig. 13. Attenuation coefficients for control, botrytis and pseudomonas onions at 636, 700, 728 and 804 nm for top, middle and bottom latitude.

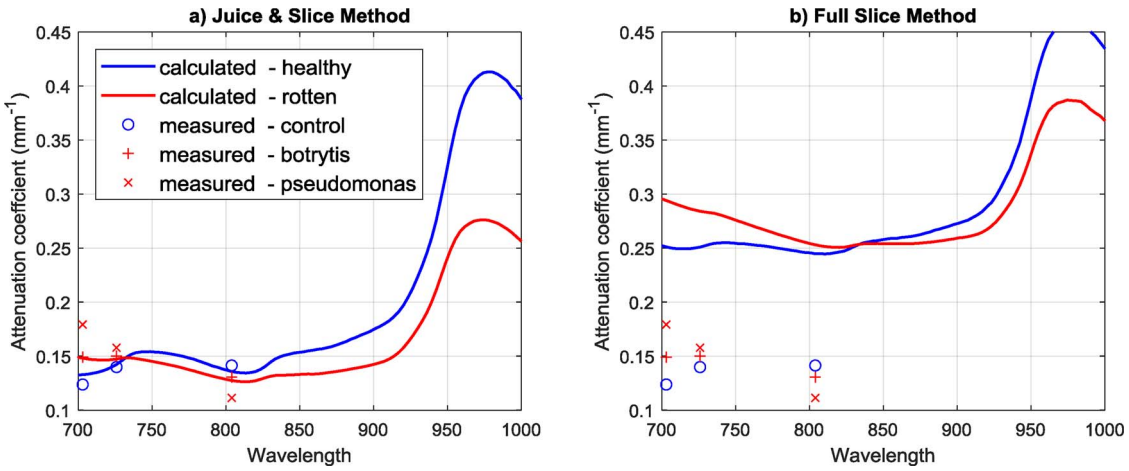

Fig. 14. Attenuation coefficients for healthy and rotten onion tissue from 700 to 1000 nm using (a) Juice & Slice method and (b) Full slice method. The measured values were also added, which were the average of the three latitude.

overestimated (Figs. 2 & Figure 3). For example, the absorption coefficients at 800 nm from the juice measurement were 0.005 and 0.083 mm^{-1} for healthy and rotten juice respectively, which were about 3 and 4 times lower than those derived from the IAD slice measurements. For the IAD method on healthy slices, our measurements were in a good agreement with the results from Wang et al. (2014), with $\mu_a = 0.013\ mm^{-1}$ and $\mu_s' = 1.4\ mm^{-1}$ at 800 nm. For the rotten slices, our results had very similar shape for both μ_a and μ_s', but μ_a (0.032 mm^{-1} at 800 nm) was about 5 times lower (Fig. 2). This could be caused by the different levels of rot in the slice sample measured in the two studies. The poor uniformity of rotten tissue in the slice sample might also cause variations that contribute to the large discrepancies. Therefore, the IAD method overestimates the absorption coefficients by a factor of 3 to 4, although spectrally correct in a relative sense from 700 to 1000 nm.

The results from Section 3.2.2 (i.e. the Juice & Slice method) indicate that attenuation coefficients through onions can be well predicted using absorption coefficients determined from extracted juice. Although the absolute accuracy was confirmed at three wavelengths (700, 728 and 804 nm), the values over the entire range of 700 to 1000 nm should also be accurate because of the consistency (not at a detailed level) with the NIRS and laser transmittance measurements. The non-soluble absorbing components in the tissue must therefore be relatively low in the 700–1000 nm range, either in concentration or in absorbance. For fresh biological tissue, such as onions, the insoluble solids mass is typically very low (Hansen, 1999). In our previous unpublished study, the average dry matter (DM) and soluble solids concentration (SSC) of 95 healthy onions were 11.2% and 9.51%, respectively. The difference between DM and SSC is the concentration of insoluble solids, which was 1.65 ± 0.6%. Carbohydrates are the dominate absorber after water in the 700 to 1000 nm NIR range (McGlone and Kawano, 1998). However, soluble and non-soluble carbohydrates are very difficult to distinguish in that NIR range, probably impossible in the overwhelming presence of water, and by far the largest fraction on mature onions are soluble sugars. The soluble solids will almost all be in the juice so it is probably not surprising that juice transmittance can afford to deliver realistic tissue absorbance measurements in the 700 to 1000 nm range.

The estimated onion tissue absorption values are only valid down to a lower limit of about 710 nm due to the absorption from chlorophyll (Munns et al., 2016). The laser light transmittance measurements showed the chlorophyll content affects the transmittance at 700 nm. This was especially pronounced when light travelled through the stem end (top latitude) of the onion where there are more green tissues (skin does not likely contain chlorophyll). To avoid the chlorophyll interference, a wavelength range above c. 710 nm should be used.

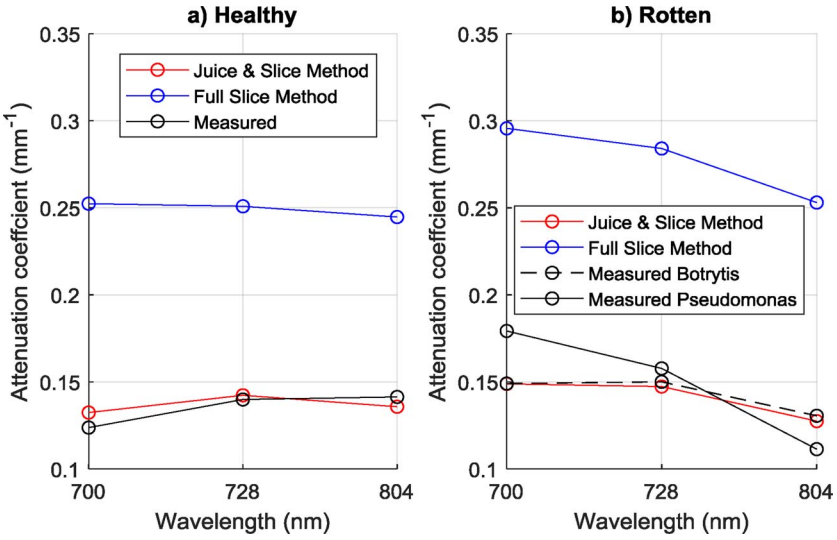

Fig. 15. Attenuation coefficients from different methods at 700, 727 and 804 nm.

5. Conclusion

The optical properties of healthy and rotten onion flesh were determined in the wavelength range of 700–1000 nm. This wavelength range is crucial for optical systems, as it allows high light propagation through the onion away from the bordering strong absorption peaks of chlorophyll (~690 nm) and water (~970 nm). NIRS transmittance measurements showed high sensitivity to the degree of rot in intact onions over the wavelength ranges 700–750 nm and 850–900 nm in the area normalised view. Transmittance measurements on extracted onion juice gave more accurate absorption coefficients for onion tissue, for both healthy and rotten tissue, than values derived using the standard IAD method used on onion tissue slices. The accuracy was confirmed by calculating attenuation coefficients from the optical properties and establishing good agreement with directly measured attenuation coefficients on three intact onions of different rot status, using a multi-laser light transmittance system at three wavelengths. With the encouraging results from the Juice & Slice method, a validation of this method over the range of 800–1000 nm should be conducted next. Furthermore, we suggest using the same onions for preparing the juice and slice samples. The results of this work aid the understanding of light propagation in healthy and rotten onions, which will facilitate the design of optical systems for internal rot detection.

Acknowledgments

This research was carried out with funding from the New Zealand Ministry of Business, Innovation and Employment, under programs C11X1601 and C11X1208. Jason Sun acknowledges the financial support of PhD scholarship from Plant and Food Research and the University of Waikato.

References

Aernouts, B., Zamora-rojas, E., Beers, R.V., Watté, R., Tsuta, M., Lammertyn, J., Saeys, W., 2013. Supercontinuum laser based optical characterization of intralipid ® phantoms in the 500-2250 nm range. Opt. Express 21, 17856–17872.

Clark, C.J., McGlone, V.A., Jordan, R.B., 2003. Detection of brownheart in 'Braeburn' apple by transmission NIR spectroscopy. Postharvest Biol. Technol. 28, 87–96.

Dehghani, H., Eames, M.E., Yalavarthy, P.K., Davis, S.C., Srinivasan, S., Carpenter, C.M., Pogue, B.W., Paulsen, K.D., 2008. Near infrared optical tomography using NIRFAST: algorithm for numerical model and image reconstruction. Commun. Num. Methods Eng. 25, 711–732.

FAOSTAT, 2016. Production of the Onion, Dry in the World. Food and Agriculture Organization of the United Nations.

Griffiths, G., Trueman, L., Crowther, T., Thomas, B., Smith, B., 2002. Onions—a global benefit to health. Phytother. Res. 16, 603–615.

Hansen, S.L., 1999. Content and composition of dry matter in onion (Allium cepa L.) as influenced by developmental stage at time of harvest and long-term storage. Acta Agric. Scand. B 49, 103–109.

Harrison, K.A., Sumner, P.E., Langston, D.B., Sparks, A.N., Riley, D.G., Culpepper, S., Hurst, W.C., Fonsah, E.G., 2008. Onion Production Guide.

Hébert, M., Hersch, R.D., Becker, J.-M., 2007. Compositional reflectance and transmittance model for multilayer specimens. J. Opt. Soc. Am. A 24, 2628–2644.

Ito, H., Hattori, G., 2012. Potential of non-destructive evaluation of internal disorder, browning of outer scale in onions using near infrared (NIR) spectroscopy. VI International Symposium on Edible Alliaceae 969, 197–202.

Ito, H., Morimoto, S., 2014. Non-destructive detection of browning of the inner scales of onions using near-infrared spectroscopy. Bull. Natl. Inst. Veg. Tea Sci. 49–53.

Jacques, S.L., 2013. Optical properties of biological tissues: a review. Phys. Med. Biol. 58, R37–61.

Khatiwada, B.P., Walsh, K.B., Subedi, P.P., 2016. Internal Defect Detection in Fruit by Using NIR Spectroscopy, 1120 Ed. International Society for Horticultural Science (ISHS), Leuven, Belgium, pp. 337–342.

Kim, A., Wilson, B.C., 2011. Measurement of ex vivo and in vivo tissue optical properties: methods and theories. In: Welch, A.J., van Gemert, M.J.C. (Eds.), Optical-Thermal Response of Laser-Irradiated Tissue. Springer, Netherlands, Dordrecht, pp. 267–319.

Kou, L., Labrie, D., Chylek, P., 1993. Refractive indices of water and ice in the 0.65- to 2.5-μm spectral range. Appl. Opt. 32, 3531–3540.

Kuroki, S., Nishino, M., Nakano, S., Deguchi, Y., Itoh, H., 2017. Positioning in spectral measurement dominates estimation performance of internal rot in onion bulbs. Postharvest Biol. Technol. 128, 18–23.

López-Maestresalas, A., Aernouts, B., Van Beers, R., Arazuri, S., Jarén, C., De Baerdemaeker, J., Saeys, W., 2016. Bulk optical properties of potato flesh in the 500–1900 nm range. Food Bioprocess Technol. 9, 463–470.

Martelli, F., Del Bianco, S., Ismaelli, A., Zaccanti, G., 2010. Light propagation through biological tissue and other diffusive media: theory. Solutions, and Software. SPIE Press, Bellingham, 2009.

McGlone, V.A., Kawano, S., 1998. Firmness, dry-matter and soluble-solids assessment of postharvest kiwifruit by NIR spectroscopy. Postharvest Biol. Technol. 13, 131–141.

McGlone, V.A., Martinsen, P.J., Clark, C.J., Jordan, R.B., 2005. On-line detection of brownheart in braeburn apples using near infrared transmission measurements. Postharvest Biol. Technol. 37, 142–151.

Munns, R., Schmidt, S., Beveridge, C., 2016. Plants in action. In: Munns, R., Schmidt, S., Beveridge, C. (Eds.), Plants In Action, 2nd ed. Australian Society of Plant Scientists.

Nicolaï, B.M., Beullens, K., Bobelyn, E., Peirs, A., Saeys, W., Theron, K.I., Lammertyn, J., 2007. Nondestructive measurement of fruit and vegetable quality by means of NIR spectroscopy: a review. Postharvest Biol. Technol. 46, 99–118.

Prahl, S.A., 2011. Everything I Think You Should Know About Inverse Adding-Doubling. Medical Laser Center, St. Vincent Hospital, Oregon, pp. 1–74.

Prahl, S.A., 2017. Inverse Adding-Doubling Program.

Prahl, S.A., Gemert, M.J.C.V., Welch, A.J., Van Gemert, M.J.C., 1993. Determining the optical properties of turbid media using the adding-doubling method. Appl. Opt. 32, 559–568.

Rowe, P.I., Künnemeyer, R., McGlone, A., Talele, S., Martinsen, P., Seelye, R., 2014. Relationship between tissue firmness and optical properties of 'Royal Gala' apples from 400 to 1050nm. Postharvest Biol. Technol. 94, 89–96.

Saeys, W., Velazco-Roa, M.A., Thennadil, S.N., Ramon, H., Nicolaï, B.M., 2008. Optical properties of apple skin and flesh in the wavelength range from 350 to 2200 nm. Appl. Opt. 47, 908–919.

Schaare, P.N., Fraser, D.G., 2000. Comparison of reflectance, interactance and transmission modes of visible-near infrared spectroscopy for measuring internal properties of kiwifruit (Actinidia chinensis). Postharvest Biol. Technol. 20, 175–184.

Sun, J., Künnemeyer, R., McGlone, A., 2017. Optical methods for firmness assessment of fresh produce: A review. Postharvest Handling. InTech.

Tomer, N., McGlone, A., Künnemeyer, R., 2017. Validated simulations of diffuse optical transmission measurements on produce. Comput. Electron. Agric. 134, 94–101.

Van Beers, R., Aernouts, B., Watté, R., Schenk, A., Nicolaï, B., Saeys, W., 2017. Effect of maturation on the bulk optical properties of apple skin and cortex in the 500–1850 nm wavelength range. J. Food Eng. 214, 79–89.

Wang, W., Li, C., Gitaitis, R., Tollner, E., 2012. 2012 Dallas, Texas, July 29 - August 1, 2012. ASABE, St. Joseph, MI. Optical Properties of Healthy and Sour Skin-Infected Onion Tissues in Vis-NIR Region.

Wang, W., Li, C., Gitaitis, R.D., 2014. Optical properties of healthy and diseased onion tissues in the visible and near-infrared spectral region. Trans. ASABE 57, 1771–1782.

Zhu, D., Lu, W., Zeng, S., Luo, Q., 2007. Effect of light losses of sample between two integrating spheres on optical properties estimation. J. Biomed. Opt. 12, 064004.

Chapter 7

Development of a Dual Laser System for Detecting Internal Rot in Onions

---

A journal paper

by

Jason Sun, Rainer Künnemeyer, Andrew McGlone, Nathan Tomer, Keith Sharrock

To be submitted

I prepared the initial draft manuscript, which was refined and edited in consultation with co-authors. Nathan conducted all the simulation work. I designed the hardware system and conducted all the experimental work. Keith Sharrock designed the method for preparing rotten onions, and wrote the section about this method. My supervisors provided guidance throughout this project.

Development of a dual laser system for detecting internal rot in onions

Jason Sun[1, 2], Rainer Künnemeyer[1], Andrew McGlone[2], Nathan Tomer[2], Keith Sharrock[2]

[1]Dodd Walls Centre for Photonic and Quantum Technologies, School of Engineering, University of Waikato, Hamilton, New Zealand

[2]The New Zealand Institute for Plant & Food Research Limited, Hamilton, New Zealand

Key word: nondestructive; laser; diffuse optical tomography; internal defect; onion

Abstract

This study details the development of a dual laser system for onion internal rot detection. The system is based on the continuous wave diffuse optical tomography (DOT) technique and a spatial pattern recognition algorithm. The two laser wavelengths were chosen through a combination of transmittance near-infrared spectroscopy (NIRS) analysis of rot affected onions, to determine wavelength sensitivities to the presence and severity of rots, and computer simulations of light transport to determine wavelength sensitivities to detection geometry and the suitability of a DOT measurement scheme. Onions (N=216) with different degrees of rot severity were prepared through deliberate inoculation of healthy onions with pseudomonas bacteria or botrytis fungus. Transmittance NIRS measurements were made close to the stem end of the onions and discriminant analysis was undertaken, involving exhaustive searches of the wavelength space (710-950 nm) in terms of the classification performances. A finite element method (NIRFast) was used to simulate light transport in onions and establish likely wavelength combinations that would minimise the influence of different source-detector distances in a proposed DOT setup where lasers were scanned across the surface of the onion with a single detector in

a fixed position on the back side. A system of two laser diodes, lasing at 728 and 805 nm, with a single photodiode was subsequently developed and used to experimentally verify the proposed spatial scanning DOT setup. The spatial transmittance profiles produced by the dual laser system allowed detection of onion rots of different sizes. A preliminary classification algorithm detected 80 % and 90 % of the rotten onions with 0 % and 8 % false positives respectively in validation. The scanning dual laser system has the potential to be adapted for online applications and can be made at low cost.

1. Introduction

Near-infrared spectroscopy (NIRS) has been used to detect internal defects in fresh produce, such as onion rot and apple brownheart. NIRS transmittance systems have shown promising results because this mode allows the light to travel over a longer path, increasing the chances of interaction with the rotten tissues (Clark et al., 2003; Kuroki et al., 2017; McGlone et al., 2005; Upchurch et al., 1997). A NIRS system is only sensitive when the defect causes detectable changes in the collected spectra (Nicolaï et al., 2007; Sun et al., 2017). As both the light delivery and detection are a single spot on the sample, the lack of spatial resolution causes it to be much less sensitive to the small and localised defects, which leads to poor detection rates and/or undesirable high rates of false positive identifications (healthy produce classified as defective). Model robustness is another issue; an NIR model may predict the attribute of interest within the normal realm of the training population, but might well fail on a new, independent set (Walsh, 2015). NIRS grader systems require frequent calibration to maintain good performance across differences in grower lines and seasons. The calibration set needs to encompass all relevant variations resulting from differences from across the range of grower sites and seasons (Nicolaï et al., 2007). The industry would benefit from an optical system where predictive models require less maintenance and, probably more importantly, a high sensitivity to small and localised defects.

Diffuse Optical Tomography (DOT) is an imaging technique used in the medical field to determine the interior composition and structure of turbid samples by NIR light (Yamada and Okawa, 2014). DOT has potential to be applied in the agricultural field to detect internal defects in produce and can be expected to perform better than NIRS in terms of model robustness and sensitivity. A typical DOT system involves a number of sources and detectors (typically >10) and a high performance computing system for image reconstruction. In order to be useful on commercial graders, the sensor must be cost

effective and able to operate at the grader speed (typically 10 fruit per second). The conventional methods used in the medical field are thus not directly applicable. Several studies have been carried out to assess the feasibility of using DOT on agricultural produce under static conditions. Kemsley et al. (2008) used a mechanical scanning based DOT system for measuring a potato phantom with a black rod as the perturbation (i.e., surrogate internal defect). Their measurements were conducted under highly simplified conditions, nevertheless the results showed the potential for internal defect detection. Numerical models were also used in some studies to simulate and validate the detection on potato (Nadhira et al., 2013) and carrot (Nadhira et al., 2015). However, to date there have been no studies assessing DOT on actual agricultural produce.

The aim of this work was to develop a static benchtop system for detecting internal rot in onions based on the continuous wave (CW) DOT technique. The system should have the potential to be developed into an online high speed system. To achieve this goal we also

- developed a method to generate onions with different level of internal rot,
- determined a small number of discrete wavelengths to build classification models through an exhaustive wavelength search, and
- simulated the proposed hardware setup using the finite element method (FEM) simulation software package NIRFast (Dehghani et al., 2008).

This paper is divided into three separate sections: wavelength selection, simulation and hardware development.

2. Wavelength search

2.1. Methodology

2.1.1. Sample preparation

Cultures of *Botrytis allii* Munn (ICMP 18376) and *Pseudomonas gladioli* pv. *alliicola* (ICMP 9209) were obtained from the International Collection of Micro-organisms from Plants,

administered by Landcare Research NZ Ltd. To prepare the fungal inoculum, *B. allii* was cultured on malt extract agar plates in a dark room illuminated only by long wavelength UV light on a diurnal cycle to promote sporulation. Spores were harvested from the agar plates by flooding with 0.05 % Tween 80 in water and scraping to detach all the surface growth. The resulting slurry was suctioned from the plate surface, vortexed in a sterile 50 mL conical-bottomed centrifuge tube (Falcon) to separate the spores, filtered through a sterile 70 µm nylon cell strainer (Falcon 2350) into a second identical centrifuge tube and centrifuged at 3000 g at 4 °C for 10 minutes. The supernatant was discarded and the pellet of spores was washed free of dissolved nutrients by re-suspending in sterile deionised water (Milli-Q) followed by centrifugation for 10 minutes at 3,000 g, repeated twice. The washed spore pellet was finally re-suspended in sterile deionised water at a density of 7×10^6 mL^{-1}, assessed using a haemocytometer, and subdivided in 1 mL aliquots into 1.5 mL screw-capped cyrotubes before freezing at -80 °C. When required to produce fresh inoculum, one tube was removed from -80 °C storage, thawed and diluted in sterile distilled water to a spore density of 2×10^6 mL^{-1} (the fungal inoculum).

To prepare the bacterial inoculum, *P. gladioli* pv. *alliicola* contents of the original freeze-dried ampule were briefly suspended in a basal mineral salts medium supplemented with trace elements and vitamins as described for *Thermoanaerobium brockii* (Zeikus et al., 1979) further supplemented with 0.3 % yeast extract, and immediately streaked onto a plate of nutrient agar and incubated at 28 °C. Once discrete colonies had formed, sub-cultures from representative colonies were grown for 24 h at 28 °C on slopes of yeast salts agar (YSA) (Dye, 1969) in 10 mL sealed vials. The vials were transferred to cold storage at 4 °C while culture growth was still in its logarithmic growth phase. When required to produce fresh inoculum, plates of potato dextrose agar were streaked with inoculum retrieved from a cold-stored YSA slope and incubated at 28 °C for 2-3 days. Bacteria from one of the resulting gelatinous colonies were then transferred by loop to ca. 5 mL of sterile distilled water and agitated to produce a visibly turbid suspension (the bacterial inoculum).

A hot (200 °C) 1 mm diameter copper wire attached to a soldering iron gun was used to create a puncture wound in the centre of the leaf scar. A 50 µL aliquot of inoculum was applied to the surface of the stalk scar using a pipette, centred on the visible hole created by the hot wire. After the inoculum soaked into the stalk scar, the onions were covered with high density polyethylene box liner film loosely sealed inside a cardboard box and incubated at 22 °C in saturated humidity. After two weeks the temperature of the incubator was reduced to 2 °C in order to slow down rot growth

2.1.2. Transmittance spectra and search procedure

Transmittance spectra were collected with the setup illustrated in Figure 1, the details previously described by Sun et al. (2018). The source and detector were targeted on the stem end so the collected spectra were more characteristics of the rotten tissue. The source-detector distance would also be more consistent then, minimising variations caused by different onion sizes. The measurements were taken in two different onion orientations, at 0° and then at 180° rotation around the stem-root axis, doubling the number of spectra to 432 from 216 onions. The dark current was first subtracted from the raw spectra. The relative transmittance spectra were obtained by dividing the spectra by a reference spectrum for the light source recorded with reduced integration time taken when nothing in the light path. To accentuate the effect from the internal rot for demonstration, the spectra were further normalised using a standard normal variate (SNV) transformation, commonly employed with NIRS analysis, to minimise light path variations caused by the different sizes and geometries of the samples.

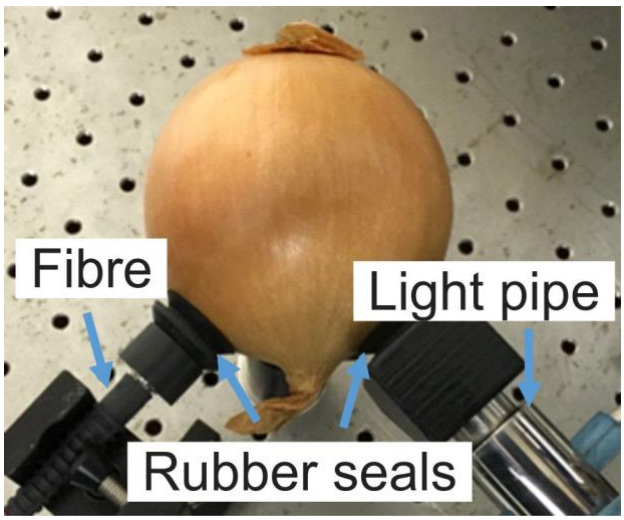

Figure 1: Hardware setup of NIRS transmittance measurements. The light entered from the light pipe, and was collected by the fibre (Sun et al., 2018).

The key objective of wavelength search was to determine whether a small number (1-4) of discrete wavelengths can be used to create a binary classification model for detecting onion internal rot. The raw spectra were used to conduct the wavelength search. No spectral pre-processing was performed to keep the application of the data more general, since the pre-processing method may not be appropriate for a discrete wavelength model (Shafie et al., 2015). The data were randomly split into two independent sets: a calibration set consisted of 323 spectral samples and an independent validation set of 109 spectral samples. For each classification algorithm, the optimal set of wavelengths was found by applying a brute force search to go through all 1 to 4 wavelength combinations from 710 to 950 nm of the calibration set. This wavelength region was chosen because it is within the transmission window of the onion, and it is away from chlorophyll absorbance effect that are measurable up to c. 710 nm (Sun et al., 2018). The model with optimal wavelengths was then applied to the validation set for confirmation and comparison of performances. Full multiple linear regression (MLR) and partial least squares discriminant analysis (PLSDA) models, generated using the full wavelength range (710 to 950 nm with 5 nm spacing), were used as benchmarks.

2.2. Results

2.2.1. Inoculation

The success rate of the inoculation was nearly 100 %. After removing some severely rotten samples, a total of 216 onions were prepared including the control, healthy onions. The longer the inoculated onions were incubated, the larger the internal rot was, but the rot developed at various rates in different onions. After two weeks both pseudomonas and botrytis caused different levels of rot close to the stem end, providing a wide spread of rot severities. The rots were close to the stem-end, which is also the case for naturally occurring rots in onions. It can be seen that pseudomonas caused rotten tissues on certain layers (Score 2, 3 and 5 in Figure 2), while botrytis infected more layers together as a block of tissue (score 1 and 4 in Figure 2). Onions were cut vertically (from the stem-end to the basal plate) after the transmittance measurements and were scored visually according to the severity level of rot visible in the cross section (Figure 2). The dataset consisted of 74 healthy onions and 128 rotten onions (Figure 3). There were only a few samples in the score 1 and score 5 range, which had 14 and 7 samples, respectively.

Figure 2: Severity score according to the level of rot from the cut surface. For these examples, Score 1 and 4 were caused by botrytis; score 2, 3 and 5 were caused by pseudomonas (Sun et al., 2018).

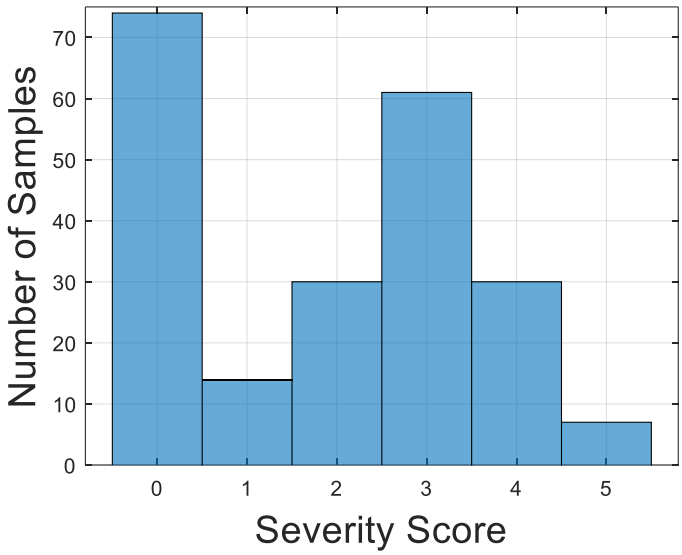

Figure 3: Severity score of the 216 onion samples used in the experiment.

2.2.2. Wavelength search

Figure 4a shows the raw spectra recorded on the healthy and rotten onions. Within the range 680-1000 nm, the spectra have good signal to noise ratio due to the lower absorbance from water and pigments. Normalisation cannot fully eliminate path length variations and could mask some spectral characteristics, but the general spectral features should be preserved. Figure 4b shows the average SNV normalised spectra for each severity score, with the score 5 spectra being appreciably different. Consistent with the observations on brownheart apples (Clark et al., 2003), rotten onions had lower transmittance in the wavelength range 680 to 750 nm and higher transmittance in the 800 to 950 nm range. Wavelengths chosen from these two ranges are likely to be useful for detecting the presence of rotten tissue. The middle region, from 770 to 810 nm, might then be used as a reference with which to normalise light intensity variations and/or spectral drift as the spectra are all closer to each other in that region (Figure 4a), even overlapping in the normalised view (Figure 4b). So a simple transmittance ratio at two wavelengths may be an effective classification algorithm.

We used the area under the receiver operating characteristics (ROC) curve (AUC) to assess the performance of classification, which is a widely used technique in areas such as

bioinformatics and statistics (Hand, 2009). Figure 5a displays AUC values for ratios of all combinations of two wavelengths from 710 to 950 nm. The plot is a matrix of values representing classification performance, indexed by the denominator on the y axis and numerator on the x axis. The values were scaled for better display of the images; the higher the value, the better classification the matrix pixel represents. The image is symmetric to the 1 to 1 line as classification was the same when the denominator and numerator were swapped. The 1-to-1 line indicates the lowest classification performance where all onions had a ratio of 1. There are regions with low classifications, where the denominator and numerator are both from 740 to 820 nm and 930 to 950 nm. The rest of the AUC image had similar classification with scaled AUC values between 50 and 65. The ratio of 880 to 905 nm had the highest AUC value, its ROC curves for the calibration and validation set are shown in Figure 5b. The ROC curve is a plot of true positive rate (TPR) versus false positive rate (FPR). There is a trade-off between TPR and FPR, and the actual detection rates (both TPR and FPR) on the validation set depend on the chosen model threshold. A ROC curve with higher AUC value does not guarantee better detection rates on any point on the curve. For example, in Figure 5b the calibration and validation curves had similar TPR values when the FPR was above 20 %, even though the validation curve had a higher AUC. In practice, the concern is often more with the FPR as a high FPR will result in an intolerable amount of healthy onions being removed and probably dumped to waste. Therefore, a TPR of 90 % (meaning 90 % of the rotten onions will be detected) was set as the target and the corresponding FPR was used for comparisons.

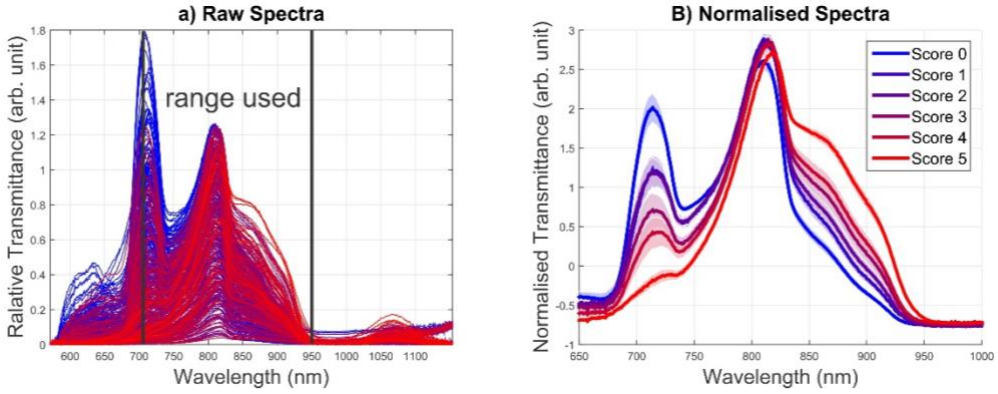

Figure 4: NIRS transmittance spectra: (a) the raw spectra used for wavelength search, vertical lines indicate the range used for analysis. (b) average normalised spectra of onions with each severity score, with the shading representing a quarter of the standard deviation at each wavelength.

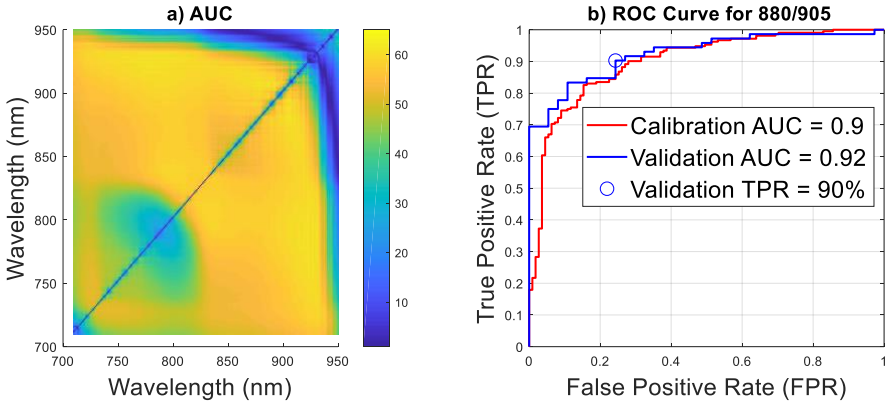

Figure 5: (a) Image indicating scaled values of AUC for measuring classification performance. (b) The ROC curve of the transmittance ratio of 880 to 905 nm on the calibration and validation set. The blue and red circles are the points where the TPR = 90 %.

The same evaluation procedure was applied to other types of algorithms (Table 1). Interestingly, the 880/905 ratio had the highest AUC in calibration, but its AUC was lower in validation than that of the 705/805 ratio. This probably means the classification is also dependent on the samples used in the model; different samples producing different optimal wavelength combinations. For the MLR models, the AUC value in validation increased with increasing number of wavelengths used. The full range MLR and PLSDA models used 49 wavelengths in the range of 710 to 905 nm with 5 nm spacing, and their AUC values were 0.89 and 0.93, respectively. Using FPR at 90 % TPR as the comparison metric, the full wavelength MLR and PLSDA models were still the best with FPR = 24 % and 14 %, respectively. The low wavelength MLR models were inferior to the ratio models with the lowest FPR = 43 % when four wavelengths were used. The difference ratio algorithms,

using three and four wavelengths, did not improve the AUC in validation and had higher FPR values at the same 90 % TPR. Practical design issues, such as instrument size limitations and the difficulty of multiplexing separate sources, means smaller numbers of wavelengths are better. The two wavelength ratio showed the best results compared to other discrete models for both AUC and FPR values, and even similar to the full wavelength MLR model. So the two wavelength ratio becomes the preferred choice.

Table 1: Classification performance on the validation set for various algorithms with the optimal wavelengths. The 728/805 ratio is also included.

Algorithm	Wavelength used (nm)	AUC in validation	FPR at 90% TPR in validation
λ_1/λ_2	880 905	0.92	24 %
	728 805	0.93	30 %
$(\lambda_1-\lambda_2)/(\lambda_3-\lambda_2)$	900 930 915	0.91	35 %
$(\lambda_1-\lambda_2)/(\lambda_3-\lambda_4)$	870 935 915 880	0.91	38 %
MLR	930	0.70	89 %
MLR	805 815	0.73	76 %
MLR	790 840 850	0.77	70 %
MLR	710 780 840 855	0.86	43 %
MLR	710-950	0.89	24 %
PLSDA	710-950 (9 latent variables)	0.93	14 %

3. Simulation

3.1. Methodology

Light transport simulations were run at wavelengths from 710 to 950 nm using the method of Tomer et al. (2018) which is based on the finite element model (FEM) software

package NIRFast (Dehghani et al., 2008). The required FEM meshes representing the onions were generated using the iso2mesh algorithm (Qianqian and Boas, 2009). The source and detector locations are illustrated in Figure 6a, a typical circular fan-beam geometry as used in DOT (Pogue et al., 1999). There are in total 63 sources and three detectors, which are distributed on the top, middle and bottom latitudes of the onion mesh. On each latitude, taking the detector position as 0°, the 21 sources are evenly located from 67.5° to 292.5° with respect to the detector. A spherical region inside the onion represents the rotten tissue (Figure 6b). The optical properties of healthy and rotten tissues were chosen from the results obtained in previous work and reproduced here for clarity (Figure 7; Sun et al. (2018)).

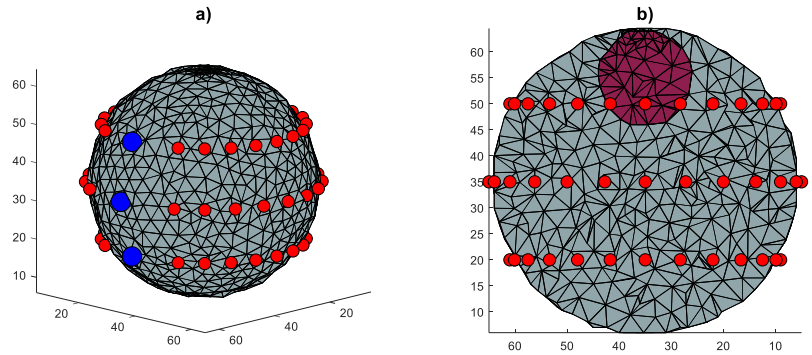

Figure 6: (a) The optical setup used in the simulation (blue is detector and red is source). (b) The cross section of the rotten onion mesh, the purple part is the rotten tissue.

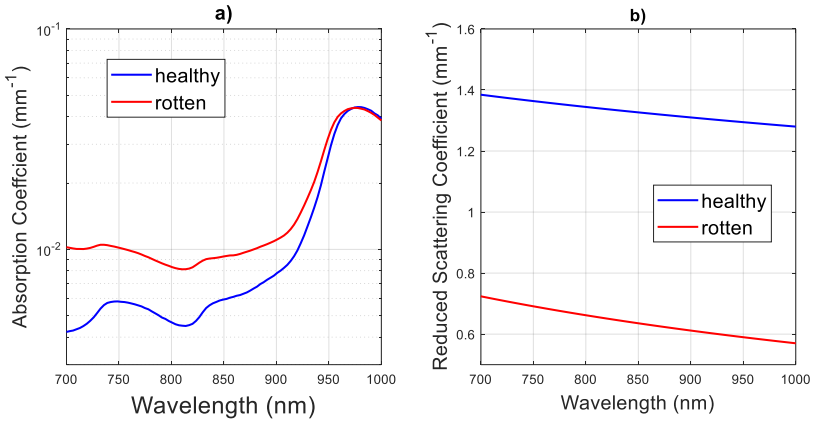

Figure 7: The average optical properties of healthy and rotten onions (reproduced from Sun et al. (2018)): (a) absorption coefficient. (b) reduced scattering coefficient.

3.2. Results

3.2.1. Source-detector distance

The results in Section 2.2.2. have shown that the ratio of light transmittance at two wavelengths can be used to identify rots, under the setup described in Figure 1. The simulations however indicate that this ratio is dependent on the source-detector separation (Figure 8).

This effect can be explained by the diffusion approximation of the radiative transfer equation, which is widely used to calculate the light transport in diffusive medium. The fluence (light energy per unit area), Φ, is calculated as (Martelli et al., 2010):

$$\phi(r) = \frac{3\mu'_s}{4\pi r} e^{-\mu_{eff} r} \qquad (1)$$

where

$$\mu_{eff} = \sqrt{3\mu_a \mu'_s} \qquad (2)$$

is the attenuation coefficient, r is the source-detector separation distance, μ_a and μ_s' are the absorption and reduced scattering coefficients, respectively.

For two wavelengths, λ_1 and λ_2, the corresponding fluences are ϕ_1 and ϕ_2. Using equation 1 the ratio can be expressed as:

$$\frac{\phi_1}{\phi_2} = \frac{\mu'_{s_1}}{\mu'_{s_2}} e^{(\mu_{eff_2} - \mu_{eff_1}) r} \qquad (3)$$

This ratio is not only dependent on the optical properties at these two wavelengths but also on the separation distance, r. This problem was not noticeable in typical NIRS applications as spectra preprocessing methods are often used to minimise this type of variations. This is not the case in the simulation of the tomography setup, the separation distance varied depending on source and detector positions. For example, with a healthy onion in Figure 8 the 880 to 905 nm transmittance ratio increases, while the 750 to

800 nm transmittance ratio decreases, with increased source-detector distance (180° is the largest separation). Thus a change in transmittance ratio depends on the source-detector distance as well as the level of rot.

Measuring the source-detector separation distance could be a solution but will not be practical for online applications. According to equation 3, the transmittance ratio changes depending on the difference of μ_{eff} at the two wavelengths. If the two attenuation coefficients are equal, $\mu_{eff_1} = \mu_{eff_2}$, the ratio becomes:

$$\frac{\Phi_1}{\Phi_2} = \frac{\mu'_{s_1}}{\mu'_{s_2}} \qquad (4)$$

This is now a ratio of the reduced scattering coefficients, independent of the source-detector separation distance. Figure 9 is an image where each pixel value indicates the logarithm of the absolute difference, $\log(|\mu_{eff_1} - \mu_{eff_2}| + C)$, indexed by λ_1 on the x axis and λ_2 on the y axis. The lower the difference value, the closer the difference is to zero, then the more independent the ratio will be of separation distance. There is only a small area, the green-blue loop in the lower left quadrant of Figure 9, where the two wavelengths have similar attenuation coefficients. Previously it was observed that 728 and 805 nm wavelength ratio had good classification performance (Table 1). Now it is observed that the attenuation coefficients are similar at these wavelengths (Figure 9), resulting in a transmittance ratio that is almost constant with distance (Figure 8). Moreover, there are commercially available laser diodes close to these two wavelengths.

Compared to healthy tissue, rotten tissue has higher absorption and lower scattering coefficients from 710 to 950 nm (Figure 7), resulting in different μ_{eff}. Therefore, the target ideal of $\mu_{eff_1} = \mu_{eff_2}$, for separation distance independence, will likely not hold if there is rotten tissue intersecting the light path. The presence of rotten tissue will more likely cause a peak or trough on the scanned spatial profile. Obviously such pattern differences in the spatial profiles could be the basis of a detection method, possibly with

higher sensitivity than indicated with NIRS and the two wavelength ratio (Table 1) because the method would be using additional spatial information with the ratio.

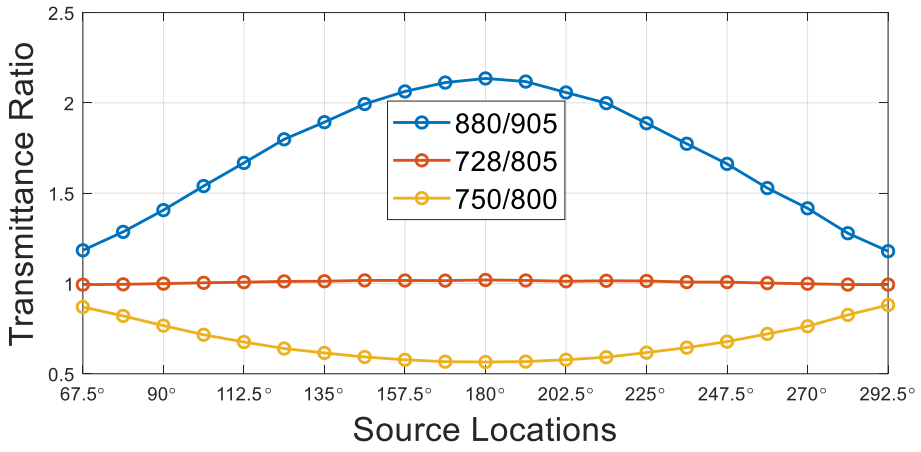

Figure 8: Transmittance ratios at different source locations on the middle latitude of a healthy onion with typical optical properties.

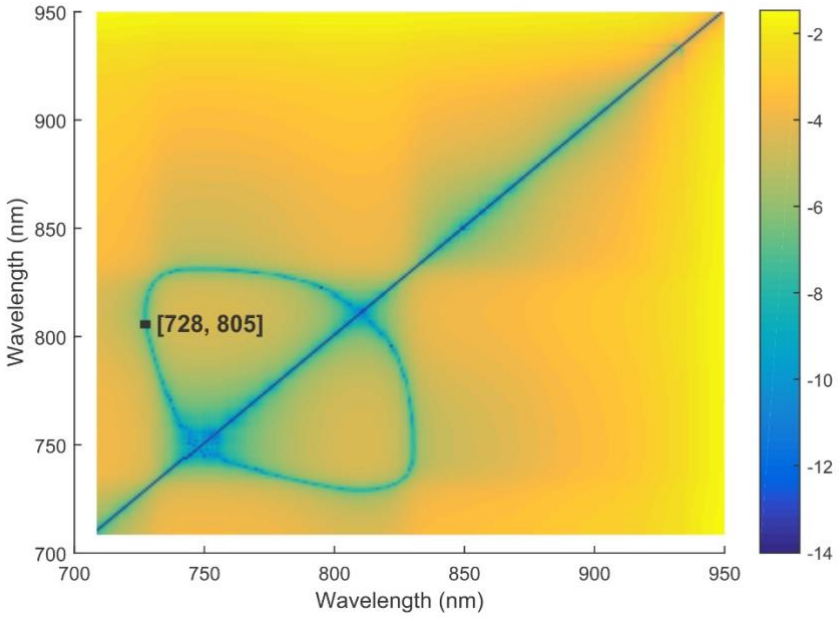

Figure 9: Image of absolute μ_{eff} difference with wavelength. The value on the plot is log transformed.

3.2.2. Spatial profile method

The effect on the transmittance ratio profile was simulated for rots located at different positions in the onion mesh. In Figure 10, 1a to 3a, the rot was located close to the stem end and horizontally moved to three different positions. In each case, the rot produced a

distinctive trough in the profile of the top latitude (Figure 10, 1b to 3b). The trough position corresponds to the position of the rot. In Figure 10, 4a, the rot was located close to the basal plate of the onion and the bottom profile displayed a trough at the centre (Figure 10, 4b). In Figure 10, 5a, a bigger rot at the top latitude caused a wider trough in the top profile and a shallower trough in the middle profile. Overall, the results show the ratio profiles at three latitudes can indicate the position and size of the rot.

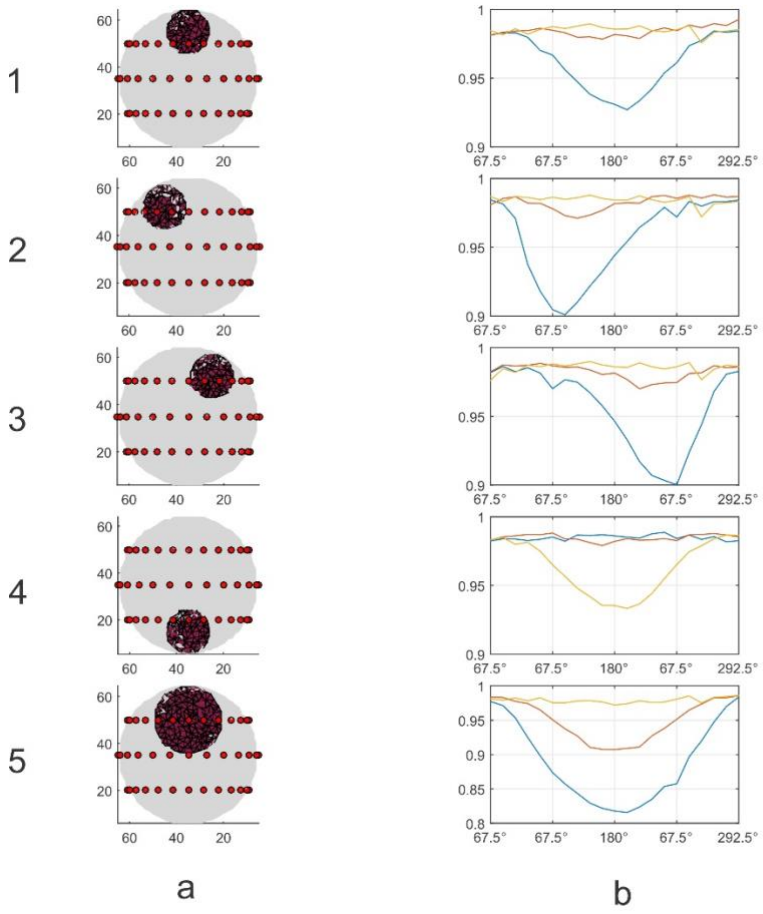

Figure 10: (a) Cross section of the rotten onion mesh. (b) The simulated ratio profile at top (blue), middle (red) and bottom (yellow) latitudes of each rotten onion.

4. Hardware development

A hardware implementation of the simulated setup was developed using two laser diodes as light source and one silicon photodiode as detector. The mechanical scanning gives flexibility and cost reduction with the compromise of longer data acquisition times. In the design process we considered practical aspects such as speed and signal to noise ratio

(SNR) so that the system would be easily adaptable for further development for use on a high speed grader.

A key component of this system is the frequency modulation and demodulation, sometimes referred to as synchronous detection. Frequency modulation allowed simultaneous measurements of two different light signals, and significant reductions of noise using a low pass filter at the output stage of the lock-in amplifier. However, there was a trade-off then between the signal noise and the acquisition speed.

4.1. Dual laser system design

4.1.1. System overview

The overview of the dual laser system is shown in Figure 11. The system consists of two lasers, at 728 and 805 nm, which provide intense light within a small illumination area on the fruit, allowing for fast, spatial measurements. They were modulated with a square wave of frequencies, F_1 and F_2, provided by the pulser (function generator). A silicon photodiode (FDS100, Thorlabs, Newton, NJ, USA) was used to collect the light and a trans-impedance amplifier (DLPCA-200, Femto, Berlin, Germany) converted the current to voltage for further processing. This voltage signal was then fed into a digital lock-in amplifier (MFLI, Zurich Instrument, Zurich, Switzerland) which was able to extract each of the two light signals, V_1 and V_2, concurrently. The processing unit such as a PC recorded the output of the lock-in amplifier and computed the ratio profile.

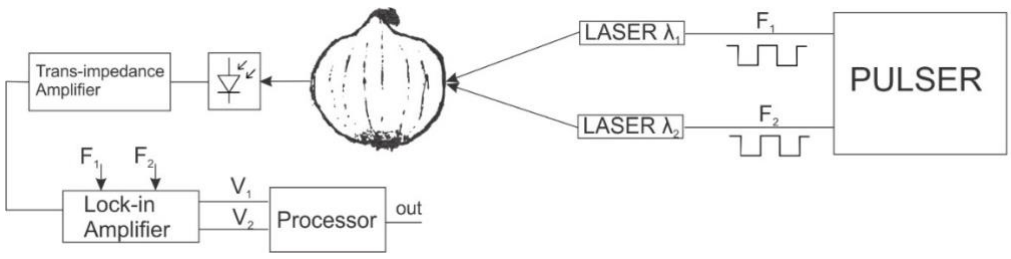

Figure 11: Schematic of the laser system for onion internal rot detection.

4.1.2. Frequency modulation

Square wave modulation allows for the driver circuit to be simplified in the future, as it requires a digital switch rather than a more complicated analogue current control. The laser controller (ITC102, Thorlabs, Newton, NJ, USA) was set to constant current mode, the analogue modulation input can take a voltage from -5 to 5 V, which was provided by a function generator (pulser in Figure 11). Each laser was modulated between its threshold and maximum current, so we could achieve the highest signal from the lock-in amplifier. The power input to the onion from each laser was measured at about 15 mW using a power meter (Nova, Ophir Optronics, Jerusalem, Israel).

The modulation frequency should be as low as possible, but still able to meet the speed requirement, to achieve the highest (optimal) trans-impedance gain and simplify the electronics design. It was found that 10^7 was the highest gain that did not saturate the lock-in amplifier when the source and detector positions on the onions were close together (smallest separation corresponds to largest signal). The DLPCA-200 has a bandwidth of 50 kHz in its low speed, low noise mode, 400 kHz in high speed mode. For better SNRs, the low noise mode was used. The 728 and 805 nm lasers were modulated at selected frequencies of 17 and 19 kHz, respectively.

4.1.3. Demodulation

The lock-in amplifier demodulated each of the two signals according to its frequency, and used a low pass filter at its output stage. Normally, a small bandwidth is selected to filter out noise. However, with the onion potentially moving at 10 onions per second rates, on a grader line, enough bandwidth is needed to handle the signal changes as an onion moves in and out of the system. It is assumed that 10 measurements on each onion is sufficient, at the speed of 10 onions per second, the time for each measurement is then 0.01 s. A typical lock-in requires five time constants (τ) to settle to a steady reading, so the

required τ is about 2 ms. The necessary bandwidth of the low pass filter can then be calculated using this equation:

$$f_{3dB} = \frac{1}{2\pi\tau}$$

For a time constant τ of 2 ms the f_{3db} bandwidth frequency is 80 Hz.

A simple test was conducted to investigate how the low pass filter bandwidth limited the sample processing speed and SNR of the detector. An optical chopper was used to test the processing speed capacity, the maximum chopper speed being determined as the speed at which the light signal started not returning to zero when light was blocked by the chopper. Table 2 summarises the results.

Table 2: Signal to noise ratio and maximum chopper speed at three different low pass filter bandwidth for 728 nm light signal.

f_{3dB} (Hz)	Max Chopper Speed (Hz)	SNR (healthy)	SNR (rotten, score 4)
50	40	917	214
100	80	729	184
200	160	428	81

As expected, the maximum chopper speed increased with the bandwidth while the SNR became lower. At bandwidth f_{3db} of 100 Hz, the SNR was 184 for rotten onion and 729 for healthy onions. At that bandwidth the maximum chopper speed of 80 Hz indicates an ability to handle eight measurements on one onion travelling along a grader conveyor running at a rate of 10 onions per second.

4.1.4. Scanning process

The detector consisted of a silicon photodiode and a trans-impedance amplifier, mounted on a turn-table (Figure 12), and connected by a cable made as short as possible to reduce noise. A stepper motor was used to rotate the turn table, which was driven by an Arduino based controller with a microstep driver (JK1545, Jingkong Motor & Electric Appliance,

Changzhou, China). A Matlab script was written to control the turn table and record the subsequent data.

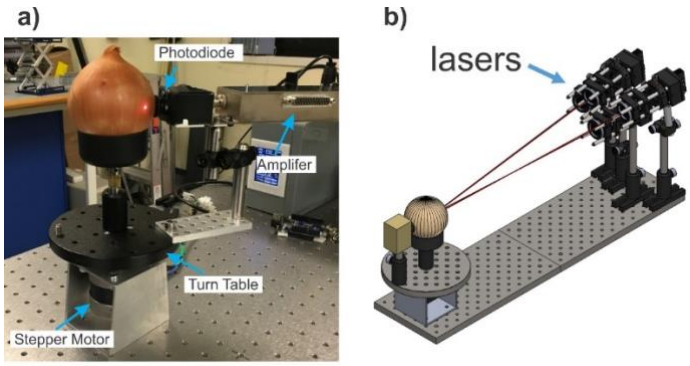

Figure 12: (a) Experimental setup of the dual laser system, the red spot is the laser illumination (b) CAD model of the dual laser system.

Figure 13 shows al engineering drawing of the photodiode housing, which was cylindrically symmetric. The photodiode had a 13 mm^2 active area. A rubber grommet was used for the attachment to the onion to reduce the amount of stray or ambient light entering the housing. The photodiode was located approximately 18 mm from the surface of the onion.

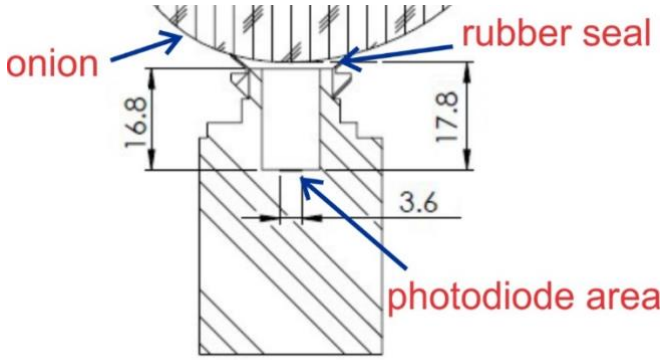

Figure 13: Sensor head geometry (dimensions in mm).

The onion was placed on a small soft rubber cup (20 mm diameter) so that it rotated with the table and meant the detector, which was mounted on the turntable, was stationary in the reference system of the onion and did not change its position on the onion (Figure 12). Hence for each scan, the detector position was fixed, and it was the source (laser beam) location that effectively rotated around the onion. The table rotated 11.25° each

time, which formed 21 source locations from 67.5° to 292.5° just as for the setup used in the simulation (Figure 6). The same onions that formed the validation dataset in section 2.2.2 were measured on the top latitude only because the onion rot always developed from the stem end part.

4.2. Results

4.2.1. Spatial profile

The measured spatial profiles were very similar to the simulation results in Figure 10. For the healthy onions (Figure 14, 1a), there was a largely flat line with some minor fluctuations, possibly caused by the variegated light absorbing character of the onion skin (Tomer et al., 2015). Rotten onions in Figure 14, 1a-6a had a trough on the spatial profile. Both pseudomonas and botrytis caused the rot to develop first in the top middle core of the onion, so the troughs appeared in the centre of the profiles. From Figure 14, 1a to 5a, the larger the rot, the deeper the trough became. The clear presence of the trough in Figure 14, 2b indicates that the system is sensitive to a very small rot. The onion in figure 14, 6a had rotten tissue occupying almost the entire volume at the neck end. The profile level in that case was dramatically reduced compared to the other profiles but there was still a clear trough in the middle of the profile. Hence the profile level in addition to profile pattern may be useful in the discrimination of severity of rot.

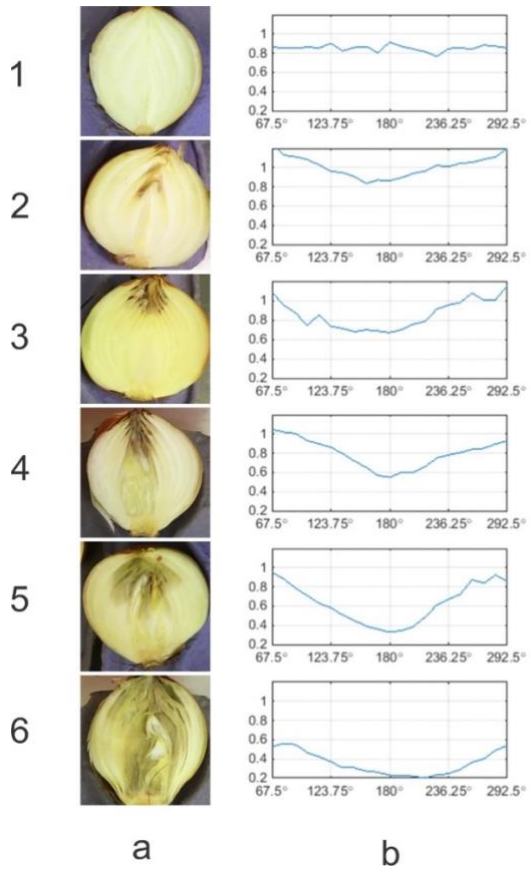

Figure 14: (a) Cross section of the onions with severity score from 0 to 6. (b) The ratio profile of the top latitude of the corresponding onion.

4.2.2. Detection

A simple algorithm was developed to discriminate profiles for rot:

$$Discriminator\ value\ = \frac{(meanSidePoints - meanCentrePoints)}{meanProfile} \quad (5)$$

$meanSidePoints$ is the average of the first and last four points (red squares in Figure 15a). $meanCentrePoints$ is the average of the five points in the centre (black square in Figure 15a). $meanProfile$ is the average of all the points.

A deeper trough on a profile will be associated with a higher discriminator value, therefore a threshold can be set to segregate the onions. Figure 15b shows the ROC curves for the new discriminating algorithm on the same validation datasets used previously. The algorithm gave higher AUC values than the full wavelength model used in section 2.2.3. When the TPR was 80 % and 90 %, the FPR was 0 % and 8 %, respectively, better performance than that of the various NIRS algorithms reported in Table 1.

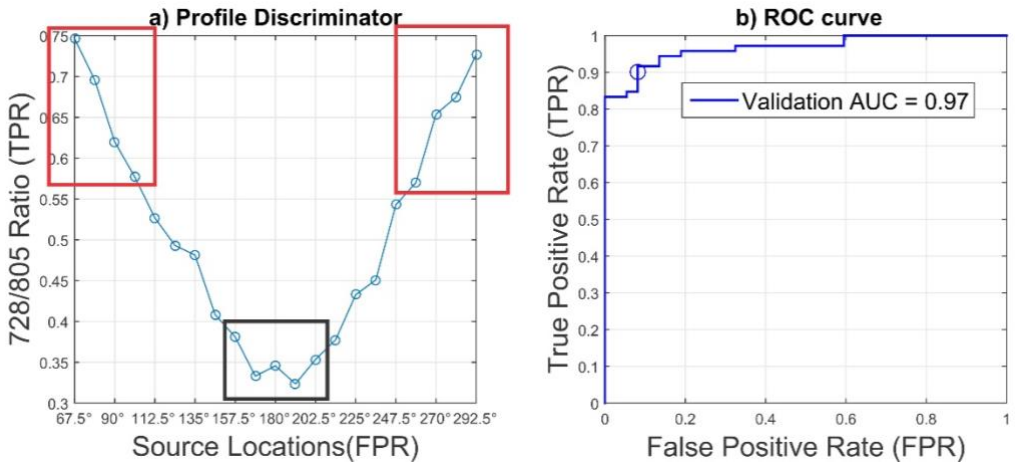

Figure 15: (a) A spatial profile of a rotten onion with score 5.(b) The ROC curve of the discriminator value on the validation set

5. Conclusion

The wavelength pair for the dual laser system here, at 725 and 805 nm, were chosen through a combination of NIRS transmittance experiments, separate light transport simulations of a DOT setup and, finally, the commercial availability of suitable laser diodes. The developed dual laser system, working through a spatial pattern recognition algorithm, proved much superior in practice to the best NIRS transmittance models that were built using PLSDA and/or MLR on full spectra range from 650 to 1000 nm. The system may have an advantage over those more typical NIRS systems, that rely on the complexity of full spectrum chemometric models, in being considerable simpler in involving measurement of a simple intensity ratio at just two wavelengths. Similarly, the simple pattern recognition algorithm involved would appear to offer the system a considerable advantage over typical DOT systems in not requiring the time-consuming iterative inverse simulation steps necessary to construct the internal properties.

The dual laser system is not perfect, the AUC was 0.97 in the single validation trial here. The hardware system is still very preliminary, the limited scanning capability makes it difficult for testing this technique to its full potential by scanning the entire volume of a sample and it is also challenging to include more samples in the trial due to the slow scanning speed. Therefore, further work is warranted to substantially improve the

scanning technique by optically and/or mechanically scanning both the light source and detector at much higher speed for real-time applications. The scanning mechanism used in a barcode scanner and laser printer could be adapted.

Acknowledgments

We would like to acknowledge Paul Martinsen for his contributions to the hardware development. This research was carried out with funding from the New Zealand Ministry of Business, Innovation and Employment, under programs C11X1601 and C11X1208. .Jason Sun acknowledges the financial support of PhD scholarships from The New Zealand Institute for Plant & Food Research Limited and University of Waikato.

References

Clark, C.J., McGlone, V.a., Jordan, R.B., 2003. Detection of Brownheart in 'Braeburn' apple by transmission NIR spectroscopy. Postharvest Biology and Technology 28, 87-96.

Dehghani, H., Eames, M.E., Yalavarthy, P.K., Davis, S.C., Srinivasan, S., Carpenter, C.M., Pogue, B.W., Paulsen, K.D., 2008. Near infrared optical tomography using NIRFAST: Algorithm for numerical model and image reconstruction. Communications in numerical methods in engineering 25, 711-732.

Dye, D., 1969. A taxonomic study of the genus Erwinia. III. The'herbicola'group. New Zealand Journal of Science 12, 223-236.

Hand, D.J., 2009. Measuring classifier performance: a coherent alternative to the area under the ROC curve. Machine Learning 77, 103-123.

Kemsley, E.K., Tapp, H.S., Binns, R., Mackin, R.O., Peyton, A.J., 2008. Feasibility study of NIR diffuse optical tomography on agricultural produce. Postharvest biology and technology 48, 223-230.

Kuroki, S., Nishino, M., Nakano, S., Deguchi, Y., Itoh, H., 2017. Positioning in spectral measurement dominates estimation performance of internal rot in onion bulbs. Postharvest Biology and Technology 128, 18-23.

Martelli, F., Del Bianco, S., Ismaelli, A., Zaccanti, G., 2010. Light Propagation through Biological Tissue and Other Diffusive Media: Theory. Solutions, and Software (SPIE Press, Bellingham, 2009).

McGlone, V.A., Martinsen, P.J., Clark, C.J., Jordan, R.B., 2005. On-line detection of Brownheart in Braeburn apples using near infrared transmission measurements. Postharvest Biology and Technology 37, 142-151.

Nadhira, V., Juliastuti, E., Kurniadi, D., 2015. Image Reconstruction of Continuous Wave Domain Diffuse Optical Tomography for Quality Control on Carrot. International Journal of Tomography & Simulation™ 28, 60-68.

Nadhira, V., Kurniadi, D., Juliastuti, E., 2013. Feasibility study on image reconstruction of continuous wave domain diffuse optical tomography for quality control on seed potatoes, Instrumentation, Communications, Information Technology, and Biomedical Engineering (ICICI-BME), 2013 3rd International Conference on. IEEE, pp. 421-424.

Nicolaï, B.M., Beullens, K., Bobelyn, E., Peirs, A., Saeys, W., Theron, K.I., Lammertyn, J., 2007. Nondestructive measurement of fruit and vegetable quality by means of NIR spectroscopy: A review. Postharvest Biology and Technology 46, 99-118.

Pogue, B., McBride, T., Osterberg, U., Paulsen, K., 1999. Comparison of imaging geometries for diffuse optical tomography of tissue. Optics Express 4, 270-286.

Qianqian, F., Boas, D.A., 2009. Tetrahedral mesh generation from volumetric binary and grayscale images, 2009 IEEE International Symposium on Biomedical Imaging: From Nano to Macro, pp. 1142-1145.

Shafie, K.A., Künnemeyer, R., McGlone, A., Talele, S., Vetrova, V., 2015. An Optimised Six-Wavelength Model for Predicting Kiwifruit Dry Matter. Journal of Near Infrared Spectroscopy 23, 103-109.

Sun, J., Künnemeyer, R., McGlone, A., Tomer, N., 2017. Fruit orientation in NIR transmission for vascular browning in apples, 11th International Conference onSensing Technology IEEE, Sydney, Australia, pp. 139-142.

Sun, J., Künnemeyer, R., McGlone, A., Tomer, N., 2018. Optical properties of healthy and rotten onion flesh from 700 to 1000 nm. Postharvest Biology and Technology 140, 1-10.

Tomer, N., McGlone, A., Kunnemeyer, R., 2015. Registering optical measurement to simulation models. 2015 Ninth International Conference on Sensing Technology, 716-719.

Tomer, N., McGlone, A., Künnemeyer, R., 2018. Validated multi-wavelength simulations of light transport in healthy onion. Computers and Electronics in Agriculture 146, 22-30.

Upchurch, B.L., Throop, J.A., Aneshansley, D.J., 1997. Detecting internal breakdown in apples using interactance measurements. Postharvest Biology and Technology 10, 15-19.

Walsh, K., 2015. Nondestrutive assessment of fruit quality In: Wills, R.B., Golding, J. (Eds.), Advances in postharvest fruit and vegetable technology. CRC Press, pp. 39-64.

Yamada, Y., Okawa, S., 2014. Diffuse optical tomography: present status and its future. Optical Review 21, 185-205.

Zeikus, J., Hegge, P., Anderson, M.A., 1979. Thermoanaerobium brockii gen. nov. and sp. nov., a new chemoorganotrophic, caldoactive, anaerobic bacterium. Archives of Microbiology 122, 41-48.

Chapter 8

Synthesis and Conclusions

8.1 Firmness

Previous studies that have compared actual penetrometer firmness with predictions made using either the SRRS system or the NIRS system have achieved correlations as high as r = 0.8 to 0.9. However, no experimental studies have compared NIRS with SRRS on the same samples. We measured a total of 100 'Royal Gala' apples non-destructively using the MSI and NIRS interactance systems. MSI measurements were also taken on a cut surface of each apple. The MSI system was validated using different concentrations of intralipid with known optical properties. The results showed that a standard light diffusion model did not predict absorption coefficients as well as the scattering coefficients. We therefore used a heuristic modified Lorentzian model to describe the scattering images at each wavelength.

Single wavelength MSI models provided poor correlations for penetrometer firmness, with r much less than 0.7 in most cases. Although we used a mathematical model to correct for the effects of instrument response and apple curvature, the poor correlation on the intact apple may suggest that this approach is not valid for the very inconsistently curved surface of 'Royal Gala' apples. The multiple wavelengths MSI models, that combined the model parameters estimated at each wavelength by MLR, significantly improved the correlations. The modified Lorentzian model parameters outperformed the use of optical properties estimated by the standard light diffusion model. The correlation with penetrometer firmness on intact apples (r = 0.87) was only a little different from that obtained on the surfaces of cut apples (r = 0.88). This indicates that the MLR model using all 16 modified Lorentzian parameters compensated for the effects of skin interference and non-uniform geometry. However, the best intact apple measurements were achieved using the NIRS method (r = 0.90 and RMSECV = 6.99 N).

The SRRS system and the NIRS system performed similarly, and the results agreed well with the previous studies discussed in the literature review. For both, the NIRS and the SRRS systems, the results from this and previous studies provided correlation coefficients lower than 0.94, which may be taken as the minimum for a system considered for grading purposes. Moreover, NIRS sensors are likely to perform worse between grader lines and across seasons. Evidence from predicting other parameters, like fruit dry matter or sugar content, suggests NIRS calibration models are not particularly robust against such variations.

For the SRRS system, further research will be required to investigate the feasibility of online applications. High-speed operation, inconsistent surface curvature and sample orientation are not normally problems for the NIRS system, but are very likely to be an issue when designing an online SRRS system. NIRS is not commonly used for firmness, but it is an established technique that has been used for fruit quality grading of parameters, such as sugar content, for more than two decades. SRRS might be more advantageous in theory since it can provide scattering properties, possibly allowing for the retrieval of more information about physical attributes such as firmness. Other than NIRS, a couple of impact response and deformation-based mechanical sensors have been commercialised for online application. Therefore, before the SRRS systems can be considered for commercial implementation, they will have to be improved and demonstrate better performance than the existing online sensors.

8.2 Internal disorders

8.2.1 NIRS sensors

Internal disorders that are small and spatially confined inside produce, such as apple internal browning and onion neck rot, are difficult to detect using NIRS due to its lack of spatial resolution. It might still be possible to improve detection with a better optical geometry (locations of source and detector), as there are fewer limitations on obtaining high light levels with more advanced sources and detectors.

To detect VAB in 'Braeburn' apples, we investigated two common optical geometries (Systems 1 & 2) and five sample orientations in System 2. We used the MC method to simulate light propagation inside the apple, assuming a 35 mm radius sphere with uniform optical properties (μ_a = 0.003 mm^{-1}, μ_s' = 1 mm^{-1}).

The simulation results indicated that light travelled much further (977 mm on average) inside a sample using System 2, compared with 259 mm using System 1. System 2 performed only slightly better with a higher AUC value and could detect 80% of defective apples with a misclassification rate of 21% for healthy ones. This poor performance can be explained by the absorption sensitivity distribution of System 2, which showed that 50% of the received signal was influenced by only 14% of the total volume lying immediately along the straight path between source and detector. Altering the optical properties in the remaining 86% would not make

any difference to the corresponding signal. The results revealed the fundamental limitations of the NIRS system when defects such as VAB are localised to a small internal volume, often outside the sensitive measurement regions. Rotating the samples and taking multiple scans may improve the detection rate. Moreover, an optical system using spatial resolutions such as HSI and DOT has the potential to resolve this issue.

8.2.2 Optical properties

The next step of our research was to develop a SRS system to improve detection. To investigate its feasibility, we used NIRFast, a FEM software package, to simulate a DOT system. Accurate optical properties were required for the simulations. We made an initial attempt using literature values from IAD measurement on onion slices, but the resulting simulation results did not match well with the NIRS transmittance measurements, and the absorption values from IAD had to be reduced to get accurate simulations. A new method was developed, which used a direct transmittance system to measure the absorption coefficients of the extracted onion juice. This juice method complemented by scattering coefficients from the standard IAD method was then validated by transmittance measurements using a NIRS system and a multi-laser system.

Experiments with the NIRS system showed that transmittance was sensitive to rot in the ranges 700 nm to 750 nm and 850 nm to 900 nm and was less sensitive in the range 780 nm to 810 nm. The laser light transmittance measurements showed that the chlorophyll content affects the transmittance at 700 nm. This effect was especially pronounced when light travelled through the stem end of the onion, which comprised more green tissue. To avoid the chlorophyll interference, only wavelengths above approximately 710 nm should be used.

An experimental laser system allowed measurements of a number of transmittances over a wide range of source-detector distances around a single onion. The resulting attenuation coefficients at 700, 728 and 804 nm respectively were compared with the calculated values using the measured optical properties from the new method and the standard IAD method. The results showed that transmittance measurements on onion juice provided accurate absorption coefficients, for both healthy and rotten tissue. The standard IAD method used on onion tissue slices overestimated the absorption coefficient by a factor of 3 to 4. The high accuracy of the onion juice

method also indicates that the non-soluble absorbing component in onion tissue must be very low in either concentration or absorbance, so the juice absorption is representative for the intact onion, at least within the range 700 to 1000 nm.

8.2.3 SRS (dual laser) system

Lasers were used as the light sources, since they can provide powerful light with a small illumination area on the fruit, allowing for fast and spatially localised measurements. Furthermore, they can also be modulated at high frequencies for synchronous detection and could be further developed into a FD system, which has the capability to distinguish light absorption and scattering. But laser light is monochromatic, so we conducted an exhaustive wavelength search (710 nm to 950 nm) to determine if a small number of discrete wavelengths can be used to create a classification model for detecting onion internal rot. Several algorithms with one to four wavelengths were investigated, including transmittance ratios and MLR models. We used full range (710 nm to 950 nm) MLR and PLSDA as benchmarks. The results showed that the transmittance ratio at two wavelengths provided the best classification results, almost as good as the full range PLSDA model.

The optical properties from the previous work were used to simulate a DOT system. Using only two wavelengths, we simulated a circular fan-beam geometry with 63 sources and three detectors, and placed it around a simulated onion. The FEM modelling results showed that the transmittance ratio was dependent on the source-detector separation. This issue was solved by finding two wavelengths that have similar attenuation coefficients, which meant that their transmittance ratio would be almost constant with distance for a homogenous medium. A suitable pair of wavelengths needed to show good classification performance and to be insensitive to the source-detector separation distance. A transmittance ratio of 728/805 nm was selected as there are commercial laser diodes available at these two wavelengths, and that wavelength ratio met the above criteria.

Simulated rotten tissue was created inside the onion mesh at different locations and with various sizes. The transmittance ratios for each source location formed a spatial profile. Classification was based on the different spatial profile patterns for healthy and rotten onions. The rotten tissue produced a distinctive trough in the profile, the location and size of the trough indicated the location and size of the

simulated rot. The three spatial profiles at top, middle and bottom of the simulated onion could detect the simulated rot anywhere in the onion.

Finally, the simulated setup was tested experimentally, using two laser diodes of 728 nm and 805 nm respectively as light sources and one silicon photodiode as a detector. The laser light was delivered at various positions around an onion by a low-cost mechanical scanning system, which provided flexibility, although increasing the data acquisition time. The measured spatial profiles agreed very well with the simulations, supporting the accuracy of the simulation methods. Results showed that the system could detect 80% of rotten onions with 0% FPR using a simple algorithm to identify the trough on the spatial profile. The detection rate was much better than that provided by a typical NIRS system.

The system has the speed and SNRs that makes it suitable to be further developed for use on a high-speed grader. More importantly, the spatial profile reveals the internal structure of the examined produce without the need for reconstruction of an internal image, which is a particular time consuming problem with full DOT schemes. Unlike the NIRS systems, it will probably not require frequent calibrations as it uses a simple ratio of signals at two wavelengths, and its performance is likely to be consistent across seasons and devices.

8.3 Future perspectives

SRRS could not predict firmness better than NIRS, even under ideal conditions. A number of issues have been identified when SRRS is used on a grader, such as slow data acquisition and computation speed, inconsistent sample geometry and orientation, and interference from the skin of the produce. Future developments may help to overcome some of these issues, but it is possible that the light that is scattered or absorbed within produce, may not contain enough information about firmness.

Mechanical methods based on impact response and force deformation, may be more promising for high-speed grading. Mechanical sensors have been commercialised in the past, but their performances have often not matched requirements for commercial grading. More studies should be carried out to improve accuracy of these methods. To better correlate to the human feel a system might need to simulate

hand touching of produce, a primary mechanism governing consumer selection of quality produce in terms of firmness.

Limitations of NIRS sensors for internal defect detection have been quantified in this study. The main cause of inferior detection is the small volume that NIRS light examines during each scan. Rotating the produce and taking multiple scans may improve the detection rate. Since the NIRS light is highly diffusive within produce, detection might be further improved by reducing the illumination area so that the light can be more focussed on certain regions. Taking a large number of scans while the produce is rotating would then make the sensor similar to a full DOT system. However, a smaller illumination area will cause the input light level to be lower, increasing integration time of a spectrometer and reducing the number of possible scans. This approach might be feasible if the spectrometer sensitivity could be increased by reducing spectral resolution, that is, by combining several pixels together, while still retaining enough spectral information.

The dual laser system developed here has potential to detect internal disorders better than an NIRS system. More accurate algorithms for distinguishing the spatial profiles may be developed. The future challenge is to achieve a similar measurement scheme, while the fruit is moving at high speed on a grader. A system that scans both, the light sources (lasers) and the detectors (photodiodes), might work. Using the frequency-division multiplexing technique would allow simultaneous measurements at multiple wavelengths to improve detection speed. It might also be possible to apply the scanning mechanism used in a barcode scanner, or a hyperspectral camera could be adapted.